BARRIER ISLAND'S SHALLOW COASTAL AQUIFER RESPONSE TO STORMS AND TIDAL FLUCTUATIONS: CASE OF SAPELO ISLAND

by

PARKER RUSSELL WHITLEY

(Under the direction of Charlotte Garing)

ABSTRACT

Several studies have focused on groundwater flow within barrier islands and how it is affected by tides and storms. However, predicting the hydrological response of a barrier island's surficial aquifer to dynamic tidal and storm conditions remains a challenge. This thesis aims to bring more insights into the effects of precipitation, evapotranspiration, tides, and storm surge on the water table of a barrier island's surficial aquifer. Water levels in ponds, used as a proxy, were monitored on Sapelo Island and the significance of the aforementioned variables was assessed through cross correlation and wavelet analysis methods. The data show that all variables have a consistent effect on the water table, with precipitation and storm surge having the strongest effect and the spatial location of the ponds controlling the overall response to tides. In particular, the water table increases rapidly following a sustained high sea-level from storm surge coupled with significant precipitation.

INDEX WORDS: Groundwater flow; Surficial aquifer, Storm, Barrier Island, Ponds, Storm surge, Tide; Wavelet analysis.

BARRIER ISLAND'S SHALLOW COASTAL AQUIFER RESPONSE TO STORMS AND TIDAL FLUCTUATIONS: CASE OF SAPELO ISLAND

by

PARKER WHITLEY

B.S., Geophysics, University of South Carolina, 2019

A Thesis Submitted to the Graduate Faculty of the University of Georgia in Partial Fulfillment of the Requirements for the Degree

MASTER OF SCIENCE

ATHENS, GEORGIA

2022

BARRIER ISLAND'S SHALLOW COASTAL AQUIFER RESPONSE TO STORMS AND TIDAL FLUCTUATIONS: CASE OF SAPELO ISLAND

by

PARKER RUSSELL WHITLEY

Major Professor: Charlotte Garing

Committee: Christof Meile
Adam Milewski

Electronic Version Approved:

Ron Walcott
Vice Provost for Graduate Education and Dean of the Graduate School
The University of Georgia
December 2022

DEDICATION

This thesis is dedicated to my grandfather, Richard Franklin Rozzelle, for instilling a love of learning and the importance of education.

ACKNOWLEDGEMENTS

First and foremost, I would like to thank my advisor, Dr. Charlotte Garing, for guiding me through grad school and helping me in innumerous ways. I will be forever grateful to her for the opportunity to study under her guidance at the University of Georgia. I would also like to thank Dr. Christof Meile and Dr. Adam Milewski from my committee; Dr. Meile for the project opportunity and for the knowledge and guidance from a marine perspective, and Dr. Milewski for the encouragement throughout this process. I would also like to thank the Georgia Coastal Ecosystems Long Term Ecological Research for allowing me to use Sapelo Island as a research site.

I would also like to thank my family for always showing support for me as I went through this process. To my mother and father, thank you for exposing me to nature from a young age and beginning my journey of interest and sense of wonder within the world of natural sciences. To my sister, thank you for always being there for me just a call away and able to distract me from whatever I may be distraught over and come to the realization of how to handle it.

To my friends, thank you for always being there for me. Whether a friend to talk to or a few beers to let loose I sincerely appreciate each and every one of you. Michael, Elliot, Steffan, Bailey and many other friends, thank you for making my experience here in Athens amazing, you are all awesome.

TABLE OF CONTENTS

LIST OF TABLES

LIST OF FIGURES

CHAPTER 1

INTRODUCTION

Coastlines and surrounding coastal areas around the world have a high population density and in turn their coastal aquifers are put under immense pressure to sustain constantly growing water use. These include excessive pumping of groundwater that may exceed the recharge rates, drought, and imminent sea level rise all of which encourage saltwater intrusion into coastal aquifers. Saltwater intrusion coupled with contamination and pollution from surface interactions degrading groundwater quality seriously impacts the availability of fresh groundwater resources for millions of people relying on coastal aquifers as their source of freshwater. Due to the increase in anthropogenic activities along coastlines the sustainability of these coastal aquifers has come into question and has raised some serious concerns from saltwater intrusion to sea level rise (Ferguson & Gleeson, 2012; Post, 2005; Post & Abarca, 2010).

Along many different coastlines in the world there are barrier islands. Located just off the coast, these islands earned their name "barrier islands" for their help in creating a barrier in between the open ocean and the mainland and sheltering the estuaries between them and the mainland. There is a significant number of barrier islands found on the east coast of the U.S. (Figure 1) and in the Gulf of Mexico, and none found along the west coast due to the different tectonic setting (Pilkey et al., 2009). These islands have become an increasingly popular destination for tourists for their diverse nature and large beaches and are also highly susceptible to storm events and contamination from seawater washover during storms (Terry & Falkland, 2009). The shape of these islands is primarily driven by coastal processes such as waves, tides, and currents, and geological materials, which mostly consist of sands (Hayes, 1979). These deposits of sands are highly permeable allowing for freshwater from precipitation to penetrate into the ground and accumulate forming and recharging a surficial aquifer known as a freshwater lens on the island. This is where the freshwater present on the island accumulates above the denser saltwater, forming a lens like shape creating a shallow freshwater aquifer for the island (Figure 2). This freshwater lens provides the island with freshwater for vegetation and inhabitants, and the lens is dependent upon its recharge from precipitation (Werner et al. 2017).

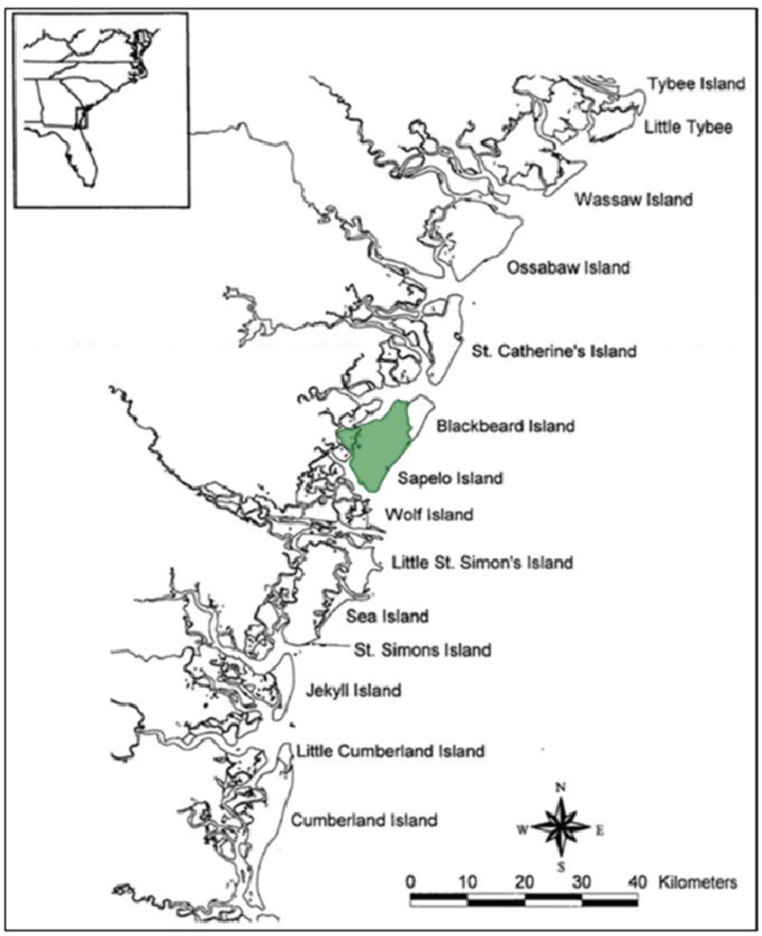

Figure 1. Map of barrier islands along the coast of Georgia modified from Dodd & Mackinnon (2003). Sapelo Island highlighted in green.

The size of the freshwater lens on an island varies depending on the geology, recharge amount and frequency, size and shape of the island, and hydrostatic pressure from the density differences between fresh and saline groundwater present (Schneider & Kruse, 2003; Ruppel & Schultz, 2007). If the island experiences a decrease in precipitation or an increase in sea level, the extent of the freshwater lens may be reduced through lessened recharge and more widespread salinity. Additionally, most barrier islands throughout the United States have been experiencing an increase in population and tourism, resulting in increased pumping of groundwater from their aquifers creating a greater strain on the island's freshwater resources (Chang et al., 2016; Post, 2005).

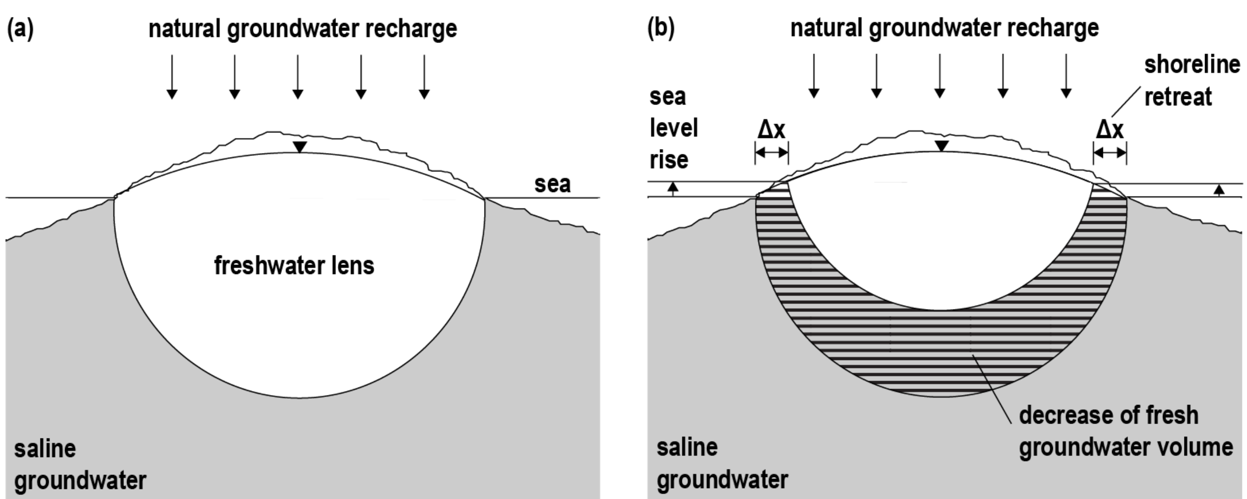

Figure 2. (a) Simplistic model of a freshwater lens underlying an island. (b) Model of effects of sea level rise on a freshwater lens aquifer. Modified figure from Essink (2001).

On barrier islands, groundwater flow within the freshwater lens is controlled by a broad range of factors that may vary both spatially and temporally. There are propagations from tidal waves, precipitation recharging the aquifer, evapotranspiration removing water, density driven flow in hypersaline areas, and sea level changes that can exert pressure onto the islands water supply (Ledoux, 2015; Wilson & Morris, 2012; Li & Jiao, 2002). Together, all these factors make the groundwater flow on barrier islands a very dynamic process that is challenging to characterize and quantify.

One key feature found on barrier islands are salt marshes, a crucial landform for both the island and the ocean. By providing protection from waves incoming from the open ocean, barrier islands allow for large salt marshes to form on the side of the island facing inland, open to the estuary. Salt marshes are inundated and drained with saltwater from the tides, creating a coastal wetland that is crucial to marine and terrestrial animals alike. They occur worldwide, and are prevalent in the Southeastern US, specifically along the South Carolina and Georgia coast. Salt marshes are essential habitats for fisheries, coastlines, communities, and economy, and are responsible for storing carbon which helps to mitigate the effects of climate change (Sanger & Parker, 2016; Deegan et al., 2012).

In recent years carbon dioxide levels in the atmosphere have noticeably increased and resulting changes in both global and small-scale climates have been observed (Lemke et al., 2007; Chang 2016). Among them is a change in the hydrologic cycle which can cause a rise in the occurrence and intensity of storms and precipitation that an area can experience. Additionally, a direct impact of global warming is the looming threat of sea level rise, which can have a negative impact on coastal groundwater. This may result in more frequent and intense flooding of salt marshes and islands, changing the dynamics of such coastal ecosystems (Koetse & Reitveld, 2009). Increased tidal forcing and pressure on the freshwater lens and groundwater system is expected from sea level rising in the future.

Given this information, it is crucial to understand the processes behind how freshwater lens operate and the factors that affect the lens. This can be done by observing the temporal evolution of the water table of the surficial aquifer at various locations across the island. The most direct way to get such data is by recording water levels in wells drilled through the freshwater aquifer (Anderson et al., 2000). An indirect way to infer the evolution of the surficial aquifer's water table is by recording water levels in the ponds located on the island.

In order to observe the water table changes over time the water level of ponds were used as a proxy. Seen as topographical depressions on the surface of the island these ponds are filled with water from a variety of sources. It is assumed that all ponds are connected to the surficial aquifer with the pond dipping below the water table. This is due to the low topography of barrier islands and the hydrostatic pressure of the aquifer allowing the height of the water table to be exposed (Chui & Terry, 2013). This means that a significant portion of the water within a pond comes from groundwater flow within the saturated zone. The pond would also be recharged through direct precipitation and runoff in its catchment area. The catchment area would vary for each pond. Flow from the unsaturated zone would also recharge some of the pond as well. It is expected that groundwater flow will have the greatest impact on recharge of ponds due to its sustained effects over time, followed by precipitation and then runoff which are localized in time relative to precipitation events, and then groundwater flow from the unsaturated zone (Corbett et al., 2000).

The ponds on Sapelo Island are not an exact representation of the water table of the surficial aquifer given that the pond level may have a higher response in magnitude or rate than the water table to certain drivers as detailed in chapter 2, but they do exemplify and give insight into the relationship that the freshwater lens has with external drivers on the island. Therefore, it is assumed that the ponds are connected to the shallow freshwater aquifer on the island. It is also important to note that the islands sediments are considered to be homogenous, and that groundwater flow within the island is anisotropic with lateral being greater than vertical flow.

There are two main objectives to this study; the first is to assess the control of each potential groundwater driver affecting the ponds and the extent of their impact on the rate and amount of the pond levels' fluctuations. The second is to assess the variability of response of freshwater ponds relative to their location and surrounding geomorphology of the island. Specific attention will be given to storm events, by focusing on the ponds response to controlling factors before, during, and after a series of selected storms, in comparison with periods of time with no recharge.

In the following chapter a literature review is provided discussing relevant work that has been done creating a knowledge base for why this project was conceived and carried out. In chapter 3 the field site of Sapelo Island is introduced and described in full detail. The fourth chapter states the objectives and hypotheses of this study. Chapter 5 covers the materials and methods used for this study. In chapter 6, the results are displayed and explained in detail. In chapter 7 the findings from the results are discussed in the context of previous studies. In the final chapter, chapter 8, conclusions are drawn about the findings of this study.

CHAPTER 2

LITERATURE REVIEW

Understanding the response of freshwater lenses to different conditions that they are exposed to gives us insight into how these aquifers will react to current and future dynamic events. With many factors such as the island geology, elevation, groundwater discharge and recharge, climatic events, and evapotranspiration affecting the distribution and flow of groundwater, it is challenging to distinguish exactly how much each factor has an effect on the freshwater lens. There are many different freshwater lenses underlying vastly different landforms; some form inland underneath sand dunes providing possibilities for vegetation and stabilization, others form under atolls in the middle of the ocean providing freshwater to the plants and inhabitants, and others can form underneath barrier islands along the coast of continents (Schneider & Kruse, 2003). Barrier islands pose a unique situation though; there are often mixed layers of sand and clay, with the clay layers acting as an aquitard separating layers of multiple aquifers creating a very dynamic system (Li & Jiao, 2002). Many aspects of this type of freshwater lens have been researched, such as the submarine groundwater discharge induced from storms, nutrient exchange in marshes from tidal forcing, and groundwater discharge from the upland to the marsh (Peterson et al., 2019; Wilson & Morris, 2012). The sole source of recharge for a freshwater lens on a barrier island is from precipitation. Understanding and quantifying how this recharge becomes part of the freshwater lens system and what other factors affect the recharge and groundwater flow in the island will help to further comprehend the interactions that occur via groundwater.

2.1 Coastal Aquifers, Barrier Islands, & Freshwater Lenses

Barrier islands are found along coasts all around the world, but typically form near river deltas and relatively low flat coastal terrain with little to no tectonic activity. Due to this, there are no barrier islands on the west coast of the US, where there is significant tectonic activity and a steep drop-off on the continental shelf. These islands are comprised of sediments that have been deposited from wind and wave action making barrier islands constantly in a state of growing, eroding, and moving (Hoyt, 1967).

Coastal aquifers are found along the coast traversing the border between the land and the ocean. Specifically, a coastal aquifer has a connection with a saline body of water, typically the ocean, leading to an interface where there is mixing of freshwater and saltwater. Coastal aquifers are usually more vulnerable than other aquifers in the sense that if the amount of freshwater that is typically held in the aquifer is lessened through withdrawal or drought, then saltwater intrusion will occur. This is where the saltwater wedge that underlies a coastal aquifer will progress further inland, or in the case of an island freshwater lens upwards, threatening to salinize the entire freshwater aquifer if it continues. As coastlines experience the highest increase in population density, and associated freshwater consumption, there is a growing concern regarding the sustainability of coastal aquifers, as they are progressively being depleted and rendered saline. Combined with a few other issues such as poor water quality from pollution, decreased groundwater recharge rates, and sea level rise from climate change can lead to much further infiltration by saline water into the aquifer (Post, 2005; Post & Abarca, 2010).

One specific type of coastal aquifer is the freshwater lens, which forms from precipitation infiltrating the islands sediments and collecting beneath the surface in a lens-like shape as seen in Figures 2 and 3. This lens acts similar to a perched aquifer as freshwater, which is less dense than the saline water, lies above saline groundwater and remains separated except for a thin layer of mixing between the two, known as the transition zone. They can occur beneath islands and sand dunes and are one of the most susceptible types of aquifers given their reliability on precipitation as recharge and density difference with the underlying salinized water. These aquifers are the main freshwater source that many island communities depend upon (Werner et al. 2017).

These aquifers are typically not very deep and can experience major changes in relatively short periods of time such as saltwater intrusion and upconing from either drought or excessive pumping, pressure from sea level rise (Figure 2), and potentially excessive recharge from precipitation events (Barlow & Reichard, 2009; Falkland, 1991). Whereas some aquifers take hundreds or thousands of years to recharge, the freshwater lenses have an almost immediate reaction to recharge. However, the shrinking of the lens as a response to prolonged periods without rainfall is slow (Bedekar, 2019).

A multitude of factors affect the size and shape of a freshwater lens: the extent of the transition zone, the hydraulic conductivity of the sediments, as well as its degree of heterogeneity and anisotropy, the rates of meteoric recharge and evapotranspiration, elevation, vegetation and densities, submarine groundwater discharge, and tidal effects (Falkland, 1991; Adyasari et al., 2021). One of the first empirical relationships identified with freshwater lens is that of the Ghyben-Herzberg relations where for every meter of freshwater above sea level the freshwater lens must extend forty meters below sea level. This is based off the simple concept that the density of saline water from the ocean is $1/40^{th}$ more than that of fresh water (Vacher, 1988). More in depth empirical relationships have been made considering more factors within the aquifer such as heterogeneity, diffusion, and dispersion, but there is still more to understand about freshwater lens ranging from the water level response, geometry of the lens, and groundwater flow under varying conditions imposed on the island (Li & Jiao, 2002). A detailed characterization and quantification of these freshwater resources is essential to accurately and properly manage such aquifers. This is especially important for freshwater lenses because their relatively small size permits rapid changes in groundwater quality due to both anthropogenic and natural processes (Werner et al. 2017).

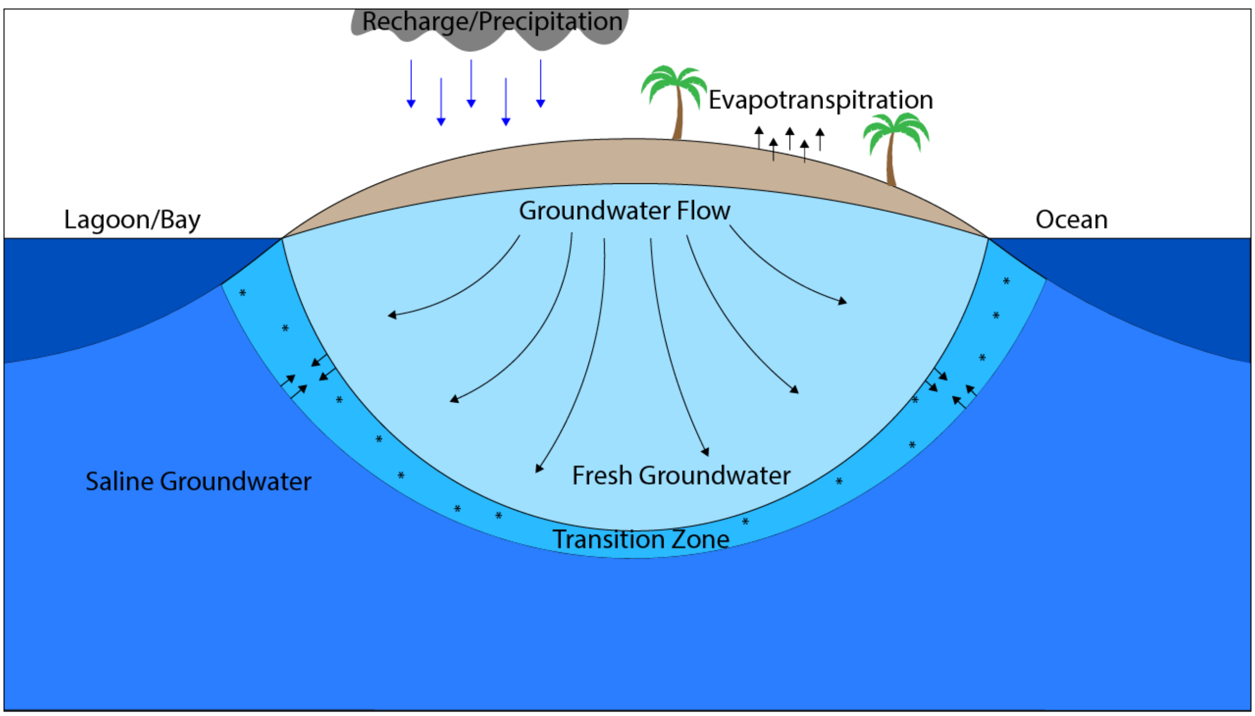

Figure 3. Conceptual model of a freshwater lens on an island with homogenous substrata. Exemplifies the shape of a freshwater lens that forms underneath an island over the denser saline groundwater. The transition zone found between the saline and fresh groundwater is shown with the mixing involved between the two.

2.2 Salt Marshes and Tidal Creeks

A large portion of the physical geography of barrier islands typically consists of salt marshes, which are naturally occurring ecosystems along the coast in the upper coastal intertidal zone and are a highly productive coastal wetland. They occur between the upland, where there are forests or urbanization, and estuaries where there is a mixing of saltwater and freshwater. The salt marsh-tidal creek systems are critical to the coastal ecosystem, being the interface between freshwater and saltwater or brackish water that is important for a variety of purposes. They act as a buffer between freshwater sources inland and the oceans constantly cycling nutrients to between the marsh and the coastal waters, physically acting as a barrier that protects the coast, and sequestering major amounts of carbon and methane that could have entered the atmosphere. Along with this salt marshes are some of the most diverse ecosystems in the world due to the hypoxic environment and varying salinities providing a home for many species of plants and animals (Sanger & Parker 2016; Deegan et al, 2012).

The systems that connect salt marshes to the estuaries are tidal creeks. Tidal creeks flood the marsh twice daily with saltwater and nutrients from the incoming tide, creating the dynamic of a salt marsh constantly at different inundation stages. At low tide they can effectively be dry, and at high tides the tidal creek will have inundated the entire salt marsh. They are typically found in between estuaries and marine barrier islands (Sanger & Parker, 2016). Barrier islands are long, low, and narrow islands parallel to coastlines. They are particularly unstable coastal environments as there are many areas of low topography that can be subject to sea water washover, and they experience constant sand migration. However, these ever-changing islands play a crucial role in protecting the coast from storms and wave action (Hayes, 1994).

Salt marshes are generally located along the backside of a barrier island where the energy from waves is lower than what is experienced on the side facing the Atlantic (Sanger & Parker, 2016). Salt marshes are typically composed of deep mud (pluff mud) and peat, which is decaying plant matter that is typically multiple feet thick, which is why it is considered marshy. Being filled with decomposing plant matter the oxygen levels in peat are incredibly low, leading to a hypoxic environment that allows for specific plants and animals to thrive as well as carbon dioxide to be trapped in the marsh (Timmerman & Chapman, 2004). Salt tolerant plants, such as *spartina alterniflora,* that thrive in salt marshes helps trap sediments and nutrients coming in with the flowing tides allowing the marsh to maintain and grow (Sanger & Parker, 2016).

2.3 Groundwater Flow on Barrier Islands

As groundwater is responsible for carrying nutrients, carbon, and contaminants through the subsurface of both the upland and the marsh, it is essential to have an accurate representation and quantification of groundwater flow and its interconnection with surface hydrology (Peterson et al. 2019, Krest et al. 2000). Within a salt marsh there are many drivers of groundwater flow ranging from propagating pressure waves from the tides, temperature differences, groundwater discharge, and sea level changes (Wilson et al. 2011, Wilson & Morris 2012, Ledoux 2015).

Peterson et al. (2019) investigated groundwater discharge from the surrounding salt marsh into the headwaters of the main tidal creek on Sapelo Island (the Duplin River) using radon as a geochemical tracer of fresh groundwater. They found the average rate of groundwater flow into the headwaters of the Duplin to be about 5.0 cm^3/cm^2 marsh/day. Their goal was to quantify net groundwater inputs to both the main channel and the headwaters of the Duplin to assess the role of inundation on driving groundwater discharge from the marsh, and it was found that there was a strong positive correlation with ebb tides and groundwater discharge rates.

Similarly, in Adyasari et al. (2021) the groundwater response within barrier islands to multiple storm events was examined and the associated discharge to the surrounding areas was assessed. The hydrological response was quantified through submarine groundwater discharge to the ocean imaged using radon as a tracer. To fully assess the reaction of the island's submarine groundwater discharge response to storm events both the hydrological and meteorological conditions were analyzed before, throughout, and after the storm events. It was ultimately found that the submarine groundwater discharge was driven mostly by marine forces, except during major storm events where it is driven by terrestrial forces.

In Ledoux (2015) drivers of groundwater flow within a salt marsh on the back of a barrier island were identified, specifically from the upland to the tidal creek. This was modeled through an equation factoring in tidal signals in (Schultz & Ruppel, 2002) and water level data from a transection of groundwater wells. By manipulating Darcy's law, using oceanographer's tools to quantify tidal forcing, and different statistical analyses the groundwater flow was determined and the impacts of each driver of flow was quantified. The influence of tides on the groundwater flow was seen 22 meters into the creek bank of a salt marsh using the hydraulic conductivity of the marsh subsurface and a tidal amplitude of .75 meters (Ledoux, 2015). Four main drivers were identified in a salt marsh environment; 1) tidal waves propagating into the marsh platform influencing the groundwater flow 2) changes in density from fluids temperatures or salinities allow for density driven flow, 3) groundwater seepages where the tidal creek is below the water level and 4) storms affecting the water level of the sea affecting pressure gradients. The main limitation of Ledoux (2015) is in applying it to a whole barrier island-salt marsh system where the upland area of barrier islands experiences vastly different groundwater flow than observed in the salt marsh.

When modelling groundwater flow in salt marshes the same drivers mentioned by Ledoux (2015) are used as the input parameters as well as changing sediment's permeability and porosity, hydraulic conductivity. When experiencing extreme inundation events, such as storm surges, there is potential for greater groundwater flow, which can in turn enhance nutrient mixing (Wilson et al. 2011). The Southeast of the U.S. frequently experiences hurricane events causing significant storm surges that inundate the salt marshes more than normal (Koetse & Reitveld 2009).

Because spatial and temporal changes in salinity create density changes that control flow patterns the study of groundwater flow in coastal aquifers is inherently intertwined with the transport of salts and both should be considered when solving for either. A huge achievement in the field was the advancement of models that can simulate groundwater flow for varying densities that may be present. Models are still striving to become more accurate and define the varying processes seen in groundwater flow (Post & Abarca 2010). The changes in salinity are evident across a salt marsh where the ebb and flow of a tide causes salinity gradients and fluctuations across the salt marshes different sections, but it is also important in the upland of barrier islands as well. The East coast of the United State frequently has hurricanes every year that can cause massive storm surges and these events cause salinized water to wash over the upland and infiltrate into the surficial aquifer (Falkland, 2009). Eventually this is flushed out of the freshwater lens, but this depends on the groundwater flow and hydrodynamics of the particular aquifer.

2.4 Effect of Sea Level Rise

Over the past hundred years there has been a significant trend in climate change, with notably global warming. Occurring at a rapid rate the average temperature of the Earth has been increasing, which in turn causes sea level rise given the amount of water that is stored in ice caps and permafrost (Koetse & Reitveld, 2009; Chang 2016). Given the upwards trend in warming of our climate this will also induce more evapotranspiration and can in turn induce more precipitation altering normal hydrologic cycles. The long-term effects of global warming and sea level rise on salt marshes and underlying coastal aquifers have been explored but are not fully known (Donnelly & Bertness, 2001). Isolated events such as storm surges and perigean tides that occur during brief periods of time give insight as to how they will react to being inundated more frequently and at a greater intensity. Wilson et al. (2011) studied groundwater flow driven by storms within a salt marsh on Cabretta Island, a Holocene barrier island in Georgia. The authors reported that small to moderate storms "can strongly increase groundwater flow and transport in salt marsh ecosystems and adjacent barrier islands" (Wilson & Morris, 2011, p. 1). Previous studies have shown that large storms have a direct effect on groundwater flow and transport (Anderson 2002). Wilson et al. (2011) used monitoring wells and radium isotopes to calculate the groundwater flow and nutrient transport during these storm events. The authors noted that there was a "significant influx of saline creek water that was into the confined aquifer below the marsh platform, by the storm surge" (Wilson & Morris, 2011, p. 1). Even from rather small storms the vulnerability of coastal aquifers near the surface of a salt marsh experience saltwater intrusion (Wilson & Morris, 2011). These studies show that storms, ranging from both small to large, have the ability to alter groundwater flow in salt marshes and barrier islands and force saline water into confined freshwater aquifers via saltwater intrusion as seen in Figure 4 for the multilayered Floridian Aquifer. One should note that whether Sapelo Island presents the same conditions of multiple confined aquifers beneath the surficial aquifer is unknown.

The effects of tides on the flow of groundwater and transport of nutrients in an estuary strongly influenced by a salt marsh were reported by Wilson et al. (2012). In particular, the authors focused on long-term changes in the mean water level (MWL) and how it is related directly to the productivity of the salt marsh and porewater salinity. If the MWL is raised high enough to inundate more of the marsh than usual, roughly around the mean high-water level, then groundwater flushes at a higher rate than normal, increasing the export of nutrients out to the marsh and ocean. If the MWL increases above the mean high-water level, then there is a decrease in groundwater flushing. The implications of the study are important in regard to the Earth's changing climate and inevitably rising sea level. The increase in the flushing of the nutrients will heighten the chance for eutrophication of the nearby bodies of water and also runs the risk of forcing saline water into aquifers.

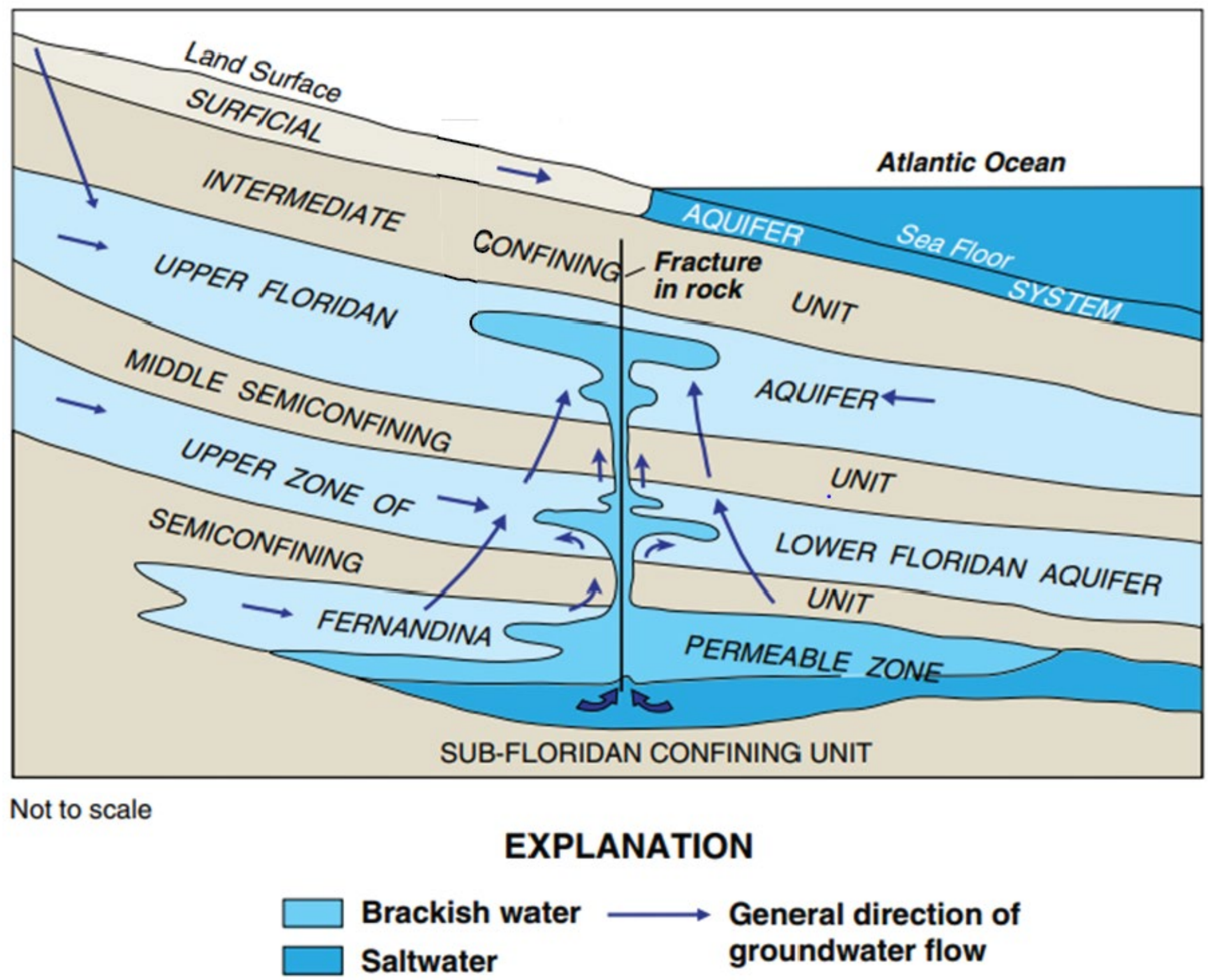

Figure 4. Modified figure from Barlow (2009), this figure shows multiple confining units that separate multiple aquifers in Florida. Potential for saltwater intrusion into the deepest aquifer is shown as well through horizontal encroachment from the ocean.

Currently, uncertainty remains in our conceptual understanding of coastal aquifers and groundwater flow, challenging predictive modeling and imminent issues such as saltwater intrusion and sea level rise. To advance the field of coastal hydrogeology the following areas require specific attention: i) better approximations of the heterogeneity of the subsurface of coastal islands, ii) a better understanding of groundwater flow in the various conditions imposed on it in the dynamic setting of a freshwater lens and salt marsh system, iii) characterizing the response of a freshwater lens to stress events, such as sea level changes, evapotranspiration, tides, precipitation, and storm surges and iv) understanding the geographical and geomorphological conditions such as vegetation density, elevation, and distance from the ocean that affect the size and shape of the freshwater lens. I will be addressing part of the second, the third, and fourth points by correlating and quantifying the response of the freshwater lens (by using ponds as proxy) to precipitation and sea level rise from major storm events to extended periods of drought and examining the different geomorphological dynamics that spatially affect each specific freshwater pond.

CHAPTER 3

STUDY SITE

3.1 Physiographic Setting

Sapelo island is a barrier island found among the many along the east coast of the United States within the coastal plains. It is the fourth largest barrier island parallel to the coast of Georgia spanning a length of 12 miles and width of 3 miles for a total area of 16,500 acres (19 km long, 5 km wide, and 667073131 m^2). Most of the island has been left undeveloped as a nature preserve and research site except for a small 434-acre community, Hog Hammock, that is mostly comprised of the long-standing Gullah and Geechee community in the low country (Chalmers, 1997).

The island can be seen as having two main sections, an upland section that remains above sea level and a salt marsh. On the east side of Sapelo facing the Atlantic Ocean is the upland, which consists of primary and secondary dunes, maritime climax forests, shrub zones, and meadows. On the west side of the island, facing inland, is the salt marsh that is comprised of many different zones such as the low, middle, and high marsh, mudflats, and hammocks. Salt marshes depend on the tides, which are brought in through a tidal creek system, and the tidal creek within Sapelo Island's salt marsh is named the Duplin River (Sanger & Parker, 2016).

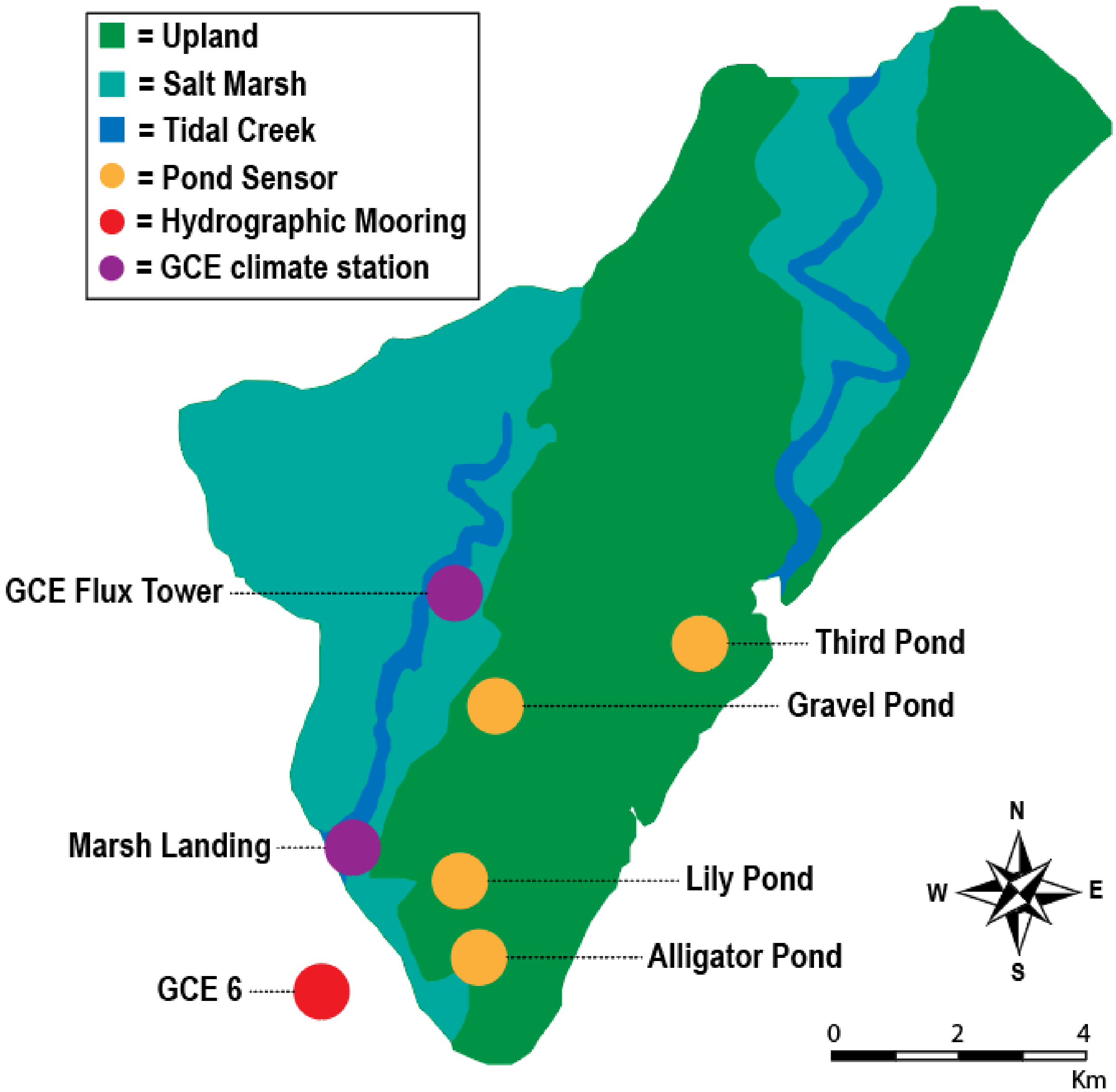

Figure 5. Map of Sapelo Island and its major physiographical components. The location of pond and tidal creeks where sensors were installed, as well as existing data (GCE) are indicated on this map. The tidal creek identified is the Duplin River.

Sapelo Island is a typical marine barrier island with a salt marsh for which the major processes have been extensively investigated over the past few decades as a part of the Georgia Coastal Ecosystems Long Term Ecological Research Project (GCE-LTER).

The tidal creek that controls the flow of saltwater to and from the salt marsh is the Duplin River, which is a relatively large at 12.5 km long, 200 m wide, and an average depth of 6.5 m. The tidal creek experiences a mean tidal amplitude of 2.4 m (Peterson et al. 2019). Fluctuation of water level, salinity and nutrient concentrations in the Duplin River are driven by the discharge from the nearby Altamaha River, tides, interactions with the groundwater, as well as exchanges with the marsh platform (Schutte et al., 2013).

3.2 Geologic Setting

Barrier islands are believed to be formed from sea level fluctuations during the Pleistocene epoch caused by alternating periods of warm and cold, changing water levels through massive amounts of storage of water in ice sheets. What were once sand dunes are believed to have been surrounded by the rising sea level and have gradually been built into barrier islands over time (Hoyt, 1967). Sapelo Island is part of a complex of Pleistocene and Holocene facies that formed during these successive sea level fluctuations that occurred across the last major regression across the Georgia Coastal plain (Hails & Hoyt, 1967; Howard & Scott, 1983).

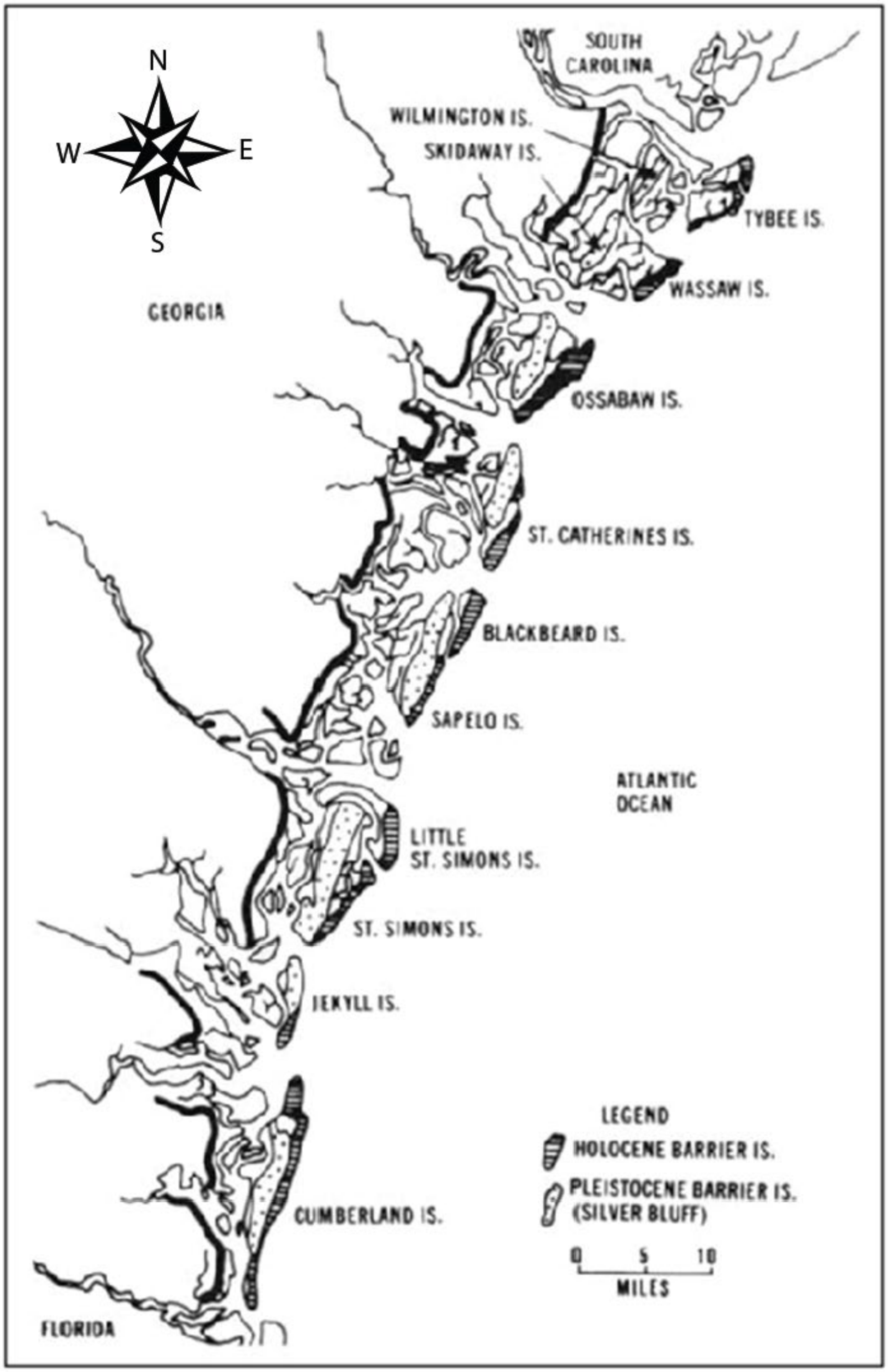

Figure 6. Ages within the geological scale of the barrier islands in Georgia, modified from Hoyt (1968). Sapelo Island is the fourth largest island of them, and the fifth from the top.

The geology of Sapelo island is similar to many of the barrier islands along the Georgia coast. As seen in Figure 6, it is comprised of late Pleistocene sands with locally distributed marsh muds and Holocene sands overlying late tertiary sediments (Peterson et al. 2019; Hoyt & Henry 1967). Sapelo Island consists of Pleistocene sands and on the seaward and southern facing side of the island there are Holocene facies that have been deposited by wave action. These sands in the upland are well-sorted and fine (Hoyt & Henry 1967; Schultz & Ruppel, 2001). A combination of geological descriptions and geophysical logs identify a clay layer that is 4-30 m thick that underlies the entire island at an average of 12 m below the surface (Krause et al., 1984; Schultz & Ruppel, 2001). It is assumed that this is the base of the upper surficial aquifer for Sapelo Island and the top of one or more confined layers beneath the island. The Floridian aquifer would extend underneath the island, albeit it is unknown if there are more aquifers below this confining clay layer. This confining layer is demonstrated in the conceptual model of Figure 7, with the surficial aquifer lying above the confining clay layer.

Below the Pleistocene sands, marsh muds, and clay layer the stratigraphy is well mapped out for the mid-Cenozoic era through multiple well logs and seismic stratigraphy. A well log on Blackbeard Island (separated from Sapelo Island by a tidal creek) found the Miocene to be undifferentiated fine to coarse sands at a depth of 108 – 122 m, the Oligocene to be undifferentiated granular limestone from 122 – 166 m, and the Eocene to be undifferentiated limestone from 166 – 217 m (Herrick, 1961). These well log results are confirmed for Sapelo Island through seismic stratigraphy tests by Adesida (2000). The mid-Cenozoic units of Miocene, Oligocene, and Eocene were confirmed around the same composition with sands and clayey silts for the Miocene and limestone for the Oligocene and Eocene. The depths of the stratigraphical units were also confirmed to be approximately the same as the well logs (Adesida, 2000).

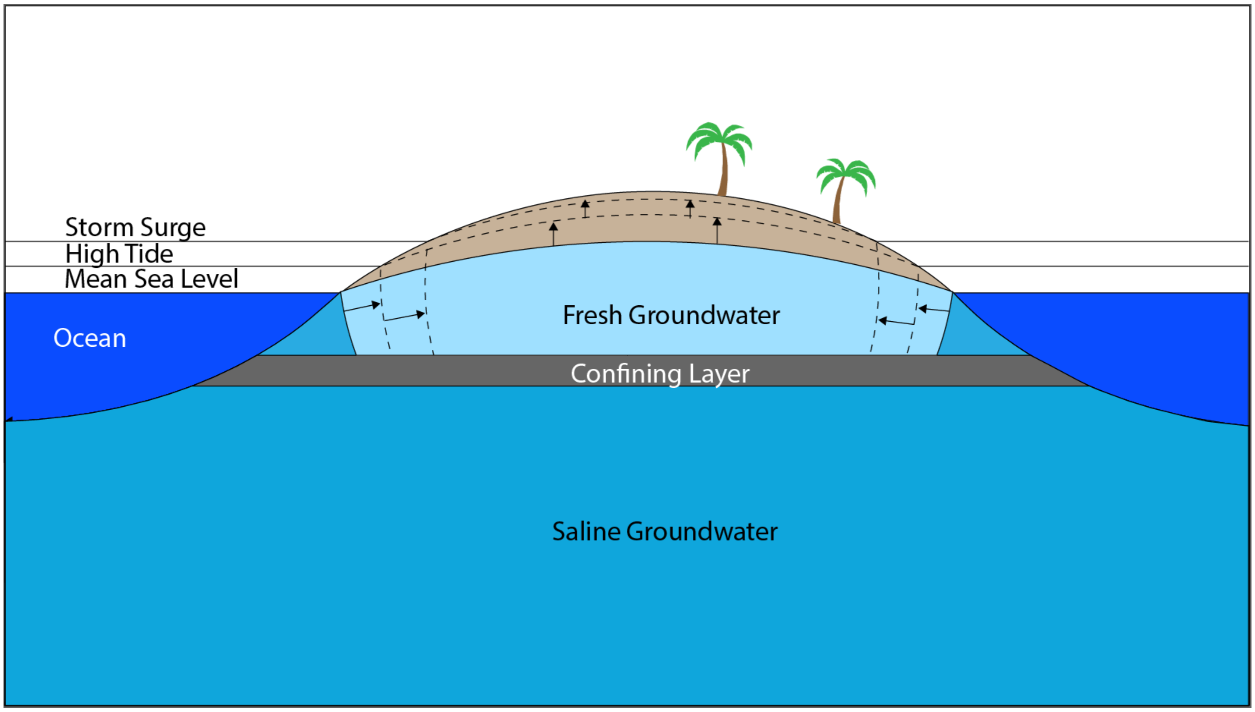

Figure 7. Conceptual model of a simplified Sapelo Island with a confining clay layer and a surficial freshwater aquifer. The dashed lines represent the effects of different tides on the shape and location of the surficial aquifer.

3.3 Hydrogeologic Setting

The recharge for the upper surficial aquifer would consist entirely of precipitation. The number of layers of aquifers is uncertain as core data would be needed for exact knowledge of the hydrostratigraphy of the island, but the Floridan aquifer system does underlie the island. This aquifer is at a much greater depth and would require expensive and time-consuming deep well drilling to fully access and characterize, so the surficial aquifer is the easiest and cheapest option to use to extract groundwater. It is also noninvasive, which causes less problems on an island protected by the state.

Sapelo Island consists of two main parts, the upland, and the salt marsh. Both have varying hydraulic conductivities given their geologies. The upland, where this research is focused, has an average hydraulic conductivity of $\sim 10^{-4}\ m.s^{-1}$ for the Pleistocene sands (Schultz & Ruppel, 2001). Towards the upland and estuary boundary there is a decrease in hydraulic conductivity by two orders of magnitude, indicating that there is a clogging layer. This clogging layer would impact tidal forcing on the upland (Schultz & Ruppel, 2001). A layer between the upland and the ocean that is not as conductive would minimize the effect of the tidal forcing on the aquifer seen.

3.4 Climatic Setting

The climate of Sapelo Island is described as subtropical with high temperatures during the summer and moderate temperatures during the winter. The hottest month is July averaging a high and low of 32 °C and 24 °C respectively. The coldest month is January averaging a high and low of 16 °C and 5.5 °C respectively. Year-round the average temperature on the island is 19.8 °C. The average amount of precipitation for the island is 128.6 cm of rain per year, with most of the rain falling from June to October, hitting a high in August with an average around 17.7 centimeters for this month.

Due to the geographical location of Sapelo Island, it is subject to hurricane impacts. Forming over the warm waters by the equator by convection of warm and cool air flow these storms have historically followed multiple paths. Some hurricanes track along the west side of Florida and into the Gulf of Mexico and some track along the east coast of the US, occasionally directly over Sapelo Island (Camargo et. al 2017). These storms can bring intense and excessive amounts of precipitation, higher than normal tides with a storm surge, and bring wave energy that can washover parts of the island and erode sediments at an accelerated rate. During Hurricane Irma in September of 2017 the wave and tidal energy from the storm surge caused a shift in a creek channel and broke off a 100-acre island from the already existing Blackbeard Island, creating a new barrier island, Little Blackbeard Island (Breslin, 2018).

3.5 Site Specific Available Data

Sapelo Island is the site of the GCE-LTER which focuses on understanding and researching how coastal areas respond to long term change, specifically the estuarine and intertidal wetland systems. The research has been ongoing for over 20 years now and covers a broad range of academic fields and studies, and thus there has been a vast amount of data collected continuously for this time.

The open-source data for research is available on the Georgia Coastal Ecosystems (GCE) Data Portal online, ranging from real time monitoring stations to long term monitoring stations of climate and hydrographs. These provide a wide range of data including tides, salinities, water temperatures, streamflow, precipitation, wind speeds, barometric pressure, and Photosynthetically Available Radiation (Georgia Coastal Ecosystems LTER, 2022). Most of the measurements are taken at 15-minute intervals except for the tides, which are taken at 30-minute intervals. The tidal datum, showing averages for tides found on Sapelo Island, can be found in Figure 8. There are no open wells to obtain water level data for the surficial aquifer, but with a permit from the US Department of Natural Resources (DNR) pressure sensors were deployed in ponds around the island and data was collected from these.

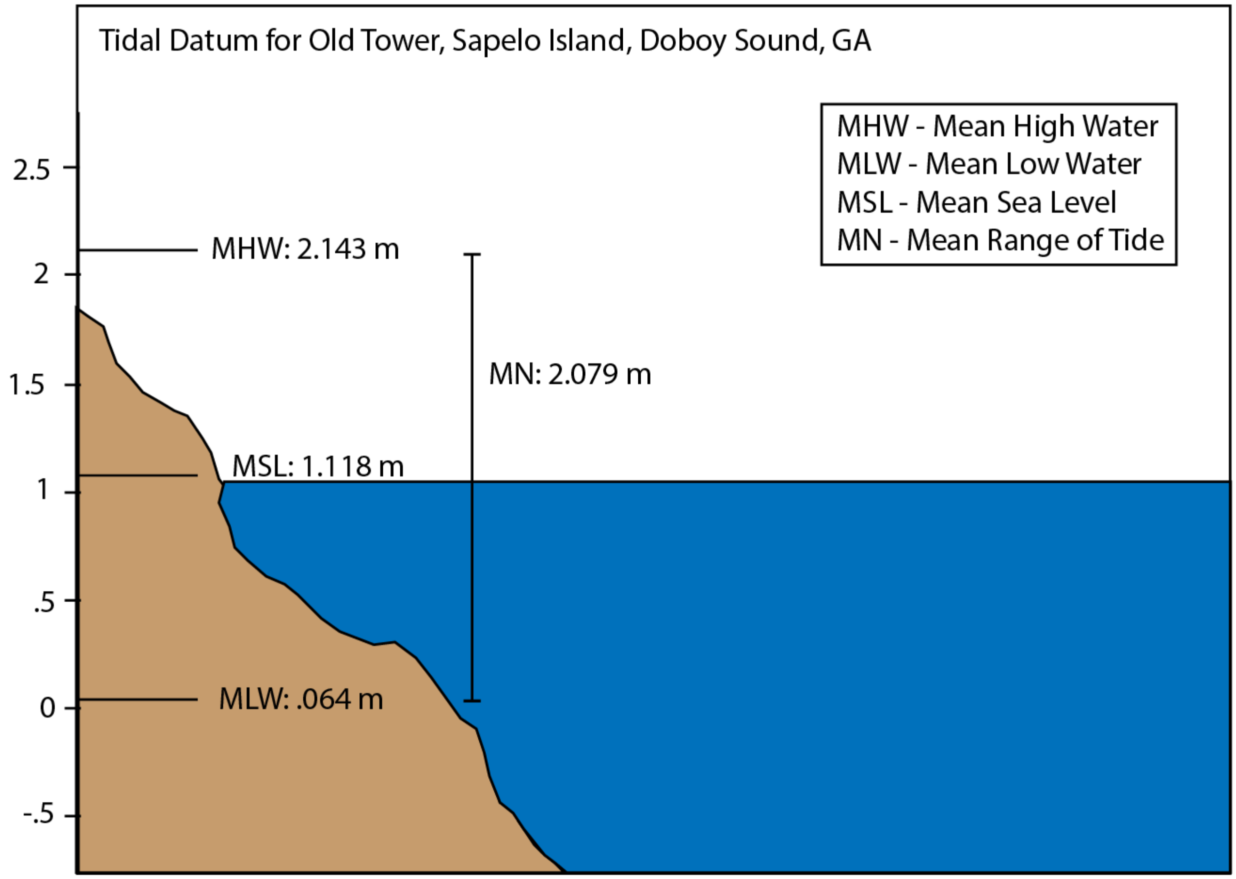

Figure 8. Tidal Datum for Old Tower, Sapelo Island. Adapted figure from NOAA (2004). Shows the Mean high-water mark, the mean low water mark, mean sea level, and mean tidal range for Sapelo Island. The station has its own set datum at a fixed elevation of 0 for the Mean Lower-Low Water (MLLW) to which all of the water level measurements are referred.

CHAPTER 4

OBJECTIVES AND HYPOTHESES

4.1 Open Ended Questions

Although there has been an extensive body of work dedicated to coastal aquifers, additional research is needed to improve the characterization of these aquifers and their dynamics. The effect of storm events and storm surges on surficial aquifers located on barrier islands has been studied by looking at the submarine groundwater discharge (Wilson et al., 2011), but the response of the water table is relatively unknown. The effect seen from tides on nutrient cycling via groundwater flow has been studied as well as the extent that the tidal wave propagates into the creekbank (Porubsky et al., 2014; Wilson & Morris, 2012; Ledoux, 2015). Despite the extensive research on the various effects of tidal wave propagation on groundwater flow in a barrier island – salt marsh system, the impact of the tides, specifically an above average and prolonged tide, on the water table and shape of a freshwater lens is relatively unknown.

This study aims to investigate these gaps in knowledge using the level of ponds as proxy for the water table height of the surficial aquifer of a barrier island to quantify the effects of storm surges, tides, precipitation, and evapotranspiration on the water level both in temporal and spatial scales.

4.2 Objectives

The specific objectives of this study are:

a) To identify and quantify the relationship between different groundwater drivers and water level of a surficial aquifer on a barrier island. This can be further broken down into each driver that will be viewed individually for its correlation and rate of change with the pond height.

   a. Precipitation

   b. Evapotranspiration

   c. Tides

   d. Storm Surges

b) To assess the spatial variability of responses to storm events by different ponds relative to their geographical locations.

4.3 Hypotheses

I hypothesize that:

a) There will be a linear relationship between the amount of precipitation and the rise in the ponds used as proxy for the groundwater level.

b) Evapotranspiration will have the least effect on the pond level in comparison to the other variables.

c) Tidal effects on the pond level will be more readily observed during the perigean tides and larger effects will be seen during storm surges.

d) Spatially across the multiple ponds it is expected that the ponds closer to the center of the island will experience more of a response in water level than the ponds closer to the water.

CHAPTER 5

RESEARCH METHODOLOGY

5.1 Field Data

5.1.1. Pressure data (water level)

Existing pressure data was collected and provided by Dr. Rick Peterson and Dr. Christof Meile from September 2016 – October 2017 of the changing water levels of a pond on Sapelo Island. This pond, known as Gravel Pond, is located near the center of the island, specifically 400 meters inland from the saltwater marsh and 12 feet above sea level (Figure 5). The data was collected to measure the temporal variations in pond level specifically in response to major storm events like hurricanes. The data was collected using a HOBOware pressure sensor that was installed in the pond taking measurements every 15 minutes. There was a second sensor gathering data on the barometric pressure just outside of the pond and the data from the pressure sensor in the pond was corrected for using the barometric pressure data.

To assess spatial variations across the island three other ponds along with Gravel Pond were identified on Sapelo Island to have their water level measured. This includes the Alligator Pond near the University of Georgia Marine Institute (UGAMI) on the south side of the island, and the third and fourth ponds, which are located in between the Alligator and Gravel Ponds and close to the east coast of the island (Figure 5). Two sections of the tidal creek also had pressure sensors installed to measure water level to get tides as accurately as possible, and near the ponds. The first pressure sensor to measure tides was installed in the tidal creek behind the UGAMI to a dock hanging using a string (Figure 9.a), and the second was installed near the post office also hanging off a dock. Unfortunately, strong tidal currents made the data inaccurate for the tidal creeks, so the GCE hydrographic moorings provided by the Georgia LTER were used instead.

Figure 9. Photos of equipment used and ponds that had pressure sensors installed in them. (a) HOBOware pressure sensor used to obtain pressure within the ponds. (b) Alligator Pond covered in green algae. (c) Glimpse of Alligator Pond, location of sensor P2. (d) The fallen tree across the water in this photo was used to attach the pressure sensor in Alligator Pond. The Third Pond having the pressure sensor installed to a dead and fallen tree. (f) The Lily Pond, covered in lilies, with the pressure sensor installed on a live pine tree branch hanging over the pond.

The water level of the ponds and tidal creeks mentioned above were monitored using a HOBOware pressure sensor at 15-minute intervals over a 226-day period from January to August in 2022. The observed pressures can be used with the barometric pressure to solve for the relative pressure. Once the relative pressure is calculated the water level height above the sensor can be calculated using the hydrostatic pressure formula as follows

$$h = \frac{P}{\rho g}$$

where h is the height of water above the sensor, P is the hydrostatic pressure, ρ is the density of the liquid, and g is the acceleration of gravity. The barometric pressure was included in the readings provided by the HOBOware pressure sensors. It was removed using the barometric pressure readings from the GCE flux tower. The height of the water above the pressure sensor was then calculated using the hydrostatic pressure formula.

The level of the pond and its change over time will be assumed to be representative of the groundwater level at each pond location. The idea is that a deep enough depression in the surface of the island will expose the water table, acting like a window allowing a view into the surficial aquifer (Chui & Terry, 2013). While this may not hold completely true in all scenarios, given that the pond level may overreact compared to the water level, it allows for a non-invasive insight into the surficial aquifer and how it reacts temporally and spatially to multiple variables.

5.1.2. Climate and tidal data

The Georgia LTER has been collecting climatic data and tidal data for multiple years now, and this data was used for this study. The near real time monitoring stations at Marsh Landing and the Georgia Coastal Ecosystems (GCE) flux tower were used for precipitation, temperature, and PAR data (Figure 5). All were collected at an interval of 15-minutes. Data from the Marsh Landing and GCE flux tower were used to calculate daily evapotranspiration rates using the FAO-56 method of the Penman-Monteith equation (Zotarelli et al., 2020). The data acquired for the Penman-Monteith equation from the two climate monitoring stations was air temperature, relative humidity, solar radiation, wind speed, and barometric pressure (Georgia Coastal Ecosystems LTER, 2022).

The hydrographic mooring station GCE6, located just south of Sapelo in Doboy Sound, was used for tidal data at an interval of 30 minutes (Georgia Coastal Ecosystems LTER). These intervals for the tidal data were resampled for every 15 minutes by taking the mean between the 30-minute intervals. Storm surge data was calculated from predicted tidal data and observed tidal data from Fort Pulaski, GA. Fort Pulaski was used as it was the station closest to Sapelo Island with similar tides and with known harmonic constituents that allowed for accurate predictions of the tide at the same observation intervals. The storm surge was calculated as the difference between the predicted and observed tide. Given that there is a 65 km distance between Sapelo Island and Fort Pulaski they may be experiencing peaks and troughs at different times. It was observed over a month of data that Sapelo Island experiences the tides on average 15 minutes after Fort Pulaski, so the time series of storm surge was shifted 15 minutes back to accurately reflect the tides of Sapelo Island.

5.1.3. Salinity Data

The conductivity of each pond used for this study was measured to assess their salinity (freshwater, brackish, or saline) during multiple trips in the second acquisition campaign. There was only one true freshwater pond, the one in the middle of the island, P4 also known as Lilly Pond. The rest of the ponds were brackish.

Table 1. Electrical conductivity (EC) of the ponds water measured in September 2022. Temperature (T) is the water temperature when EC was measured. For reference: EC < 1.5 mS/cm for freshwater and EC = 55 mS/cm for seawater.

	P1 *Alligator Pond*	**P2** *Gravel Pond*	**P3** *Third Pond*	**P4** *Lily Pond*	
EC (mS/cm)	2.65	8.33	6.59	0.202	**17-Sep-22**
T (°F)	76.2	80.7	84.9	78	

5.2 Data Analysis

5.2.1 Cross Correlation

All the collected data from the field and from various sources were collected over time, making them time series that will be used to see the effect on the pond over extended periods of time. One of the analytical methods used to see the relationship between two time series is cross correlation, measuring the similarities between two time series. Cross correlation was calculated using the cross-correlation function in MATLAB with the time series x being independent and the time series y being dependent.

5.2.2. Wavelet Analyses

Wavelet analysis is commonly used when two nonstationary time series do not present a strong cross correlation even though theoretical knowledge suggests linkage. It is a relatively recent and new alternative to windowed Fourier transforms, producing a two-dimensional plot that shows the strengths of variations within a time series as a function of both frequency and time.

For this study the Continuous Wavelet Transform (CWT) is calculated to show the wavelet power spectrum across both varying time and frequency for each time series. The Cross Wavelet Transform (XWT) then characterizes the interaction between the CWT of two time series and reveals areas where the two share high power. These areas of high power display the nature of the relationship through phase arrows that show the relative lag between the two time series. The circular mean of the phase angle is calculated and used to quantify the exact relationship of the phases, albeit the phase arrows do not indicate that two signals are in a causal relationship; rather they could be randomly related or there may be a third unknown variable linking the two (Grinsted et al. 2004).

The Wavelet Coherence (WTC) can be calculated using two CWTs. It exemplifies the correlation between the two time series localized in both time and frequency. Wavelet coherence is similar to a traditional correlation coefficient, such as Pearson's rank correlation, of two time series within time frequency space. The WTC finds frequencies within the two time series and relates the phase behavior to one another indicating the relative lag (Grinsted et al., 2004). All of the wavelet analyses were completed using adapted MATLAB code from the cross wavelet and wavelet coherence toolbox provided by Grinsted et al. (2004).

5.2.3 Continuous Wavelet Transform (CWT)

The basis of wavelet analysis is using a wavelet to extract one or many different frequencies from a time series that contains nonstationary power. A wavelet is a signal of limited duration with an amplitude that begins, oscillates, and ends at 0. There are numerous wavelets that exist, and many are useful for CWT. Which wavelet to use depends on what signal features are trying to be detected within the time series signal.

The wavelet used in this study was the Morlet wavelet, as it is well balanced in both time and frequency. This is important as there is an inverse relationship between higher resolution in time and frequency, the higher one is the lower the other will be, and having a balanced approach allows for an accurate view of both. The Morlet wavelet was introduced in the 1980's to be applied in the world of geophysics and subsequently began continuous wavelet analysis. The Morlet wavelet is defined as:

$$\psi_0(n) = \pi^{-1/4} e^{i\omega_0 n} e^{-\frac{1}{2}n^2}$$

where ω_0 is dimensionless frequency and n is dimensionless time (Grinstead et al., 2004; Kumar & Foufoula-Georgiou, 1997).

CWT applies the wavelet at varying scales to act as a bandpass filter at different to a time series to identify multiple different frequencies. The mother wavelet (wavelet chosen to be used for CWT) is stretched in time through the changing scale (s) and normalized to have unit energy. When the mother wavelet is translated or stretched, it is referred to as the daughter wavelet. It is stretched to identify different frequencies within the signal. The daughter wavelet is then shifted across the entire time series to identify any areas corresponding to a frequency. This is repeated for different scales to identify the varying frequencies that may be present in a time series signal. The CWT of a time series is the time series, x_n, convoluted with the mother wavelet. The time series should have uniform time steps δt, and the wavelet will be scaled and normalized. The formula for CWT is defined as:

$$W_n^x(s) = \sqrt{\frac{\delta t}{s}} \sum_{n^1=1}^{N} x_{n^1} \psi_0 [(n^1 - n)\frac{\delta t}{s}]$$

Where the wavelet power is defined as $|W_n^x(s)|^2$ which is used to produce a scalogram of time and frequency for a time series, and $W_n^x(s)$ is interpreted as the local phase (Grinstead et al., 2004; Torrence & Compo, 1998).

When calculating the CWT the wavelet does not remain completely localized within the time series used thus creating edge artifacts that are unreliable. They are found near the beginning and the end of a time series and increasing for lower frequencies (Grinstead et al., 2004). It is helpful to use a Cone of Influence (COI) to identify these regions in the time-frequency plot that are unreliable due to edge effects. The COI visible on all scalograms indicates where the edge effects are in place and where the wavelet power can and cannot be accurately interpreted.

Many time series "have distinctive red noise characteristics that can be modeled well by a first order autoregressive (AR1) process" (Grinsted et al., 2004, p.563). This AR1 process is used to calculate the stationary signal that the CWT will be assessed against for statistical significance. Having a lag-1 autocorrelation, α, the AR1 in the Fourier power spectrum is calculated by:

$$P_k = \frac{1 - \alpha^2}{|1 - \alpha e^{-2i\pi k}|^2}$$

where k is the Fourier frequency index (Allen & Smith, 1996; Grinsted et al., 2004). For our time series the background power spectrum calculated above is assumed to be a stationary process and will be the null hypothesis that the signal will be tested against to identify areas of high power of statistical significance (Grinstead et al., 2004; Torrence & Compo, 1998).

5.2.4 Cross Wavelet Transform (XWT)

The XWT between two time series x_n and y_n is calculated as

$$W^{XY} = W^X W^{Y*}$$

where * signifies complex conjugation between the CWTs of both time series. The cross wavelet power, which helps to identify where the two time series are strongly related, is noted as the absolute value of the XWT coefficients (Grinsted et al., 2004).

For a relationship to be present between two time series one would expect the oscillations to be phase locked. In other words, when one time series causes an effect to another time series, we would expect to see the frequencies within the time series as correlated to each other with a consistent lag. This would mean that they are phase locked, and not just a spurious relationship between the two time series. This phase relationship is calculated through the cross wavelet phase angle and shown by the phase arrows plotted on the scalograms of wavelet coherency.

5.2.5 Cross Wavelet Phase Angle & Phase Angle Statistics

Knowing the phase difference shows the lead and lag relationship between two time series. This is calculated from the areas with greater than 5% statistical significance, that are not within the COI. In these areas the circular mean of the phase of the frequency seen is calculated and used to determine the phase relationship between time series. The equations to calculate the circular mean of a set of angles is:

$$a_m = \arg(X, Y) \qquad X = \sum_{i=1}^{n} \cos(a_i) \qquad Y = \sum_{i=1}^{n} \sin(a_i)$$

The scatter of angles around the mean can be found by the circular standard deviation:

$$d = \sqrt{-2\ln(R/n)} \qquad \text{where} \qquad R = \sqrt{X^2 + Y^2}$$

These equations calculate the angle of the phase arrows and their standard deviation. These angles provide insight into the lead - lag relationship between time series.

5.2.6 Wavelet Coherence

To identify areas of correlation between two time series wavelet coherence is used. Like the CWT, wavelet coherence identifies correlations both within time and frequency. Wavelet Coherency of two time series can be defined as

$$R_n^2(s) = \frac{|S(s^{-1}W_n^{XY}(s))|^2}{S(s^{-1}|W_n^X(s)|^2) * S(s^{-1}|W_n^Y(s)|^2)}$$

where S is used to remove some of the noise from the data. Wavelet coherence is similar to a correlation coefficient such as Pearson's rank correlation coefficient, but occurs localized in time frequency space, with the magnitude squared coherence ranging from– 0 - 1.

Localized areas of statistical significance in wavelet coherence were found using Monte Carlo methods. The original coefficients, AR1, used to assess statistical significance of the CWT were recreated in a large group of data set pairs. For every pair of faux signals the wavelet coherence is calculated. This large number of wavelet coherences are used to estimate the significance level that the wavelet coherence of the two time series signals will be tested against. The 5% significant level is displayed on the scalogram of wavelet coherence as solid black lines (Grinsted et al., 2004).

5.2.7 Interpreting Scalograms of CWT and Wavelet Coherence

Continuous wavelet transform analysis takes an input signal and breaks it down to reveal frequencies that are within the input signal and where these lie in time. Put simply, CWT analysis breaks down the signal into a graph displaying both time, frequency, and the magnitude of the absolute value of the coefficients. CWT coefficients are calculated through the convolution of the input signal with a wavelet (Torrence & Compo, 1998). The absolute value of these coefficients is displayed on a graph referred to as a scalogram which shows both frequencies and time.

The scalogram of a CWT or wavelet coherence between two CWT's can be difficult to interpret, so 2 simple signals of sine waves have been created and analyzed via these methods to help better explain how this analysis works and how to interpret it. In Figure 10.a a signal is displayed with 2 separate frequencies at 3 different occurrences across a time of 100 seconds. The first frequency is at 0.5 hertz and an amplitude of 1 from 10 – 30 seconds, the second frequency is at 1 hertz and an amplitude of 2 from 40 – 60 seconds, and the third frequency is a combination of both the previous frequencies and amplitudes from 70 – 90 seconds.

It is important to remember that period (T) and frequency (f) have an inverse relationship with each other in that period is the amount of time that it takes to complete one full cycle of the wave and that frequency is the number of waves that pass during a given amount of time. For hertz this will be in terms of waves per second. In this study all scalograms will have the y-axis as periods instead of frequencies.

In Figure 10.b the scalogram of the CWT for the absolute value of all the coefficients of the signal in 10.a are displayed. The magnitude of the coefficients is indicated by the color bar on the right, with yellow being a clear and strong presence of a frequency and going darker to blue showing there is no discernable correlations with any frequencies. The areas of higher magnitude are then further tested against the null hypothesis of the CWT that the time series signal is stationary and red noise. Where the coefficients are higher than 5% statistical significance the area is enclosed by a black line. The cone coming to a point downwards is referred to as the cone of influence, and all of the data outside of it cannot be accurately interpreted due to influence from edge artifacts.

Figure 10.b shows 4 areas of statistical significance. From 10 – 30 seconds there is high magnitude around the period of 2 seconds, which would be a frequency of 0.5 Hz, at 40 – 60 seconds there is strong magnitude values at a period of 1 second (1 Hz), and from 70 – 90 seconds there are 2 areas of high magnitude at a period value of 1 and 2 seconds (1 and 0.5 HZ respectively). In both of the frequencies seen at a period of 1 second the magnitude is seen as brighter, and this is due to this frequency having a higher magnitude than the other frequency. The amplitudes of all the frequencies within a scalogram are normalized to each other. This uncovers the frequencies within the signal as well as where these frequencies are occurring within the times series.

It is clear in this example how the projection of the signal in Figure 10 is portrayed in the time – frequency plane of the scalogram, but it is not always so simple. Within this signal the first two frequencies are very clear and distinguishable, and the third is a little trickier with the two frequencies combined. In the real world a signal may have many different frequencies combined with varying levels of noise that make it very hard to distinguish between frequencies. This is when wavelet analysis can become rather very helpful, uncovering frequencies that are hidden within a signal across a range of frequencies and across the time series where it is present.

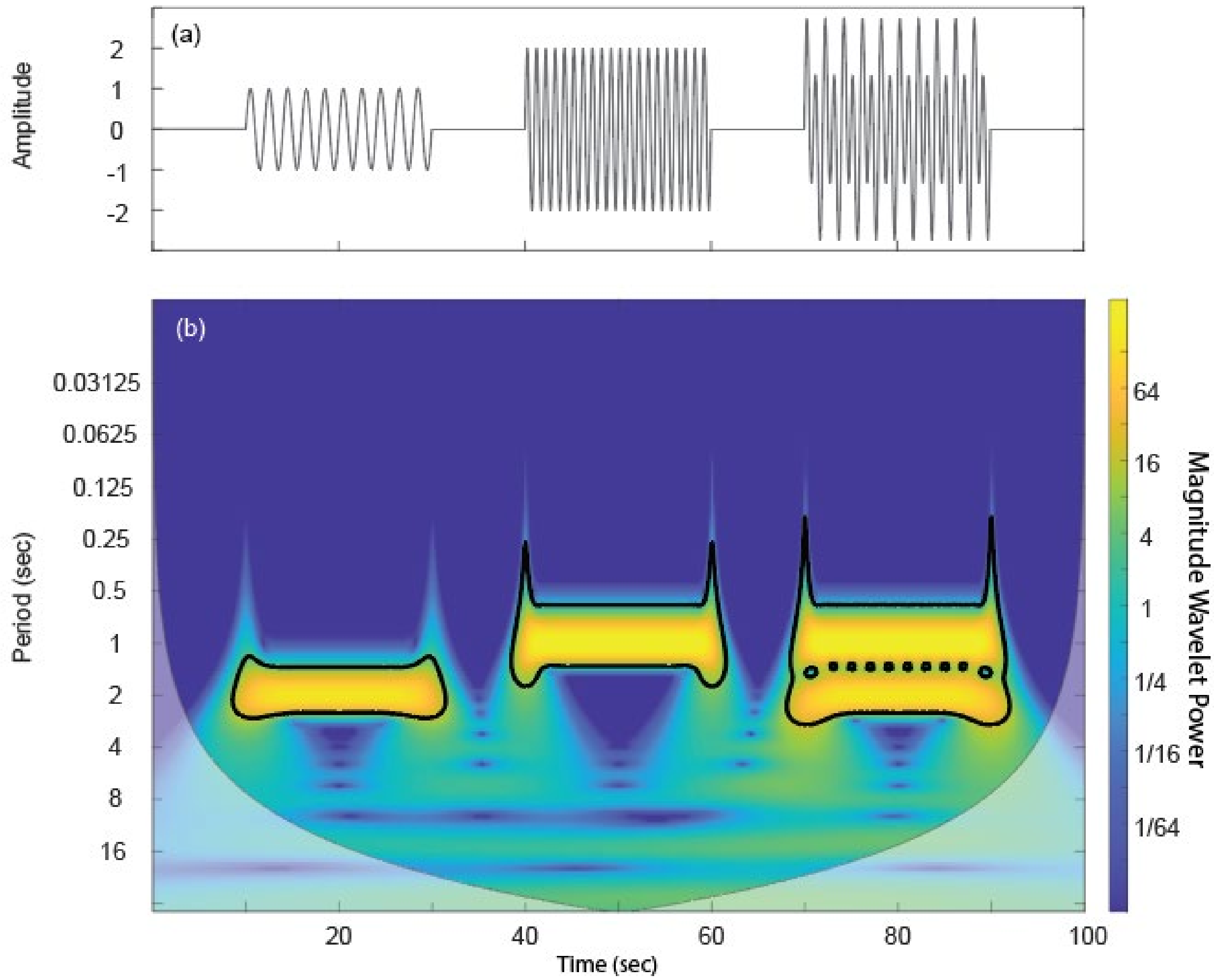

Figure 10. (a) Signal of 2 waves occurring at various times over a 100 second period. (b) Scalogram of the CWT coefficients for the signal in part (a). Black lines and any area encircled by them indicate a significance level of 5% or greater. The period of the wave is the y-axis, and the magnitude of the coefficients is displayed in the colorbar on the right. Brighter colors indicate a higher magnitude.

In Figure 11.a there is a signal across a 100 second window with 2 frequencies at separate times. The first is from 10 – 30 seconds at a frequency of 0.5 Hz and an amplitude of 1 and the second is from 40 – 60 seconds with a frequency of 1 Hz and an amplitude of 2. The first frequency seen starts at a phase 90°, or $\pi/2$, ahead of that seen in the frequency in the first signal. Throughout the whole time series signal there is also background noise. Of note, these are the exact same frequencies seen in Figure 10.a with the exception of the last two frequencies in the first time series signal. In the scalogram of the time series there can be seen a larger spread of different magnitudes due to the background noise, but still the two frequencies present in the signal are visible and statistically significant at periods of 2 and 1 seconds, matching the known frequencies in the signal.

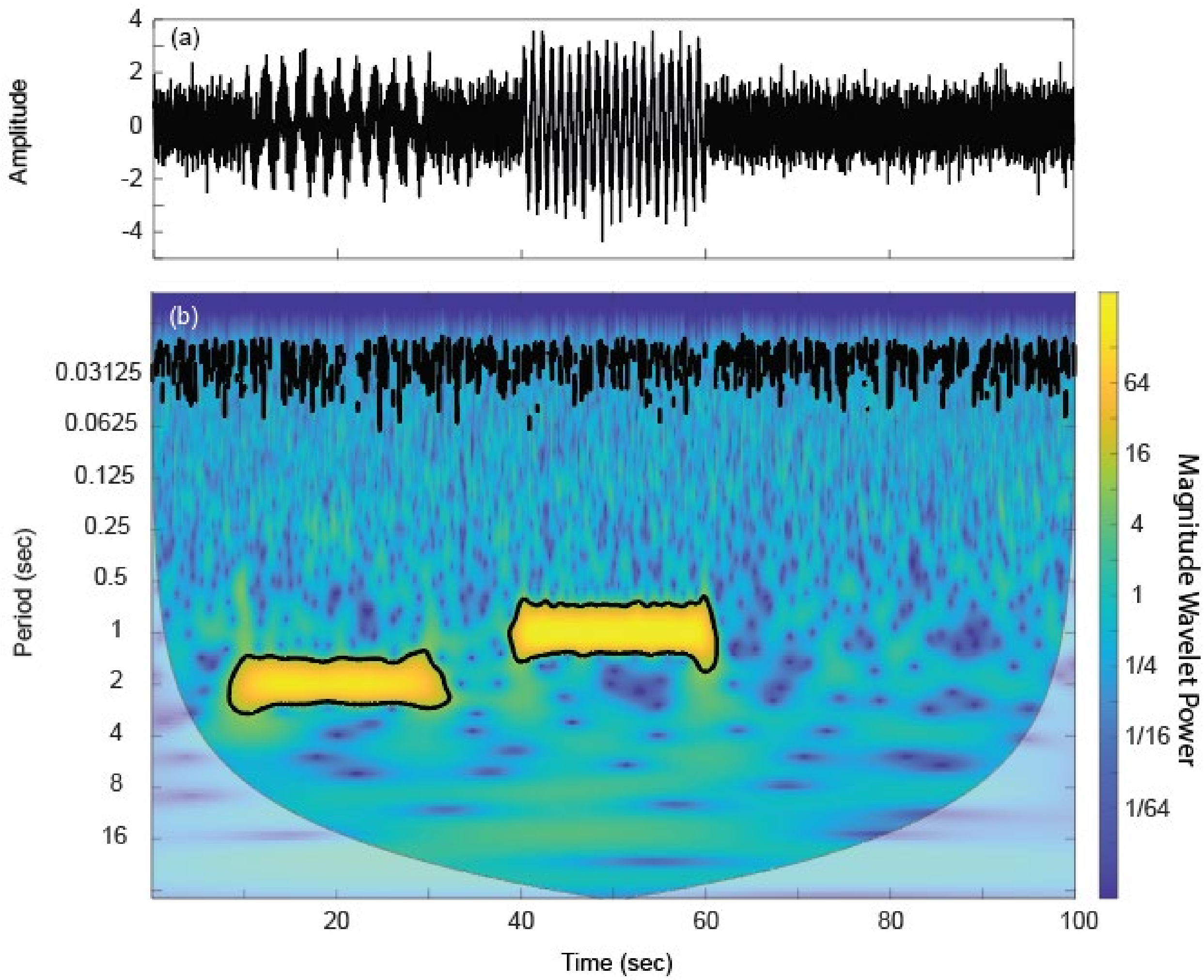

Figure 11. (a) signals of two waves occurring at two singular 20 second periods with a constant white noise background. (b) Scalogram of the CWT coefficients for the signal in part (a). Black lines and any area encircled by them indicate a significance level of 5% or greater.

The CWT identifies the frequencies present in a signal and where in time they are allowing for comparisons to be drawn between CWT's. Wavelet coherency identifies and quantifies the correlation of frequencies between two CWTs of time series to see if there are periods of correlation between the time series. The scalogram of wavelet coherence displays the correlation coefficient from 0 – 1 between the two time series and indicates any areas of statistical significance. In the areas that are above 0.6 correlation a phase arrow is calculated that indicates the relative lag of the x signal to the y signal.

Figure 12 shows the scalogram of the wavelet coherence between the CWTs of the signals in Figures 10 and 11. There are two large areas of high coherency seen in the figure; one from 10 – 30 centered around a period of 2 seconds and another from 40 – 60 seconds centered around a period of 1 second. This matches the known two frequencies that were displayed within the two CWT's. The first area of high coherence has phase arrows pointing up showing the second time series is leading the first by a quarter phase and the second area of high coherence has arrows pointing to the right showing there is little to no lag between the two, they are in phase. The first frequency sees the Y leading the X by a quarter phase because $\pi/2$ was added into the frequency making the signal a quarter of a phase ahead of signal one. There are a few other small but statistically significant areas seen around 70 – 80 seconds that are spurious correlations between the frequency in the first signal and the background noise of the second signal.

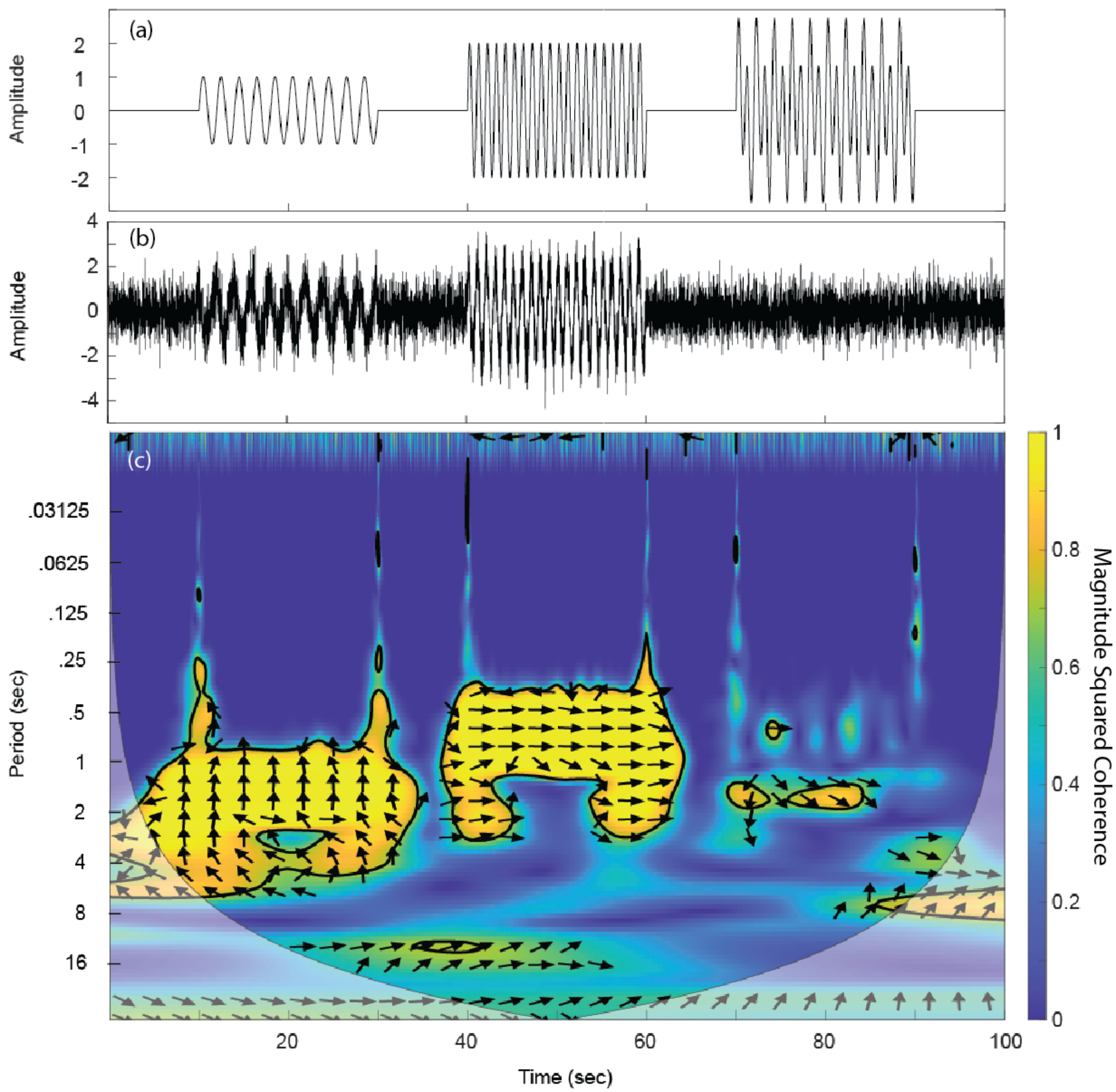

Figure 12. (a) Signal created in MATLAB used to create CWT in Figure 10. (b) Signal created in MATLAB used to create CWT in Figure 11. (c) Wavelet coherence of the two signals from (a) and (b). Color bar on the right indicates magnitude of the coherence from 0 – 1. Solid black lines and enclosed areas show statistically significant locations of coherence between the 2 signals. Arrows indicate phase lag between the two signals.

The phase arrows within the statistically significant areas give insights into the lead and lag relationship between the two signals. When a phase arrow is pointing right it means that the signals are in phase, left means they are in anti-phase, down would be X leading Y by quarter phase, and up would be Y leading X by quarter phase. This relationship can be seen in Figure 13 through the display of one full revolution of a sin wave. The radians represent a location on a circle from 0° - 360°,–0 - 2π, and show that if a signal were to lead by this amount of a frequency what phase arrow would be displayed on a scalogram of wavelet coherency. For example, if there were two time series with a signal present in both of them at a frequency of one-year and one lagged by a quarter phase, $\pi/2$ or 90°, then the effects from the leading time series would be observed in the second time series 3 months later.

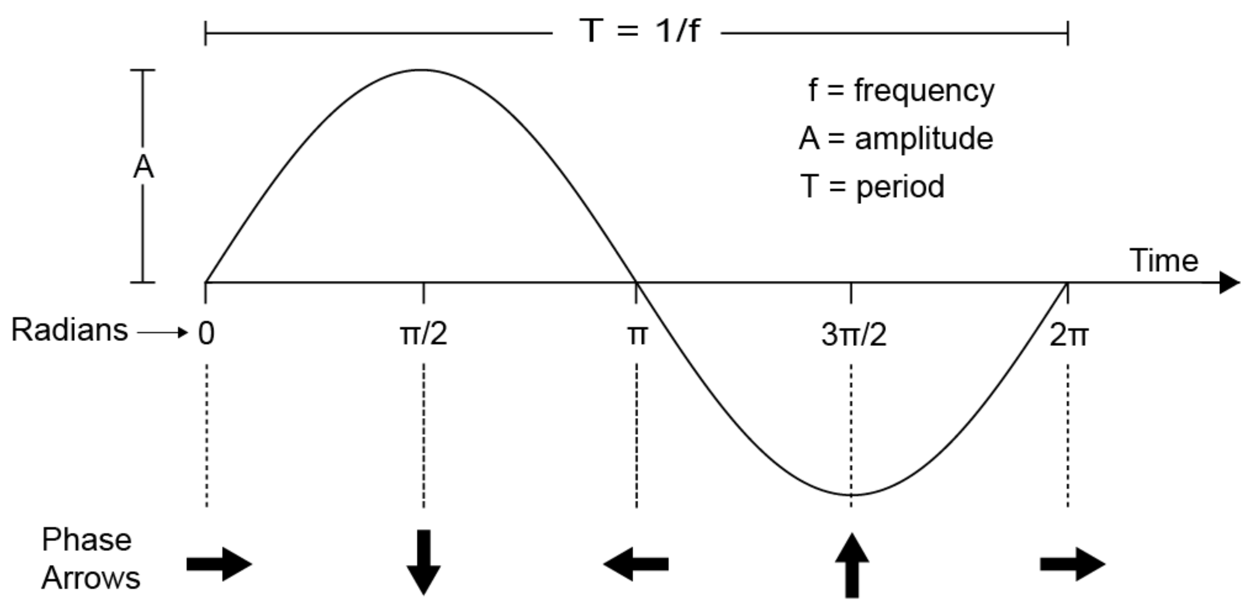

Figure 13. A complete revolution of a sin wave and all of the radian revolutions. Relationship between frequency, period, and amplitude of the wave are displayed as well. Phase arrows and their radial components are displayed. Phase arrow direction pointed indicates: Right = in phase, Down = X leading Y by $\pi/2$, Left = anti-phase, Up = Y leading X by $\pi/2$.

5.3 Rates of Drivers to Water Level

The first set of data spans a large amount of time and goes through 2 periods: one with an abundance of storm events and another with no storm events or recharge. Both periods are multiple months long. These periods helped to isolate different variables that influence the water level of the pond and identify the relationship between them. Specifically, the period of drought allows for the influence of the water level of the ocean (tides) to be seen on the pond and the periods when there is an abundance of storms allows for the combined effects of sea level and precipitation to be observed on the pond's water level.

For every storm event identified there were multiple independent variables that were quantified and graphed compared to the water level of the pond to identify potential relationships. Storms were categorized into two main categories: large and moderate. Large storms were defined as having more than 40 millimeters of overall precipitation and having precipitation rate exceeding 30 mm/hr at one point. Moderate storms were defined as having a precipitation rate at some point during the storm between 10-30 mm/hr and no limit to precipitation amount. Storms with a precipitation rate less than 10 mm/hr were not categorized due to their small effect on the surficial aquifer. The variables considered were the precipitation amount, rate of precipitation, mean sea level, and maximum tide, all measured during the storm events. These variables were also plotted against the water level of the pond during this time to denote any relationships between them.

5.4 Spatial Analysis

The second set of data from the four ponds around Sapelo Island brings insight into the spatial view of the water level across the island. All aspects of the location's proximity to the ocean and elevation will be considered when analyzing the time series of water level data. A 1m Digital Elevation Model (DEM) from the National Elevation Dataset (NED) created by the United States Geological Survey (USGS) was imported into ArcGIS to determine the exact height of the ponds and relative distance to saline water (U.S. Geological Survey, 2012). Wavelet analyses will be used to understand the relationship between the driving variables and the water levels of each pond. The wavelet coherences of pond level to variable will be compared for all four ponds to note and determine similarities or differences. Inferences can then be drawn by comparing this data to the elevation heights and proximity of the ponds to the marsh to see if there are any discernable trends.

CHAPTER 6

RESULTS

This chapter presents the data and the results from all the analyses detailed in the previous chapter. The first three parts will be dedicated to the analyses of the data available for the gravel pond during the first monitoring time period (9/2016 – 10/2016) along with storms analyzed from the 2022 data, and the last part will be the analyses of the data available for the four ponds during the second monitoring time period (1/2022 – 8/2022). The complete dataset used for these analyses is displayed in Figures 14 and 15 for the first and second dataset respectively.

The results will be presented in three sub-sections focusing on precipitation (sub-section 6.1), evapotranspiration (sub-section 6.2), and tides and storm surges (sub-section 6.3).

A last sub-section (6.4) will focus on the analysis of the data available for the four ponds during the second monitoring period (Jan 2022 – Sept 2022). The complete dataset is displayed in Figure 15. The water level of each respective pond was analyzed in relation to the precipitation data, temperature data, and tides/storm surges. Subsequently these were compared to each other and their relative location for the spatial analysis of data.

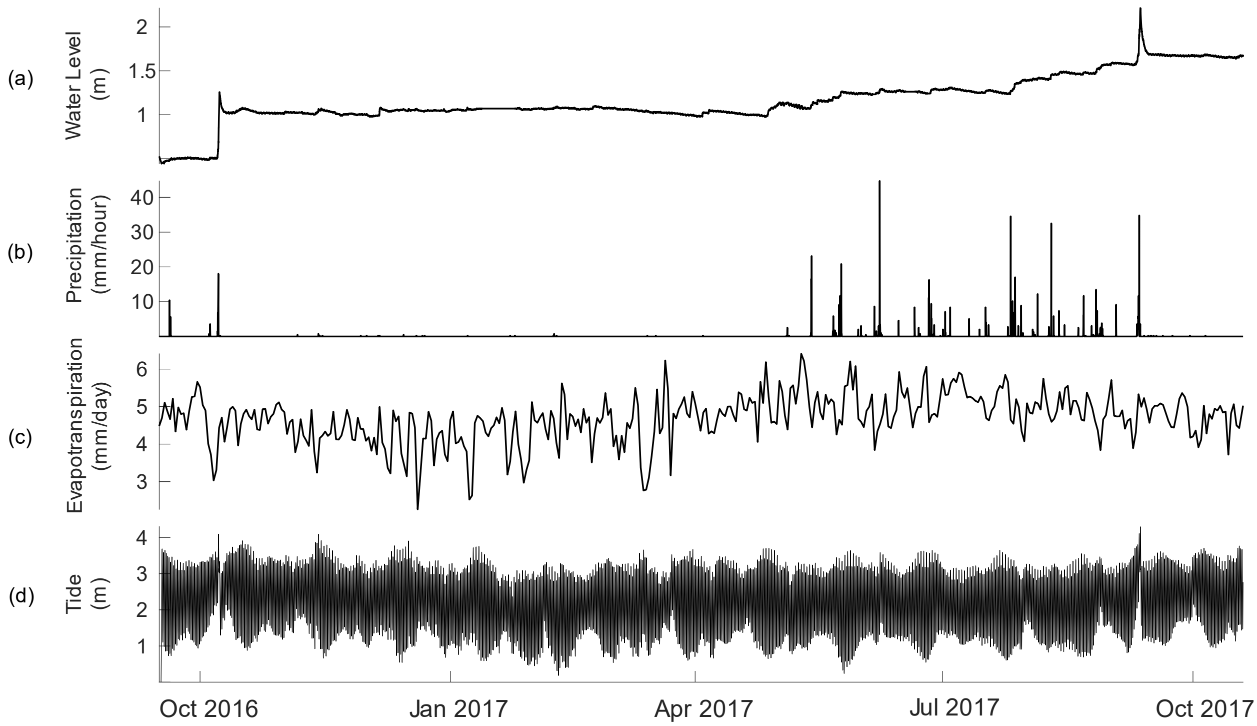

Figure 14. Data collected and used for analysis of first monitoring period. (a) Water level data of Gravel Pond during the time from September 2016 – October 2017. (b) Precipitation rates for Sapelo Island in mm/hour. (c) Daily evapotranspiration rates calculated with data from the GCE flux tower using the Penman Monteith equation. (d) Tide heights from nearby buoys to Sapelo Island.

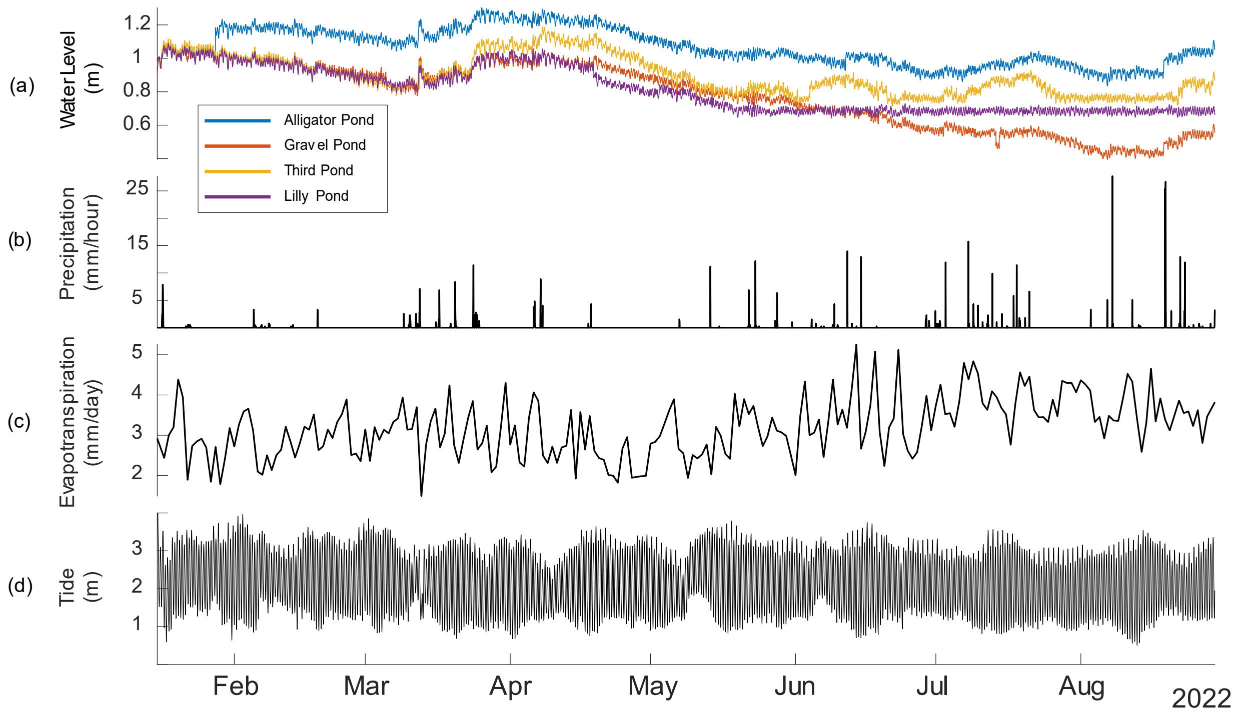

Figure 15. Data collected and used for analysis of second monitoring period. (a) Water level of all four ponds across the 2022 dataset. Of note, the Lily Pond pressure sensor was exposed above water level when retrieved in August, so the relatively flat data from mid-May on is not representative of the water level. (b) Precipitation in mm/hr on Sapelo Island during the collected period. (c) Daily evapotranspiration rates calculated with data from the GCE flux tower using the Penman Monteith equation. (d) Tide data for Sapelo Island during the collected period.

6.1 Hydrological Response of Gravel Pond Water Level to Precipitation and Storm events

A scalogram of the CWT of the water level of the Gravel Pond for the first dataset is displayed in Figure 16. The areas of high magnitude are displayed as bright spots within the scalogram. These line up well with the sharp changes in water level seen in section (a) of the figure, showing the magnitude of these events in time frequency space in section (b). In the scalogram there can be seen two main spots of high wavelet power that are circled by the 5% significance level in October of 2016 and September of 2017. Both of these events are present for about half a month. There is also a notable band of power across the time series around the 25 hour period, but it is not statistically significant.

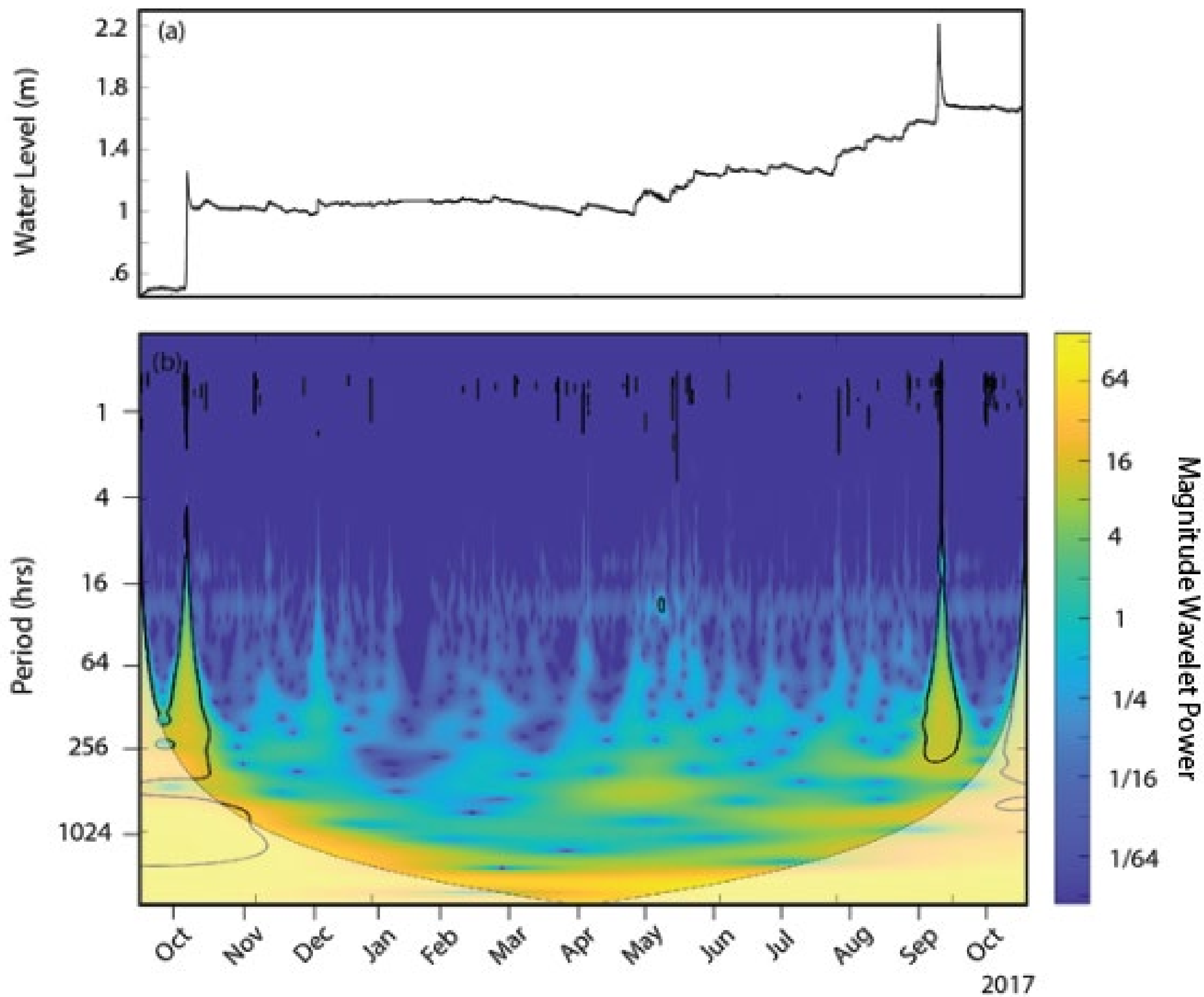

Figure 16. (a) Time series of the 2016-2017 water level (m) of Gravel Pond. (b) Scalogram of the Continuous Wavelet Transform of the water level time series of the Gravel Pond. The periodicity of the signal is indicated on the y-axis and is base 10 logarithmic. Magnitude of wavelet power is indicated by the color scale on the right-hand side.

6.1.1 Hydrological response to precipitation

Part of the first objective of this study is to see the effect that storms have on the surficial aquifer relative to the amount of precipitation from the storm. It is expected that smaller storms will have less of an effect on the recharge than larger storms will, and the relationship will be linear in regard to the precipitation amount and water level rise of the Gravel Pond.

Over the course of the first dataset collected there were two distinct periods of frequent precipitation and one period of draught. The periods of precipitation were from September to October of 2016 and from May to October of 2017. Water levels and precipitation are displayed on Figure 17 for the entire period of time (A), the first dataset, and then for the two rainy periods in 2016 (B) and 2017 (C), with moderate and large storms highlighted for each period.

Four main variables were identified during the time surrounding the storms and used for the identification of potential trends. These variables are the precipitation amount, precipitation rate, mean sea level, and maximum tide during the storm event. The data for both campaigns (in both 2016/2017 and 2022) are summarized in Table 2, where it is sorted by storm size and year of data, and then displayed in order of increasing precipitation. In this sub-section we will only focus on the variables related to precipitation.

The variables of pond level rate and amount were plotted against the precipitation amount, precipitation rate, mean sea level, and maximum tide to see if there were any noticeable trends among the data. All the data were viewed linearly and logarithmically. As expected, the scatterplot of pond level rise against the precipitation amount and pond level rate has a positive linear trend, with pond level increasing with the amount of rainfall. This can be seen in Figure 18 where the linear relationship between the pond level rise and precipitation amount of the data from 2016-2017 has an R^2 value of 0.58. In Figure 18 part (a) has all of the data and part (b) shows the data with the outliers removed to best see the trend. There is a positive trend seen in the 2022 data set for the same variables, with a weaker R^2 of 0.39 showing less strength.

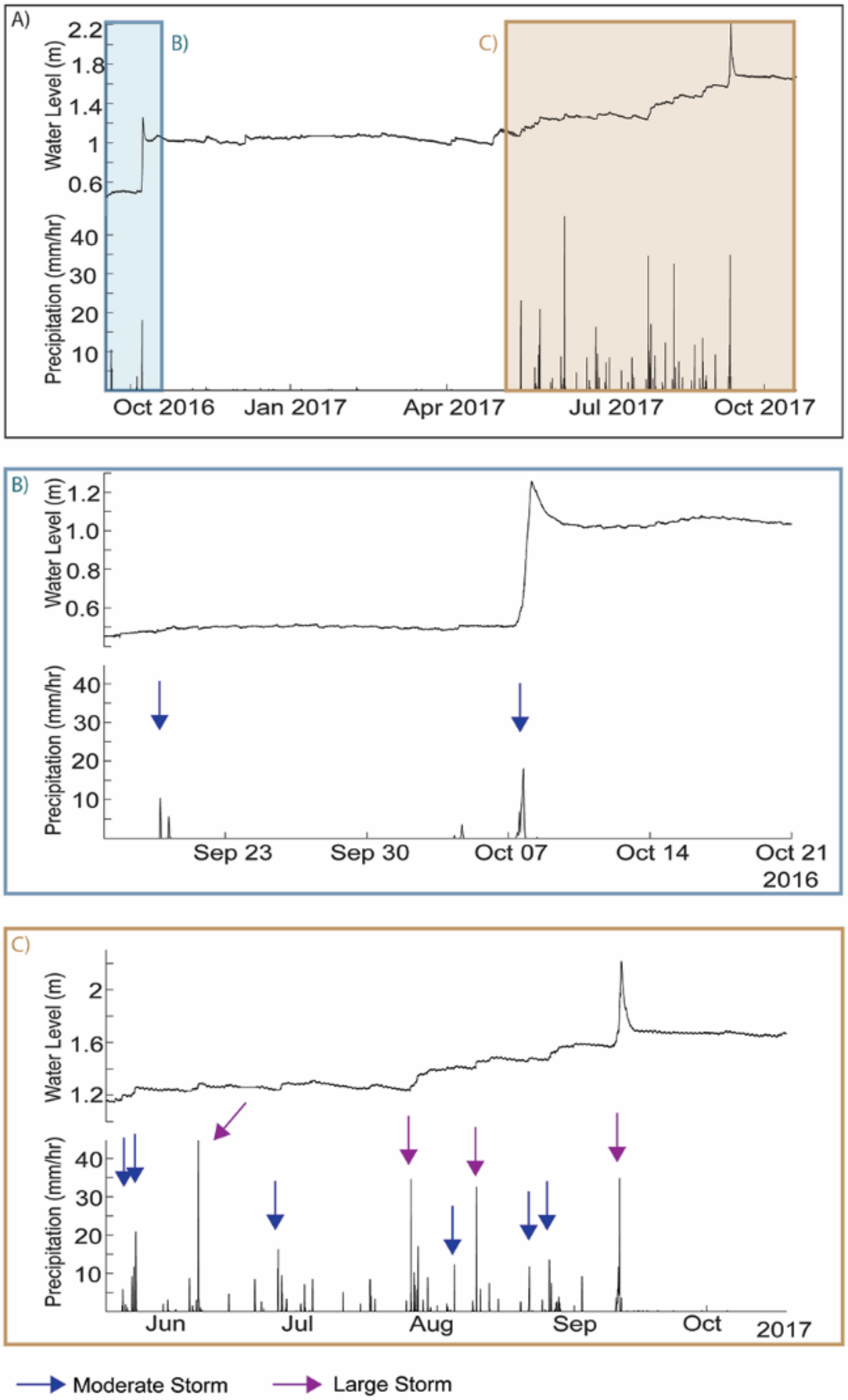

Figure 17. Temporal evolution of water levels (m) and precipitation rates (mm/hr) for gravel pond for A) the total recording period from Sept. 2016 to Oct. 2017 and zoomed for B) the first period of precipitation with 2 moderate storm events (from September to October 2016) and C) the second period of precipitation events, which contains 6 moderate and 4 large storms.

Table 2 – All storm events during both water level data acquisition periods and accompanying variables. Mean sea level is calculated as the average from 6 hours prior to the storm beginning and 6 hours after of the tide heights. Max tide includes the storm surge, so it is the maximum sea level. Large storms are defined as presenting more than 40 millimeters of total precipitation and of precipitation exceeding 30 mm/hr in some 15-minute period. Moderate storms are defined as presenting a precipitation rate at some point during the storm between 10-30 mm/hr. No large storms were recorded for the 2nd time period.

		Start	Duration	Precipitation		Mean	Max	Pond Level		Ratio
				Amount (P)	Rate	Sea Level	Tide	Rise (h)	Rate	h/P
			(hr)	(mm)	(mm/hr)	(m)	(m)	(mm)	(mm/hr)	(-)
20–6 - 2017	Moderate	9/19/2016	0.5	10.41	20.8	2.62	3.44	26	1.65	2.5
		8/4/2017	1.25	14.99	9.99	1.96	3.08	25	65	1.67
		8/21/2017	4.5	25.9	5.76	2.68	3.52	22	5.5	0.85
		8/26/2017	11.5	28.19	2.45	1.92	3.29	56	4	1.99
		6/25/2017	3.75	34.04	9.08	2.75	3.57	57	3.9	1.67
		5/13/2017	6.25	53.09	8.49	1.72	2.97	83	1.3	1.56
		5/23/2017	21.25	64.52	3.04	2.71	3.42	73	2.3	1.13
		10/7/2016	8.5	64.77	7.62	2.79	4.09	751	40	11.59
	Large	8/9/2017	1.5	42.42	24.24	2.17	3.22	42	28	0.99
		6/7/2017	5.5	81.53	14.82	1.86	3.52	50	1.78	0.61
		7/25/2017	40.5	113.79	2.81	2.61	3.36	90	2.2	0.79
		9/10/2017	21.5	122.94	5.46	2.75	4.33	641	16.5	5.21
2022	Moderate	5/14/2022	0.75	11.43	15.24	2.53	3.62	-6	-0.56	-0.52
		7/18/2022	0.75	11.68	15.5	2.1	3.12	-16	-0.66	-1.37
		7/3/2022	1.25	12.19	9.75	2.08	3.05	34	1.43	2.79
		5/23/2022	1.75	13.46	7.69	2.14	3.1	16	1.25	1.19
		6/15/2022	1	13.46	13.46	2.22	3.61	26	1.07	1.93
		6/12/2022	0.5	13.97	27.94	2.1	3.1	-5	-0.2	-0.36
		7/8/2022	5	20.57	4.11	1.74	2.82	-4	-0.17	-0.19
		8/8/2022	3.5	29.21	8.34	2.24	3.16	15	0.45	0.51
		8/22/2022	24.75	29.47	1.19	1.96	2.93	36	1.5	1.22
		3/24/2022	31.25	38.61	1.23	2.12	3.21	102	1.42	2.64
		8/19/2022	4.75	65.02	13.69	2.09	2.9	52	2.17	0.8

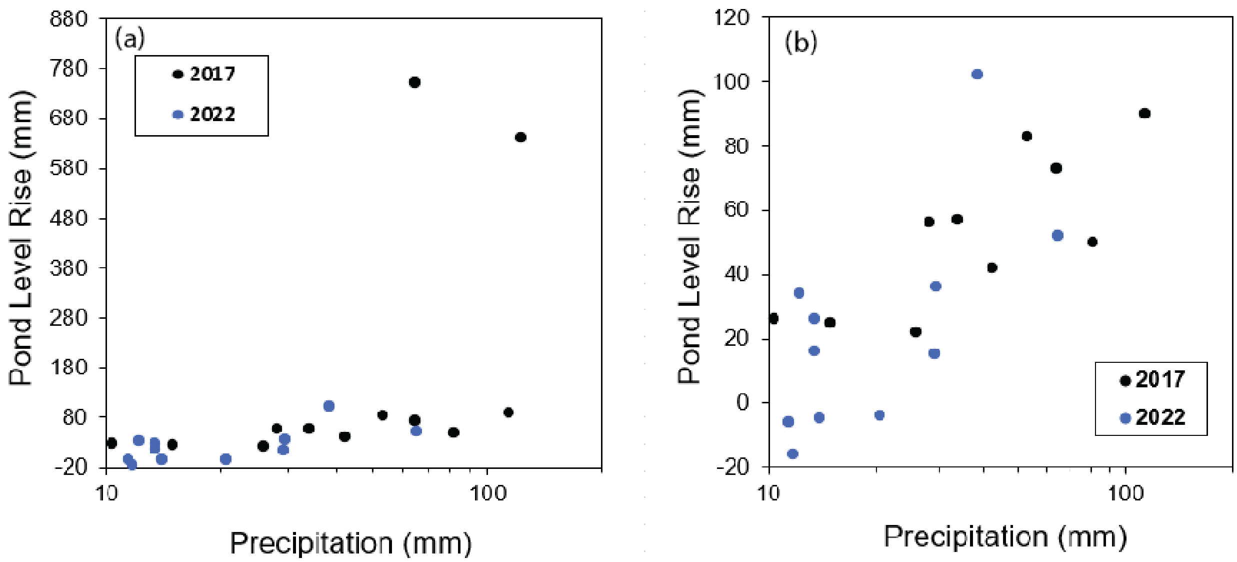

Figure 18. (a) Graph representing pond level rise as a function of precipitation for Gravel Pond during both the 2016-2017 and 2022 datasets. The y-axis is logarithmic with a base of 10, starting at 10. (b) Same data as graph (a), but with the 2 outliers removed. The linear regression of the 2017 data has an equation of $y = .58x + 25.4$ with an $R^2 = .58$. The linear regression of the 2022 data has an equation of $y = 1.28x – 7.4$ with an $R^2 = .39$.

The strong relationship between the amount of precipitation and the rise in pond level can be further viewed through the CWT of the precipitation data. The CWT highlights areas of a time series that have abrupt changes to a background signal and shows these areas of change as high magnitude in time frequency space. For the scalogram of the CWT of precipitation this is where the precipitation events are occurring in time. From mid-October 2016 past April of 2017 there were no discernable precipitation events, and this can be seen in Figure 19 by the stretch of low magnitude during this time. Areas on the scalogram within the periods of precipitation have high magnitude showing the precipitation events in time frequency space. These areas are the bright spots on the figure and the enclosed areas by the black lines have above 5% statistical significance, ranging from less than an hour to around a 1024 hour period depending on the event.

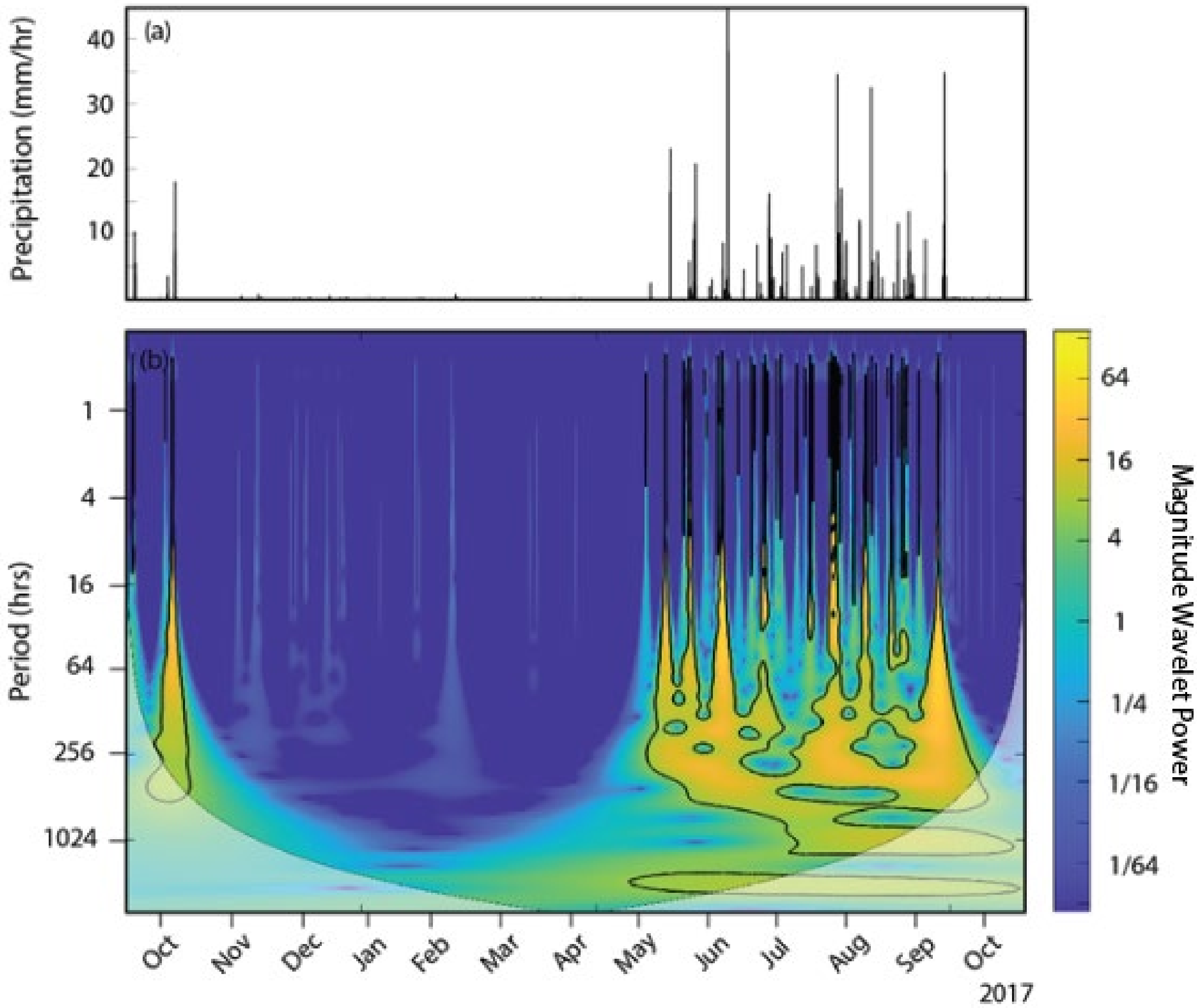

Figure 19. (a) Time series of the 2016-2017 precipitation (mm/hr) of Sapelo Island. (b) Scalogram of the Continuous Wavelet Transform of the precipitation. The periodicity of the signal is indicated on the y-axis and is base 10 logarithmic. Magnitude of wavelet power is indicated by the color scale on the right-hand side.

The CWT of the water level of Gravel Pond and the CWT of the precipitation for the 2016-2017 time period are both used to calculate the wavelet coherence. Similar to a cross correlation with a value from 0 – 1, known as the Magnitude-Squared Coherence, with 1 being a strong correlation and 0 having no coherence. The scalogram of wavelet coherence highlights areas where the two time series are connected, even if it is not as pronounced in their respective CWTs. Figure 20 shows the wavelet coherence of precipitation and water level. Strong bands of wavelet power are seen across the scalogram from 16 – 256 hours (1 – 10 days), with the highest concentration being at the 64 hour period. The connected areas of high coherence are more pronounced during times of precipitation. The phase arrows on the graph are primarily pointed downwards, indicating water level rise lagging precipitation.

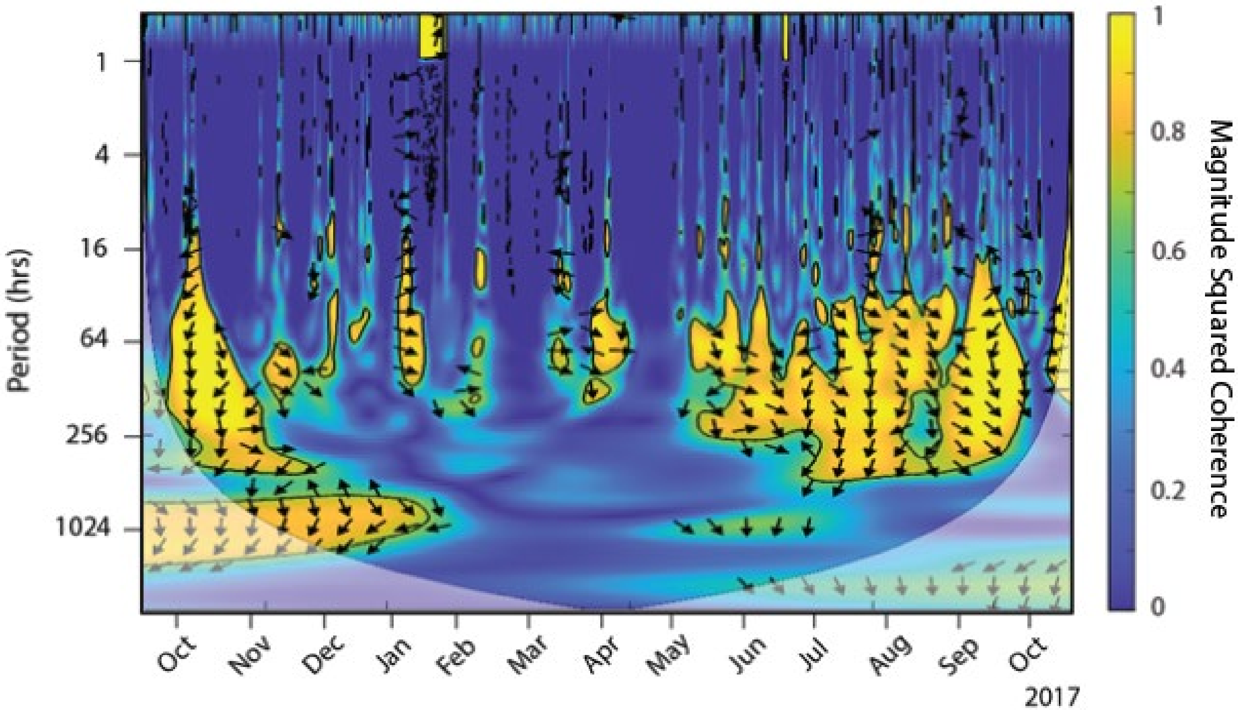

Figure 20. Wavelet coherence between precipitation and water level of Gravel Pond for the 2016-2017 dataset. Magnitude squared coherence is on a scale from 0 to 1. Phase arrows show relative phase lag between the two time series. The phase arrows are shown in areas that have greater than 0.6 magnitude-squared coherence. Magnitude-Squared Coherence is indicated by the color scale on the right-hand side.

6.1.2 Hydrological Response to Storm Events

There were two storms in the first monitoring campaign that stand out as having the largest effects seen on the water level of the gravel pond. They are the moderate storm starting on October 7th of 2016 and the large storm starting on September 10th, 2017. The first is categorized as moderate due to the fact that the precipitation per hour never exceeded 30 mm/hr, but both are hurricane events. The first event is hurricane Matthew and the second is hurricane Irene. The hydrometeorological conditions prior, during, and after the two events were analyzed to evaluate the effects on the water level of the Gravel Pond. The variables considered are the precipitation amount and rate, tide heights, and associated storm surge. The data are displayed in Figure 21 for Hurricane Matthew and Figure 22 for Hurricane Irene.

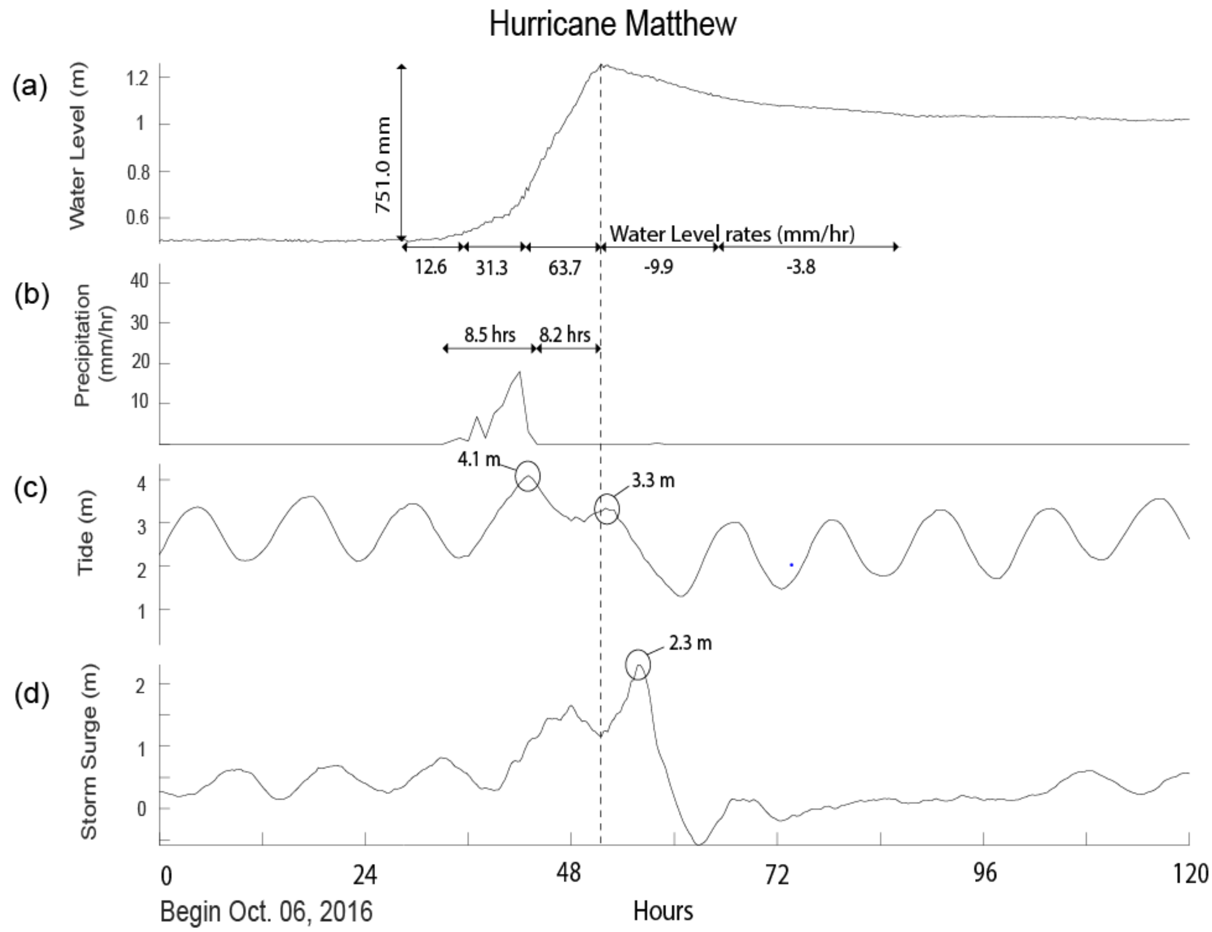

Figure 21. Water level response to hurricane Matthew's precipitation amount, tides, and storm surge. (A) Water level of the Gravel Pond during Hurricane Matthew. Height of pond level increase and rates of water level changes are included in this section. (B) Precipitation rates of Sapelo Island during storm event. Duration of precipitation and from precipitation end to water level peak included. (C) Tidal heights seen during this period. Higher than normal tides circled. (D) Storm Surge extracted from the tidal heights. Peak storm surge circled.

During Hurricane Matthew there was a relatively short period of precipitation occurring for about 8.5 hours with 65 mm at a corresponding rate of about 7.6 mm/hr. Before the storm occurred, the tides were relatively high, above 3 meters, and increased to a high tide of 4.1 meters at the height of precipitation from the storm. This high tide did not recede into a low tide and merely stayed high, at around 3 meters, and peaking at

3.3 meters at close to the same time as the peak water level of the pond. The overall pond level rose 751 mm in total during this event, having a ratio of water level rise to precipitation of 11.6. The pond level rate increased exponentially from 12.6, to 31.3, to 63.7 mm/hr to the peak. Notably the highest rate occurred after the precipitation and during the highest tides and continued for 8.2 hours until reaching the peak of the water level. After the peak the water level rate decreased at a rate of -9.9, and -3.8 mm/hr for a total loss of 230 mm until reaching a plateau that was significantly higher than the water level of the pond before the hurricane. Overall, the pond level gained 521 mm with this event.

Hurricane Irene had a relatively more prolonged period of precipitation of 23 hours dropping 123 mm of rain at a rate of 5.5 mm/hr. There was a small amount of precipitation about 8 hours after the highest precipitation peak, but it was considered insignificant due to its small amount. The tides before the storm began were already incredibly high at 3.8 meters and increased with every high tide reaching a maximum tide of 4.4 meters. Notably the oceanic water level barely dipped below 3 meters between the time of peak precipitation to peak water level (9 hours). The storm surge during this time shows the highest peak 9 hours before the highest peak in water level of the pond. Overall, the water level of the pond increased by a total of 641 mm, having a ratio of water level height change to precipitation of 5.2. The water level of the pond is seen increasing consistently and increasingly from the beginning of the data displayed in Figure 22. It increases at a rate of 2.9 mm/hr before precipitation, and after precipitation goes from 9.1, to 33.8, to -9.5, to 51.4 mm/hr up to the peak of the water level. The negative rate occurs when the tide lowers. After the peak in water level the rates of water level decreased sharply from a high negative rate to more gradual negative rate, with successive rates of

23.9, -12.0, 5.5, -5.8, 1.0, and -2.1 mm/hr. In total a net loss of 524 mm was recorded until the water level reached a plateau. Overall, this event caused an increase of the pond water level of 117 mm.

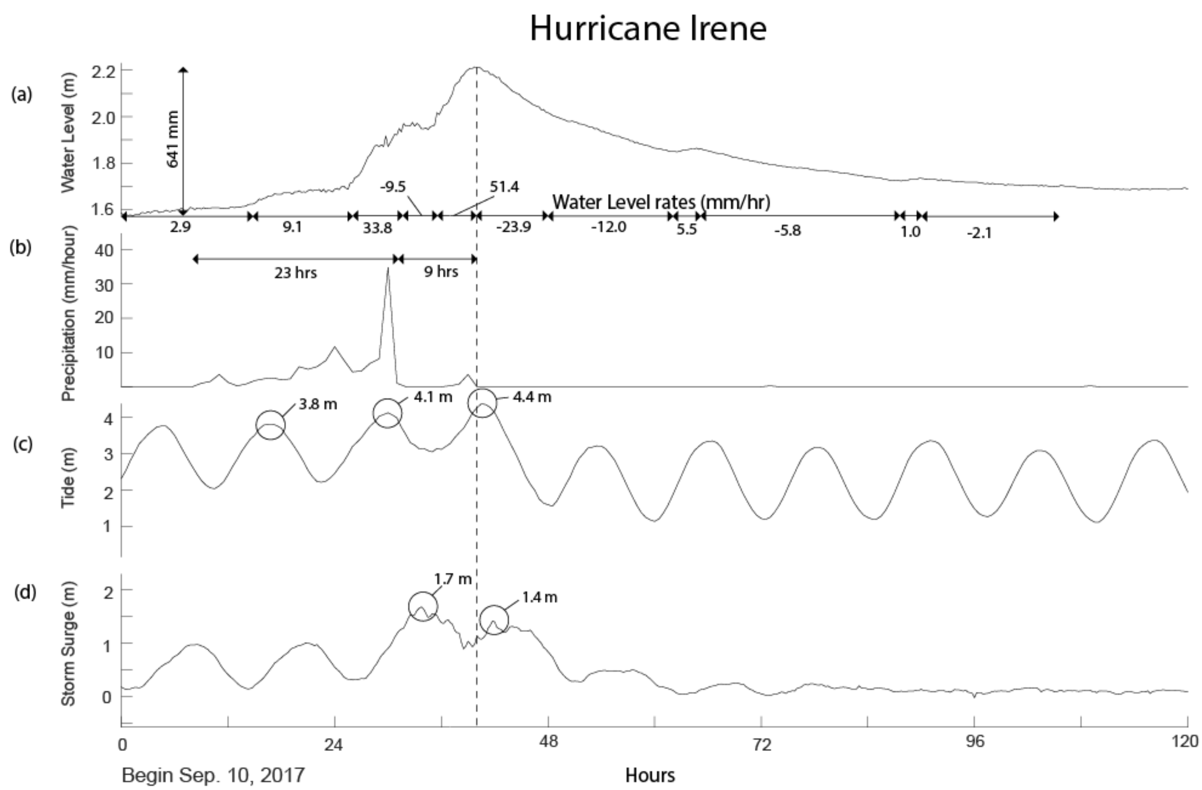

Figure 22. Water level response to hurricane Irene's precipitation amount, tides, and storm surge. (a) Water level of the Gravel Pond during Hurricane Irene. Height of pond level increase and rates of water level changes are included in this section. (b) Precipitation rates of Sapelo Island during storm event. Duration of precipitation and from precipitation end to water level peak included. (c) Tidal data, showing the combined tide and storm surge for the total oceanic water level is seen during this period. Higher than normal tides circled. (d) Storm Surge extracted from the tidal heights. Peak storm surge circled.

6.2 Relationship between Evapotranspiration and Water Level of Gravel Pond

Typically viewed together for their indistinguishability in the field, evaporation and transpiration combined have a clear effect on the water level of Gravel Pond. As seen in Figure 23.A-F, the water level fluctuates daily and decreases at a consistent rate over a 6-day period. This appears on a very small scale as the pond is fluctuating between less than a centimeter per day. During periods of precipitation or storm surges the effects of evapotranspiration will be very hard to distinguish from other factors that have a greater impact on the pond level, but during periods where these factors are not present the relationship between the pond water level and evapotranspiration can be seen clearly.

The evapotranspiration of the Gravel Pond was calculated on a daily scale using the daily values for all variables necessary to equate the Penman-Monteith equation as seen in section 5.1.2. Evapotranspiration was calculated on a daily scale because the change in water level from evapotranspiration on a 15-minute scale would be too minuscule for the HOBOware sensor to accurately record. The correlation coefficient between the calculated evapotranspiration and the daily difference for the water level of Gravel Pond was calculated to be .14 with no lag using MATLAB. This is a very low correlation and is most likely due to other variables affecting the water level. Table 3 displays the actual water level change weekly, daily, and calculated daily via Penman-Monteith for 6 weeks during the first monitoring campaign where there were no storm events present. These same 6 weeks are also presented in Figure 23.A-F for a visual representation of the rates.

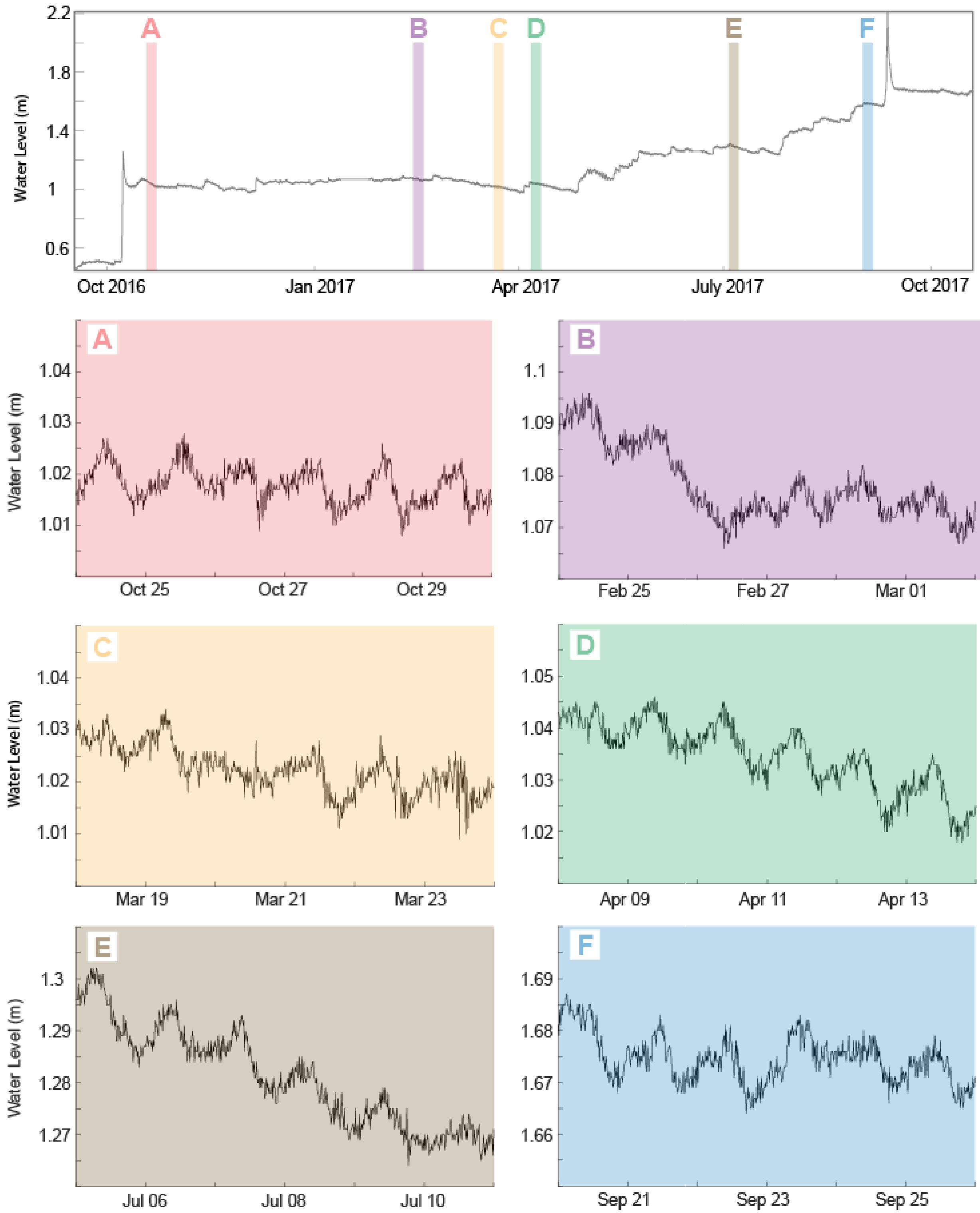

Figure 23. Water level of the Gravel Pond across the first monitoring period, 2016-2017 with highlighted sections corresponding to subgraphs showing the rate of decrease in the pond level. All subgraphs are normalized to a 6-day period and a .05 m y-axis.

Table 3. Weekly and daily water level changes, and calculated evapotranspiration for Gravel Pond across different weeks for the first monitoring period in 2016 and 2017.

Date	Water Level Δ (mm/week)	Water Level Δ (mm/day)	Evapotranspiration (mm/day)
October –4 - 30, 2016	-20.0	-2.8	4.3
February –4 - March 2, 2017	-27.0	-3.8	4.2
March –8 - 24, 2017	-27.0	-3.8	4.4
April–8 - 14, 2017	-33.0	-4.7	4.2
July 5-11, 2017	-34.0	-4.8	5.0
September –0 - 26, 2017	-28.0	-4.0	4.1

6.3 Relationship between Tides, Storm Surges, and Water Level of Gravel Pond

The entirety of tidal and storm surge data for the 2016-2017 dataset is displayed in Figure 24 for the first campaign of data collected for the Gravel Pond. Note that the dataset is across more than a year long period so there were many tidal cycles of varying sizes observed and two distinctly large storm surges were observed as well.

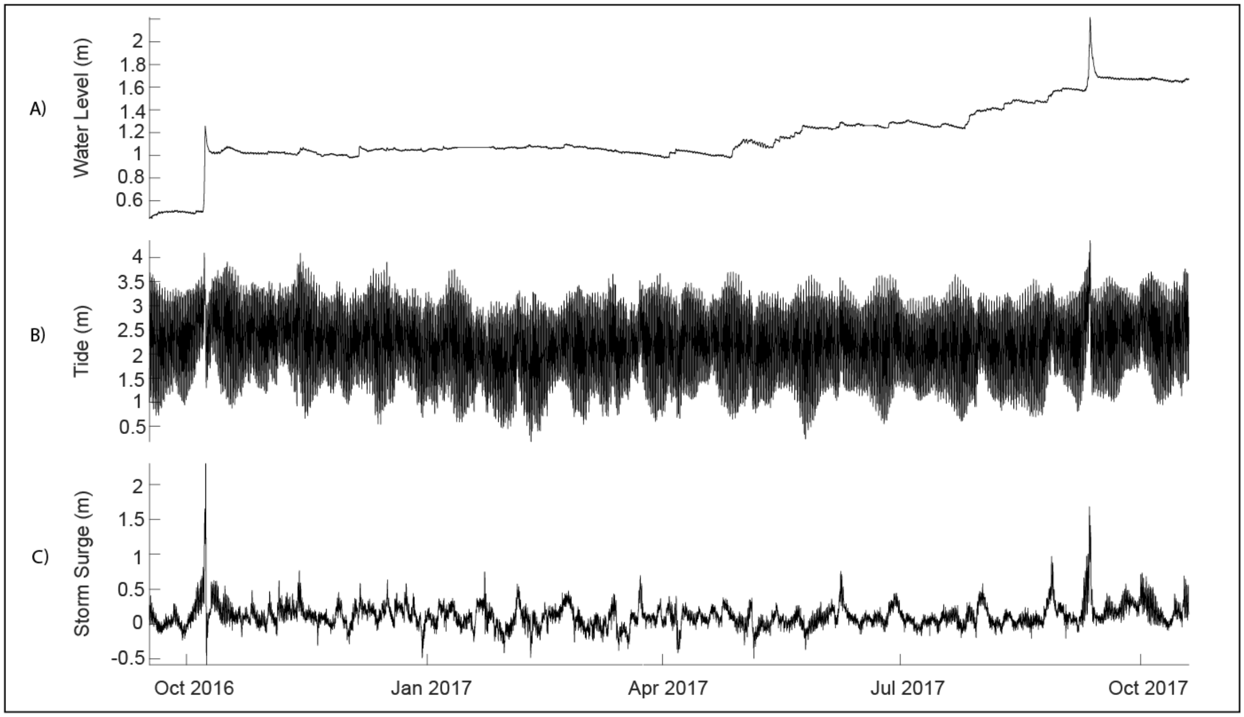

Figure 24. A) Water Level of the Gravel Pond from September 2016 to October 2017. B) Tide heights of the GCE 6. C) Storm surge observed on Sapelo Island.

More detailed data are provided in Table 4 for specific storm events. These additional variables along with the maximum tide were graphed against the pond level amount and rate to assess the presence of potential trends among variables. We note that two largest peaks of storm surge, and subsequent tide, occur during the two hurricane periods in the dataset. The first of which is storm 2, occurring on October 10th, 2016, which is when the effects from Hurricane Mathew were seen on Sapelo Island. The second hurricane was Hurricane Irene, storm 12, which occurred on September 10th, 2017.

Table 4. All storm events across the first observed period of the pond level of Gravel Pond with variables related to storm surges. Organized in ascending order by the maximum storm surge seen during each event.

	Storm	Start Date	Duration (hours)	Max Storm Surge During (m)	Average Storm Surge During (m)	Avg. Storm Surge 6 hrs before (m)	Avg. Storm Surge 6 hrs after (m)	Pond Level Rise (mm)	Pond Level Rate (mm/hr)
Moderate	1	9/19/2016	0.50	0.07	0.06	-0.04	-0.05	26.00	1.65
	8	8/4/2017	1.25	0.09	0.06	0.06	-0.02	25.00	65.00
	10	8/21/2017	4.50	0.13	0.04	0.07	0.45	22.00	5.50
	4	5/23/2017	21.25	0.13	0.01	0.11	-0.04	73.00	2.30
	6	6/25/2017	3.75	0.16	0.08	-0.01	0.06	57.00	3.90
	3	5/13/2017	6.25	0.20	0.11	0.09	0.13	83.00	1.30
	11	8/26/2017	11.50	0.46	0.32	0.28	0.45	56.00	4.00
	2	10/7/2016	8.50	1.07	0.54	0.64	1.39	751.00	40.00
Large	9	8/9/2017	1.50	0.09	0.07	0.03	0.10	42.00	28.00
	7	7/25/2017	40.50	0.31	0.12	-0.07	0.09	90.00	2.20
	5	6/7/2017	5.50	0.47	0.39	0.34	0.64	50.00	1.78
	12	9/10/2017	21.50	1.18	0.60	0.77	1.47	641.00	16.50

When graphed logarithmically on a base 10 scale, there is a visible trend in the graph of pond level rise and maximum tide during the storm events as displayed in Figure 25. The regression that explains the relationship most accurately is a power regression, where the pond level is proportional to the maximum tide raised to a power. The equation between the two variables is $y = 0.0037x^{7.96}$ with y being the pond level rise and x being the maximum tide, with a R^2 of 0.82, which shows a strong relationship between the maximum tide and pond level rise.

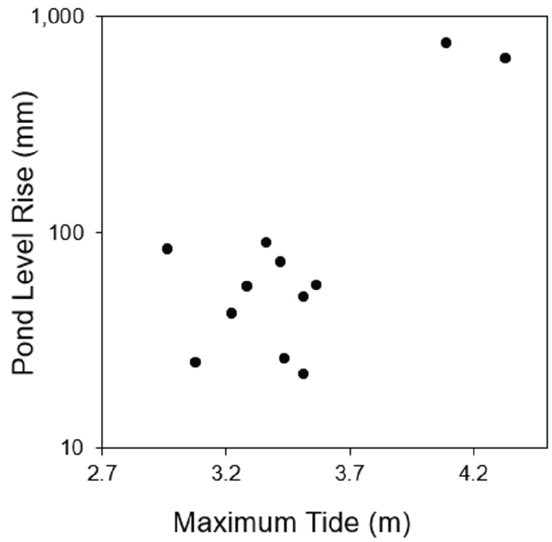

Figure 25. Graph representing pond level rise logarithmically on a base 10 scale as a function of maximum tide for storm events for Gravel Pond during the 2016-2017 data. The regression that best fits the data is the power regression, which has a formula of $0.0037x^{7.96}$ with an R^2 value of 0.8271.

Figure 25 shows that there is a clear relationship between the maximum tide and pond level rise during storm events. While precipitation events occur frequently along the coast there are still periods of drought in between rain events. During these periods, effects from perigean tides, possibly a large storm surge without precipitation, as well as normal tides can potentially be reflected in the water level of the ponds. Focusing on these events enables us to assess the relationship between tides and storm surges and the water level of the surficial aquifer in Sapelo Island. More precisely, the analysis was done using the CWT on both the tidal and storm surge data. Periods of high magnitude that represent a signal within the time-frequency plane of each respective time series, tide and storm surge, can then be identified.

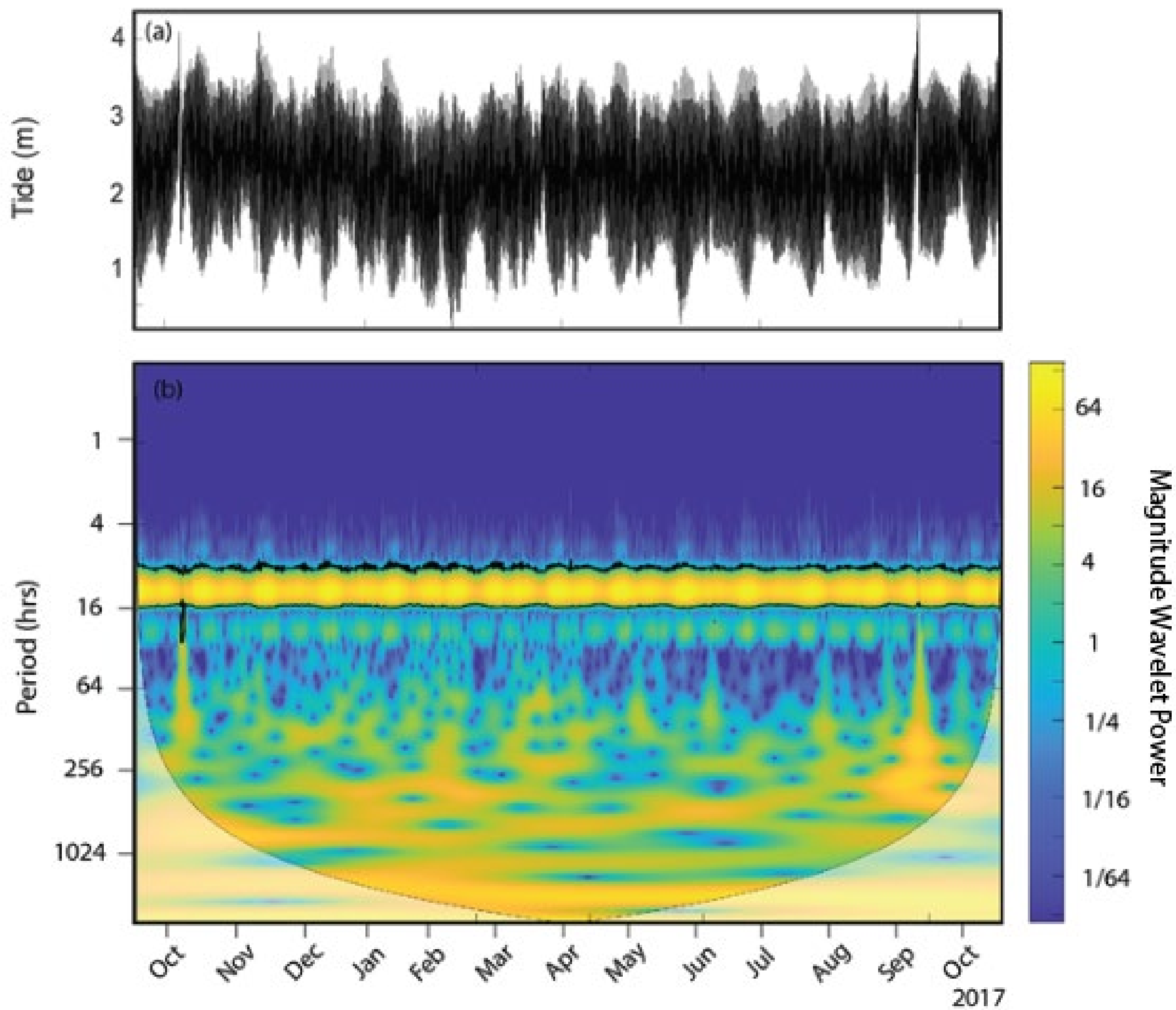

Figure 26. (a) Time series of the 2016-2017 tides of Sapelo Island. (b) Scalogram of the Continuous Wavelet Transform of the tides. The periodicity of the signal is indicated on the y-axis and is base 10 logarithmic. Magnitude of wavelet power is indicated by the color scale on the right-hand side.

Figure 26 shows the time series of the tide in (a) and the scalogram of the CWT of the tide (b). The scalogram exhibits a strong band of magnitude along the period of around 12 hours that is enclosed by the 5% significance level. This matches up with the frequency of high tides, occurring at about every 12 hours, 25 minutes during the day. The strength of the magnitude varies, with higher magnitudes matching up with the large perigean tides that occur every 29.3 days. There is also a noticeable band of slightly higher magnitude, albeit very light, at the period of 24 hrs 50 min which is presumably the highest tide seen every day. This band of frequency is not statistically significant.

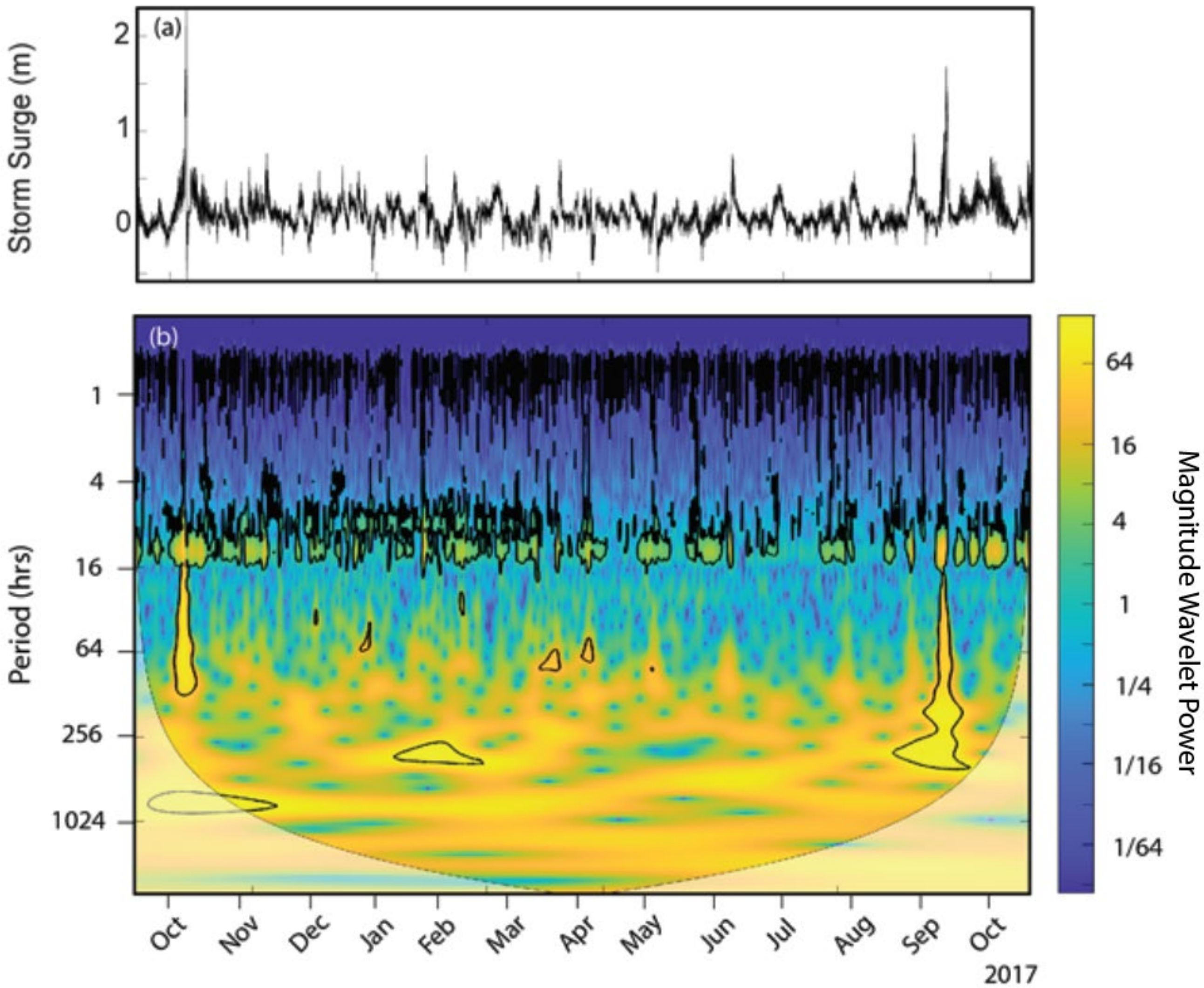

Figure 27. (a) Time series of the 2016-2017 storm surge by Sapelo Island. (b) Scalogram of the Continuous Wavelet Transform of the storm surge. The periodicity of the signal is indicated on the y-axis and is base 10 logarithmic. Magnitude of wavelet power is indicated by the color scale on the right-hand side.

The CWT seen in Figure 27 shows the time frequency analysis of the storm surge. While there are a couple of distinct peaks in the time series data seen in Figure 27.a, there are really three that stand out and are statistically significant, two of which being from hurricanes, in October 2016 and September 2017 ranging from a period of 16 – 400 hours, and peak in late January/early February around 256 hours. There is also a clear band of high wavelet power across the time series around the 12 hr 25 min period, most likely from the differences in tides between Fort Pulaski and Sapelo Island.

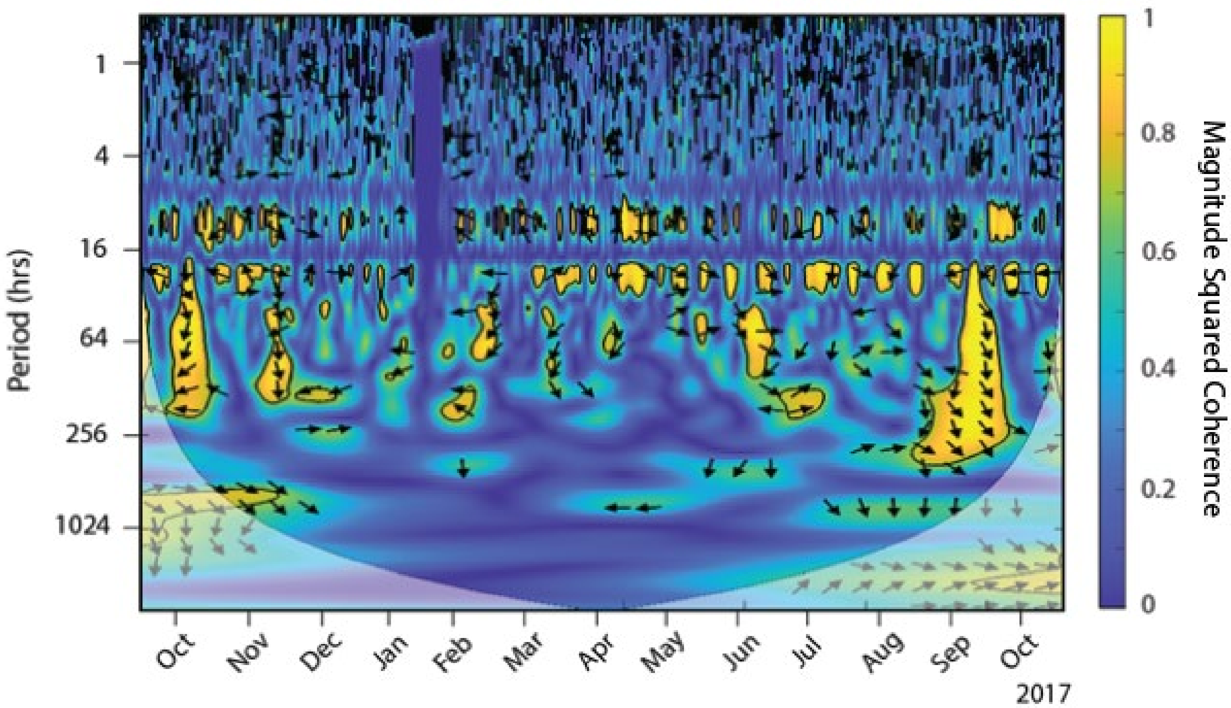

Figure 28. Wavelet coherence between tide and water level of Gravel Pond for the 2016-2017 dataset. Magnitude squared coherence is on a scale from 0 to 1. Phase arrows show relative phase lag between the two time series. The phase arrows are shown in areas that have greater than 0.6 magnitude-squared coherence. Magnitude-Squared Coherence is indicated by the color scale on the right-hand side.

Wavelet coherence between the CWTs for the tide and the water level of the Gravel Pond is shown in Figure 28. There is a clear common feature between the two time series at the period of 12 and 25 hours with the latter having more pronounced peaks and statistically significant areas on the scalogram. Both of these bands are time intervals at which tides occur. There are also a few given areas of high power at periods greater than 25 hours, primarily in October of 2016 and September of 2017. Phase arrows are displayed on the figure at areas greater than 0.6 magnitude-squared coherence. While they are not all in phase in Figure 28 with each other the calculated phase angle has a small confidence interval indicating a consistent phase lag between the tide and water level. The calculated phase angle of the Cross Wavelet Transform (XWT) within the 5% significant regions that are not in the COI has a mean angular phase 2±6° (with ± designating the circular standard deviation).

From the CWT of storm surge and water level of the Gravel Pond the wavelet coherence was calculated and plotted in the scalogram displayed in Figure 29. There are two areas of clear high power in October of 2016 and September of 2017. The first period is in a band from 16 – 100 hours, and the second is from 16 – 256 hours. There are a few other noted areas of high coherence during the 6 - 64 hour period as well. Most of the phase arrows are pointing down and to the right, indicating that the time series of storm surge and water level are near in phase or water level is lagging.

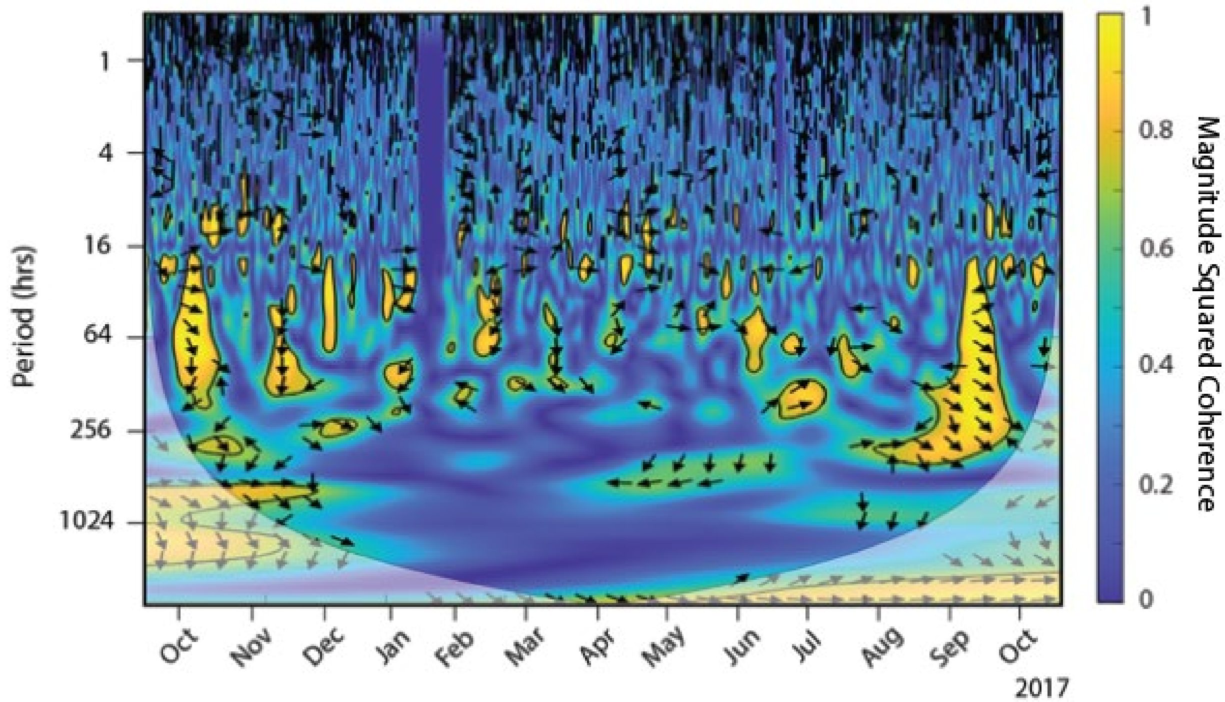

Figure 29. Wavelet coherence between storm surge and water level of Gravel Pond for the 2016-2017 dataset. Magnitude squared coherence is on a scale from 0 to 1. Phase arrows show relative phase lag between the two time series. The phase arrows are shown in areas that have greater than 0.6 magnitude-squared coherence. Magnitude-Squared Coherence is indicated by the color scale on the right-hand side.

6.4 Spatial variances between pond levels on Sapelo Island

To assess the surficial aquifer's response to variables spatially, four pond locations were chosen to collect water level data from as a spatial reference for the surficial aquifer. All of the water levels for the respective ponds were analyzed using wavelet analysis to assess the different responses spatially and temporally. The exact locations of the ponds, elevation above sea level, distance from marsh, and surface area are all shown in table 5. These will be used in analyzing the response of water to variables in multiple wavelet analyses.

Table 5. Data of exact pond locations, reference names, height of pond above sea level, distance from the closest marsh, and surface area of each pond. Height above sea level determined using national elevation dataset in ArcGIS. Distance from marsh is determined using google earth.

Location	Name	Latitude	Longitude	Height above sea Level (m)	Distance from Marsh (m)	Pond Size (m^2)
P1	Alligator Pond	31’23'52”77"N	81’16'43”91"W	1.16	184	9573
P2	Gravel Pond	31’26'9”18"N	81’16'34”41"W	1.09	346	8277
P3	Third Pond	31’26'38”48"N	81’14'34”90"W	1.47	38	1173
P4	Lilly Pond	31’24'34’’7"N	81’16'55’’4"W	1.48	360	2552

The water levels of all four ponds are displayed in Figure 30.a, and the CWTs of all ponds are displayed beneath in Figure 30.b-e. All of the pond level time series follow a similar pattern over the course of the acquisition period, losing water at a similar rate. There is a notable sharp spike in mid-March followed by a large increase peaking in April and then falling again. The Alligator Pond experienced a spike in water level in water level in early February that the other ponds did not, then followed a similar pattern. The Gravel Pond water level followed a similar pattern to the other ponds until June when it began to lose water at a faster rate but still experienced changes in rate similar to the other ponds. The Third Pond followed the same pattern as the others but responded with a higher rate of water level increase during positive water level rate changes. The Lily Pond followed the same pattern until June when the water level remains stagnant (Figure 30.a). The stagnant water level is due to the pressure sensor not being inundated during this time. Due to the sensor being exposed and not collecting water level data the portion of data that was not the pressure of the water level will be removed from the upcoming scalograms while maintaining the same x-axis to allow for easy comparison of the different scalograms.

The CWT of each pond's water level was calculated and added to separate scalograms that are stacked on each other for comparison in Figure 30. Most of the scalograms have very similar areas of power, but there are some notable differences. In all 4 of the scalograms there is a clear band of wavelet power above the 5% significance level at the 12 hour period. There is a second band at the 25 hour period, but it is much sparser and not fully connected. It is most prevalent in the Alligator and Third pond, and completely disappears the second half of the Lilly Pond (this may be due to the data logger being exposed at the Lilly Pond). There was a large peak seen in all scalograms in the 16 – 64 hour period during the middle of March. The Alligator Pond also experienced a peak in late January as well where there was an abrupt change in water level. This was an isolated event and not noted in any other scalogram.

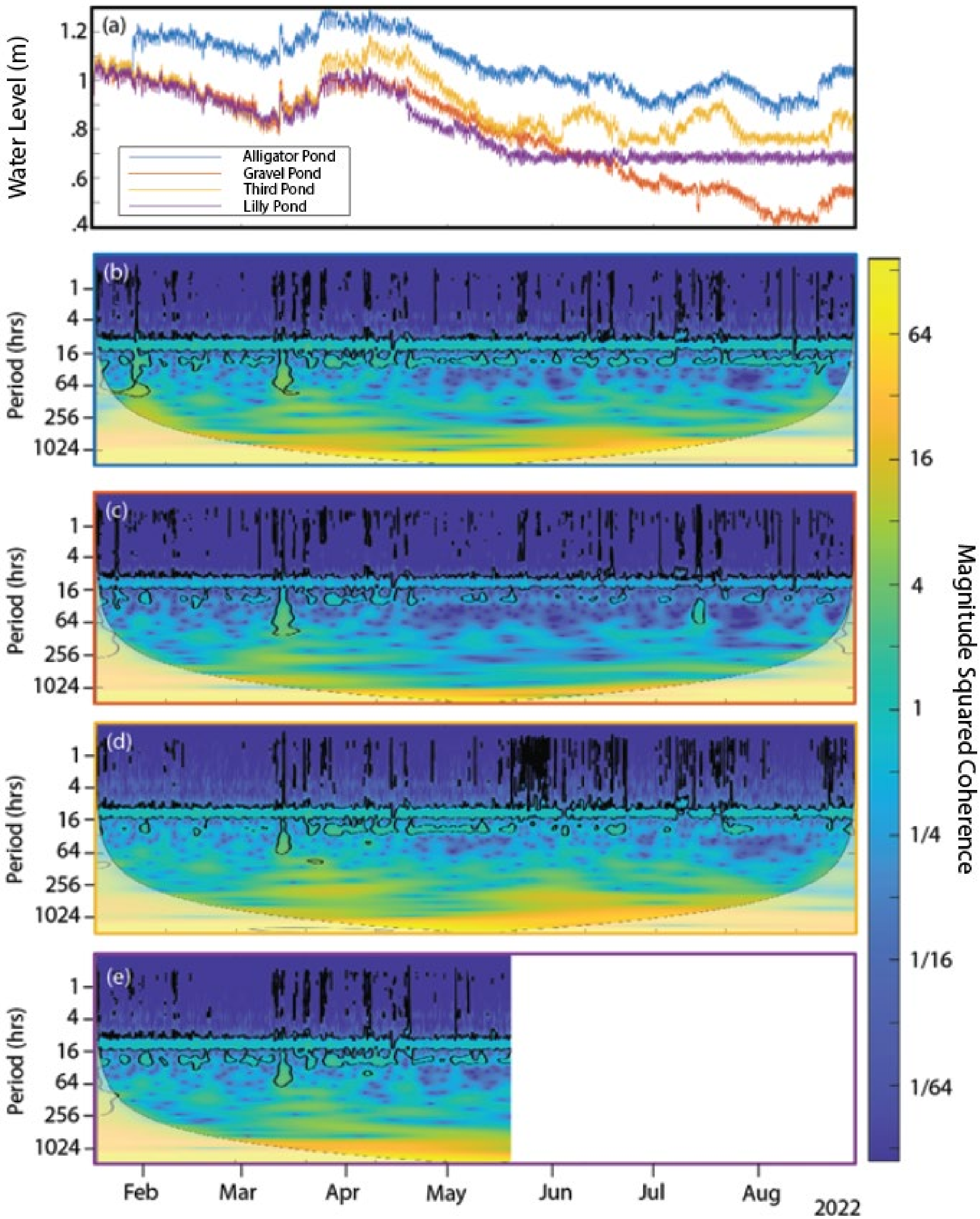

Figure 30. (a) Time series of all observed water levels measured in ponds for 2022. Of note, the sensor in the Lilly Pond was exposed when read off, so given the water level values it was most likely not showing water level from mid-May onwards. Scalogram of CWT of observed water levels in Alligator Pond (b), Gravel Pond (c), Third Pond (d), and Lilly Pond (e). Magnitude is indicated by the color scale on the right-hand side.

There were a number of precipitation events collected over the dataset from January through August as seen in Figure 31.a. The scalogram of the CWT for precipitation is shown in Figure 31.b. All of the precipitation events are clearly highlighted within the scalogram with bright vertical lines indicating the higher magnitude and ranging in period from below 1 hour up to 500. There are some high peaks seen mid-March to April from 64 – 300 hours and all of August with one huge event up to a period of 256 hours within the bounds of the COI.

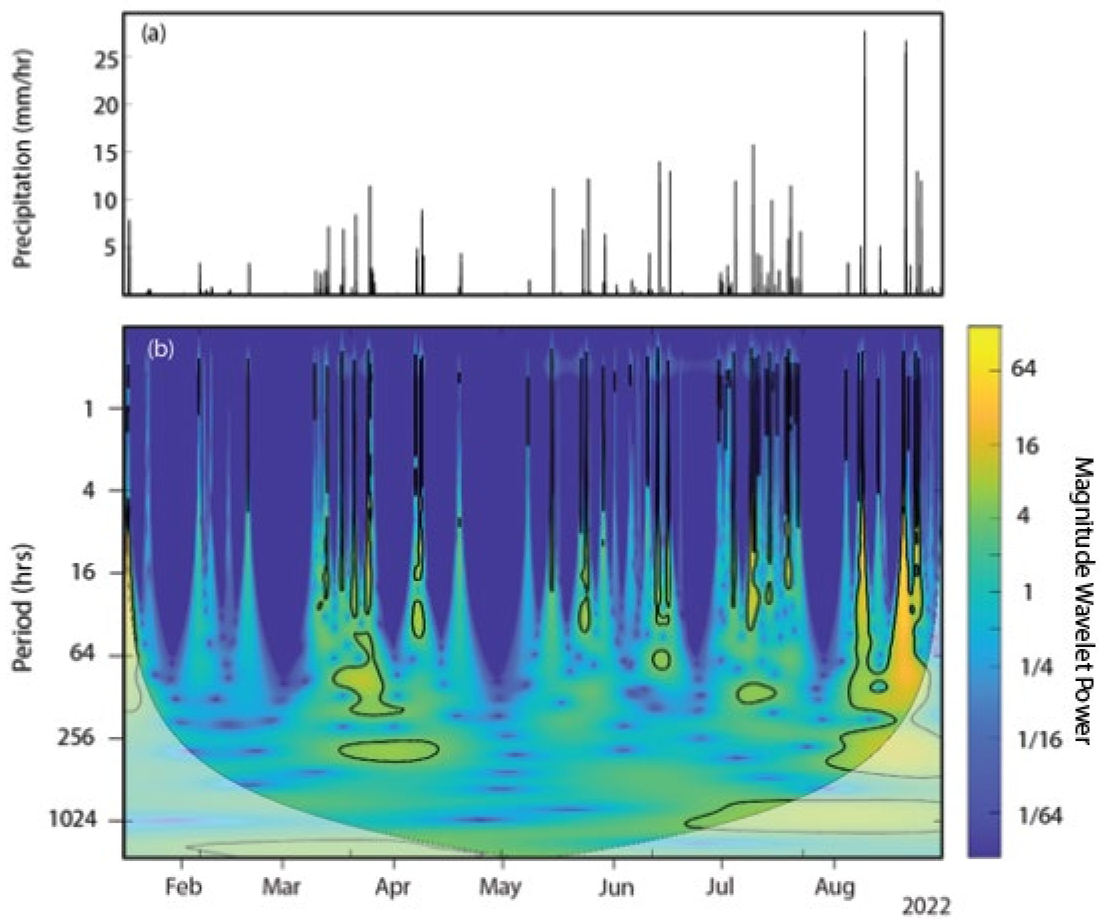

Figure 31. (a) Time series of Precipitation in mm/hr for the 2022 data. (b) Scalogram of the Continuous Wavelet Transform of the precipitation time series data. The periodicity of the signal is indicated on the y-axis and is base 10 logarithmic. Magnitude of wavelet power is indicated by the color scale on the right-hand side.

The scalogram of the CWT for tides during the second monitoring campaign (Figure 32) is rather similar to the first one, displayed in Figure 26. There is a strong band of wavelet power around 12 hours that is within the 5% significance level, with clear peaks where the larger tides are seen. Below this there is a band of higher wavelet power at around the 25 hour period, but this band is not statistically significant compared to the background noise.

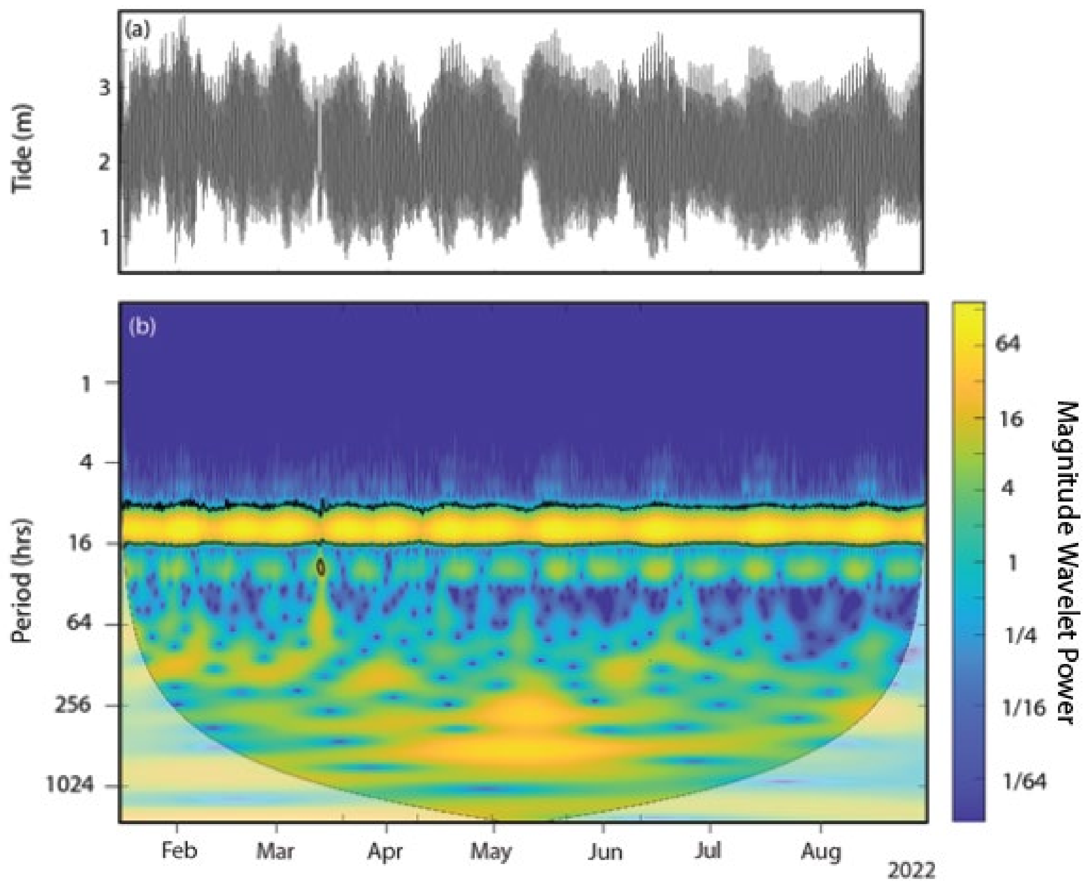

Figure 32. (a) 2022 time series of Tidal data from GCE_10, located on the backside of Sapelo Island. (b) Scalogram of the Continuous Wavelet Transform of the tidal data time series. The periodicity of the signal is indicated on the y-axis and is base 10 logarithmic. Magnitude of wavelet power is indicated by the color scale on the right-hand side.

The scalogram of the CWT for the storm surge (Figure 33) shows a band of wavelet power that is above the 5% significance level at the 10 – 16 hour period. There are a few peaks away from this that are statistically significant in late January, early February, and Late March, with the one occurring in March being the largest at a period ranging from 16 – 100 hours. Another significant peak seen is in mid-May around the 256 – 500 hour range.

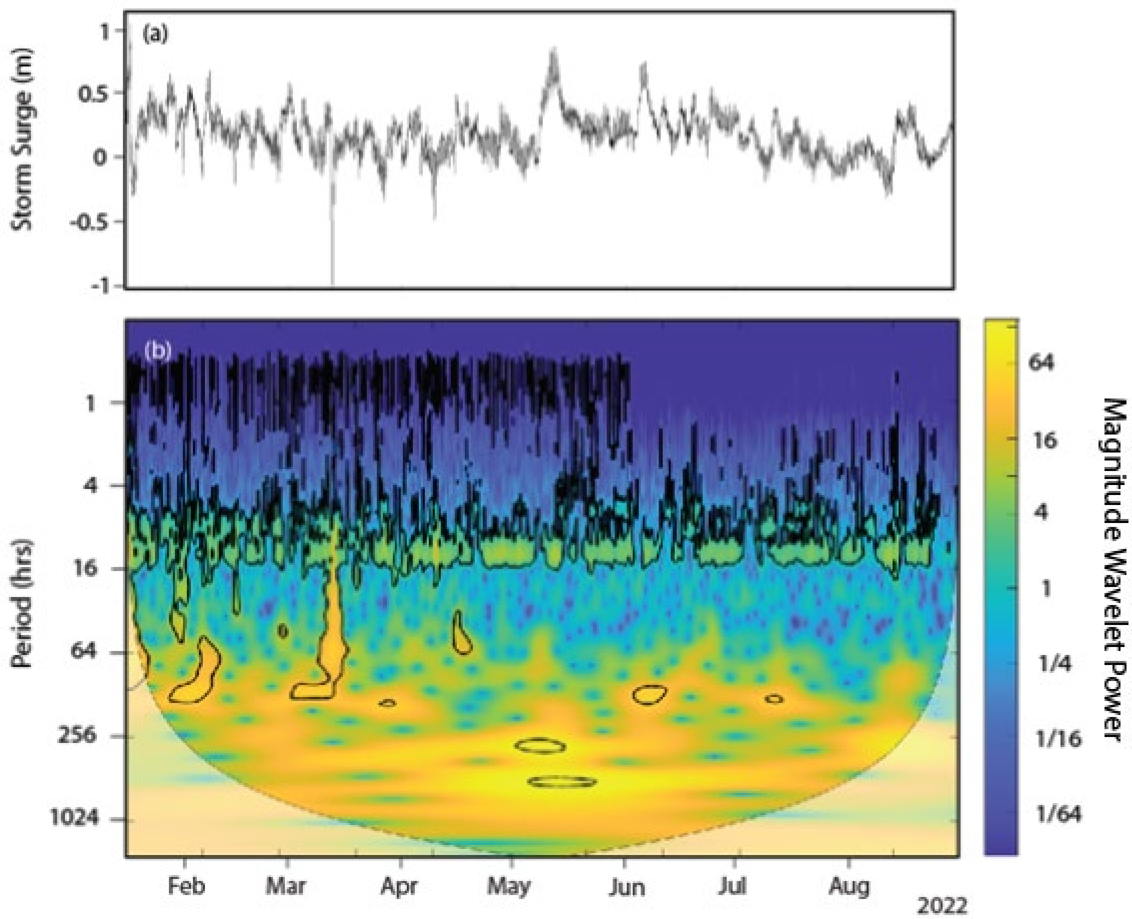

Figure 33. (a) 2022 time series of Storm Surge associated with the tides. (b) Scalogram of the Continuous Wavelet Transform of the Storm Surge time series. The periodicity of the signal is indicated on the y-axis and is base 10 logarithmic. Magnitude of wavelet power is indicated by the color scale on the right-hand side.

Figure 34 presents the scalograms of the wavelet coherence (WTC) of the four ponds CWT of water level to the CWT of precipitation. The scalogram shows disparities, but there is a semi-consistent band of magnitude-squared coherence in the 30 – 64 hour range for all of them. In the WTC of the Alligator Pond there are very large areas of coherence all above the 64 hour range. The first of which occurs from mid-February to late May in a range of 64 to 256 hours. The second and largest peak starts in April and extends to the end of the time series at a period of 256 – 1024 hours. Phase arrows are mostly directed downward, indicating a lag of the water level to precipitation.

In the second scalogram representing the WTC of the Gravel Pond in 2022 there is still the band across the 30 – 64 hour range, but more inconsistent than in the Alligator Pond. There is a similar large peak of coherence from mid-February to late May ranging from 64 to 256 hours. There's also a high peak in late January but is in the Cone of Influence. There is a continuous period of high coherence in the significance level above 5% at a range of 500 – 1024 hours across the whole dataset until entering the cone of influence. Phase arrows are mostly directed downward, indicating a lag of the water level to precipitation.

Figure 34.c is the scalogram of the WTC between precipitation and the water level of the Third Pond. Again, this has a sparse band across the range 30 – 64 hours. It has a large peak from late January to late May at a range from 64 to 256 hours. This peak is notably larger than the in the other ponds for the same time frame. Around May to late June there is a 500 hour period significant event that is not seen on the other scalograms in Figure 34, as well as a peak event in the beginning of July at the 64 – 256 hour period. There is a continuous period of coherence across the bottom at period of 1024 hours that

is connected to the first event described in January. Phase arrows are mostly directed downward, indicating a lag of the water level to precipitation.

Figure 34.d is the WTC of the precipitation and Lilly Pond water level. There are some slight peaks in coherence in the 30 – 64 hour range, but hardly enough to say there is a band across the time series. There is a large peak event from mid-February to April at a range of 64 – 500 hours, but it is the smallest of the 4 scalograms for this time frame. There are few peaks after this, most likely due to the sensor becoming exposed. For the significant events the phase arrows are mostly downward, indicating water level lagging precipitation.

Figure 35 shows all four of the WTCs of the CWT of tide compared to each respective pond's water level. All of the respective scalograms have a band of continuous and high wavelet coherence at a period of 12 hours. The WTC of the Alligator Pond also has a less continuous but still clear band of coherence around the 25 hour period. There are 2 other large peaks in wavelet coherence above the 5% significance level. One is at around the period of 64 hours from mid-February to mid-March and the other is at a period from 30 – 100 hours in late June. The calculated phase angle of the Cross Wavelet Transform (XWT) within the 5% significant regions that are not in the COI has a mean angular phase -164±21°.

The WTC of Gravel Pond with respect to tide and water level, has a band of power at both 12 and 25 hours, with the 12 hour band being more pronounced. Similar to the Alligator Pond, this scalogram has two nearly identical peaks of coherence in mid-February to mid-March and in late June at the same periodicities. There is a third peak from April to mid-May at about the 100 – 200 hour period as well. The calculated phase angle of the Cross Wavelet Transform (XWT) within the 5% significant regions that are not in the COI has a mean angular phase -1±40°.

The Third Pond's WTC scalogram shows two bands of high coherence at the periods of 12 and 25 hours with 12 being the stronger band. Nearly identical peaks to the WTC of the Gravel Pond in that there are 3 major peaks: one from mid-February to mid-March, another from April to mid-May, and another in late June all at the same periodicities. The calculated phase angle of the Cross Wavelet Transform (XWT) within the 5% significant regions that are not in the COI has a mean angular phase -15±48°.

The WTC of the Lilly Ponds water level and tide has the same bands of power seen in the other three scalograms in Figure 35 at 12 and 25 hours. There are two similar peaks in mid-February to mid-March at around 64 hours and late July around 30 – 100 hours, and an additional peak of coherence from April to June at about 500 hours. The calculated phase angle of the Cross Wavelet Transform (XWT) within the 5% significant regions that are not in the COI has a mean angular phase -132±46°.

The WTC between the CWT of storm surge and the CWT of each pond's respective water level is shown in Figure 36. All four present a band of coherence above the 5% significance level at a period of 12 hours. These scalograms are relatively similar. For all of them there are three significant events at 64 hour period occurring in late February, mid-March, and late June. The majority of phase arrows for Figure 36 are pointed left or 45° Southwest suggesting that the time series are in antiphase.

There are a few small differences seen between the scalograms. In the WTC of the Gravel Pond the peak of coherence in March is the largest among the rest of the scalograms. The WTC of the Lilly Pond has a peak around 500 hours from April to June.

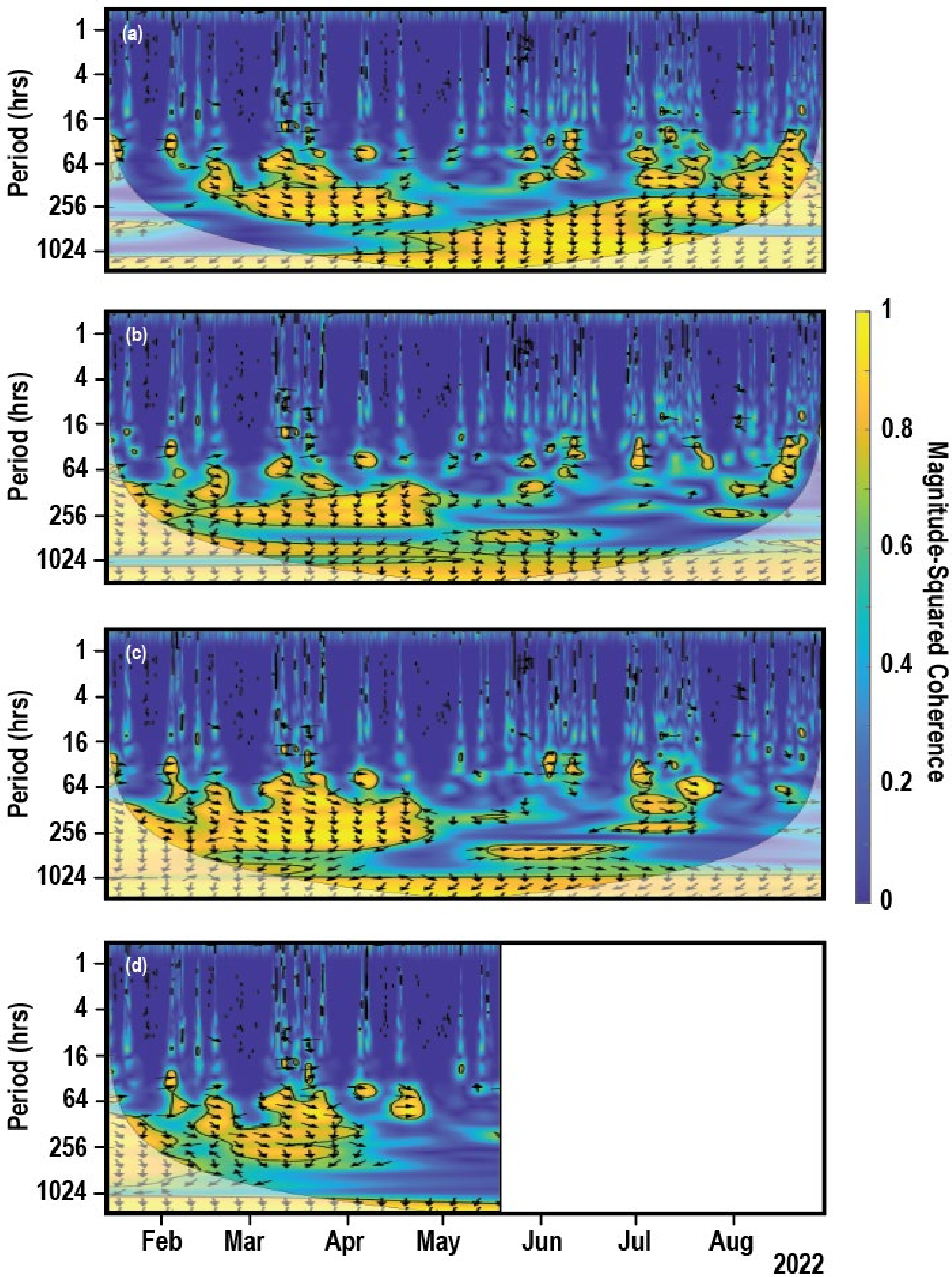

Figure 34. Wavelet coherence of precipitation and water level for (a) Alligator Pond (b) Gravel Pond (c) Third Pond and (d) Lilly Pond. Arrows show relative phase lag between the time series of precipitation and water level of the respective ponds. Phase arrows are only shown in areas of the scalogram where Magnitude-Squared Coherence exceeds 0.6. Magnitude-Squared Coherence is indicated by the color scale on the right-hand side.

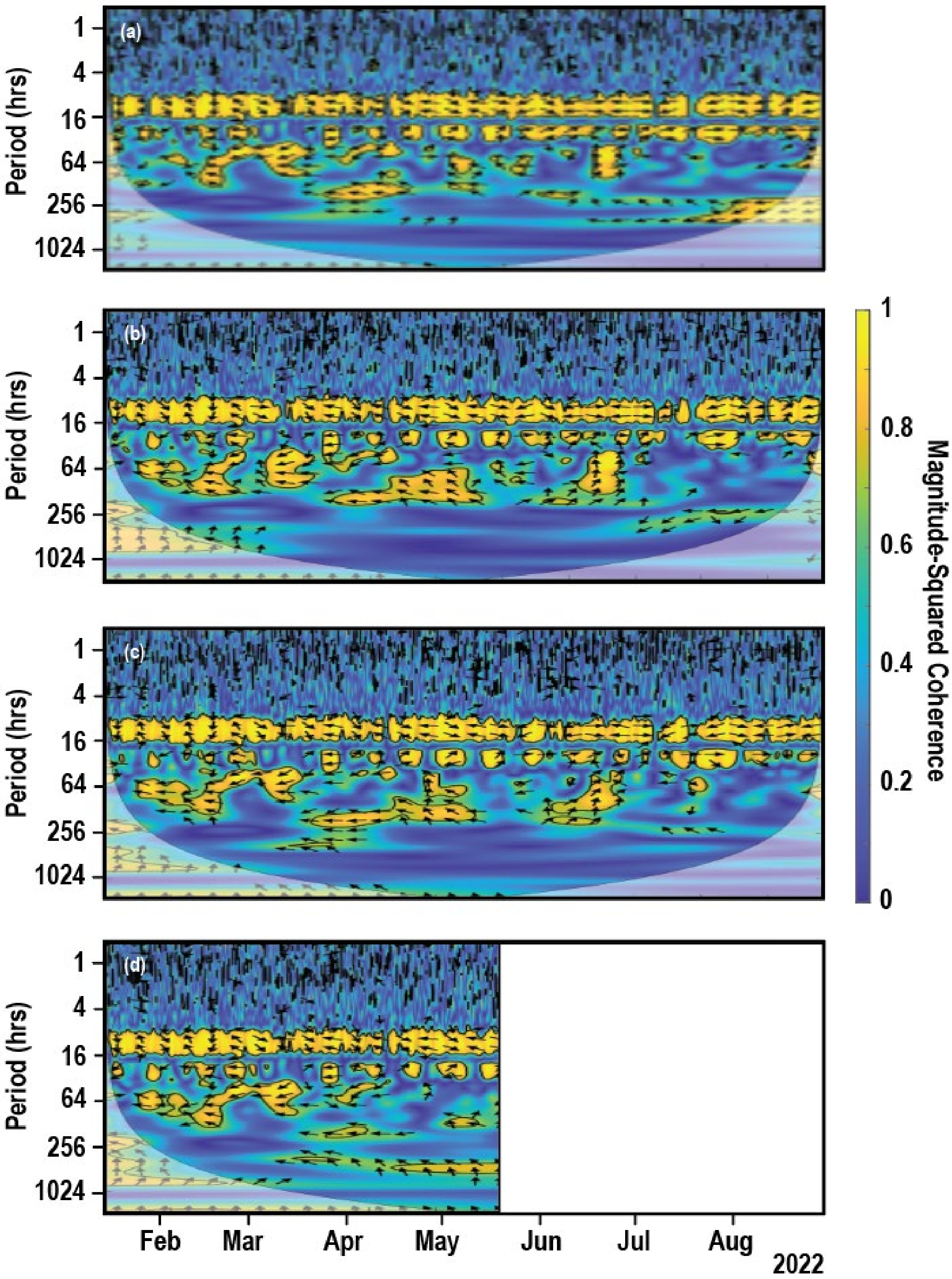

Figure 35. Wavelet coherence of tides and water level for (a) Alligator Pond (b) Gravel Pond (c) Third Pond and (d) Lilly Pond. Arrows show relative phase lag between the time series of tide and water level of the respective ponds. Phase arrows are only shown in areas of the scalogram where Magnitude-Squared Coherence exceeds 0.6. Magnitude-Squared Coherence is indicated by the color scale on the right-hand side.

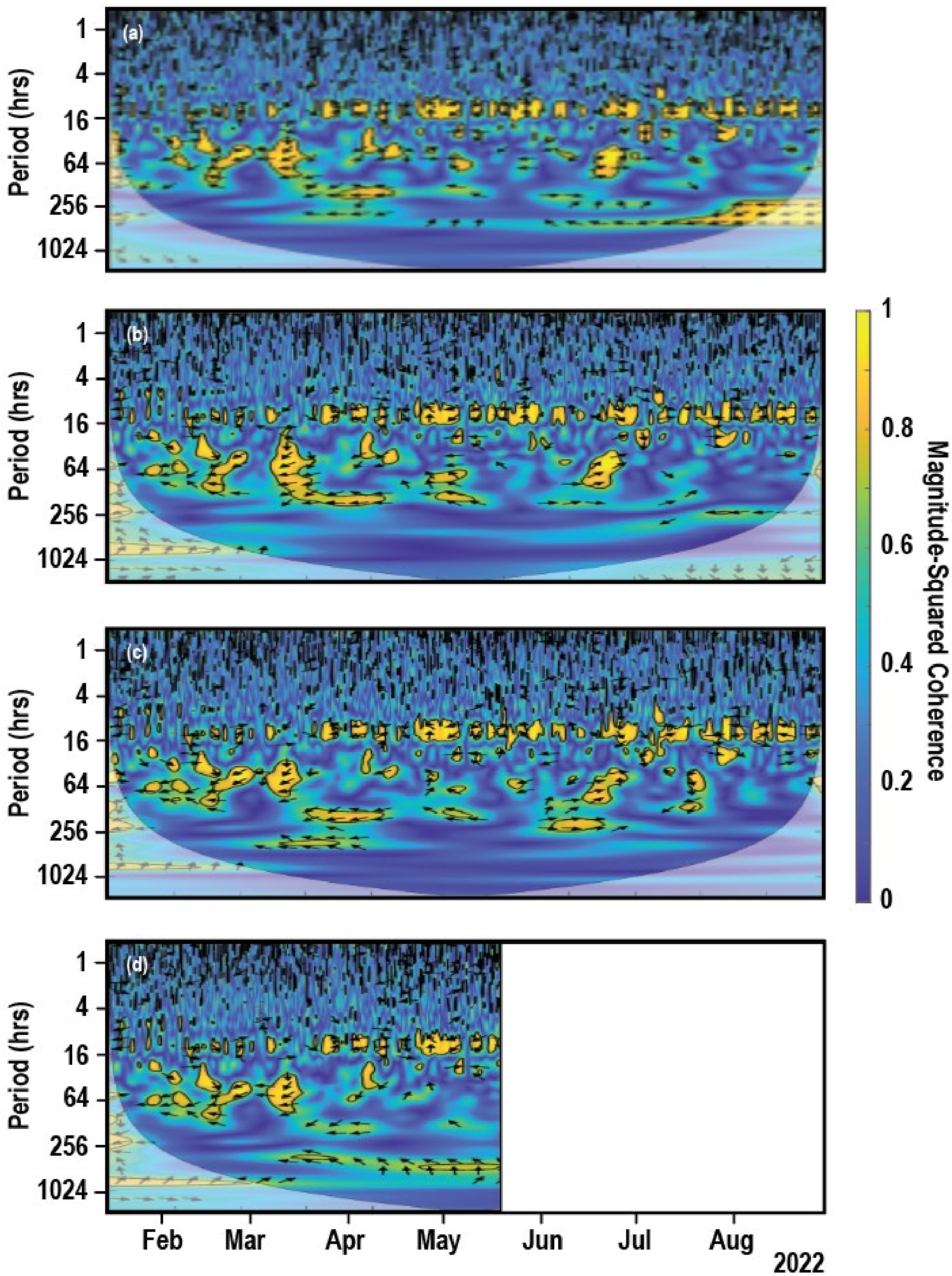

Figure 36. Wavelet coherence of storm surge and water level for (a) Alligator Pond (b) Gravel Pond (c) Third Pond and (d) Lilly Pond. Arrows show relative phase lag between the time series of storm surge and water level of the respective ponds. Phase arrows are only shown in areas of the scalogram where Magnitude-Squared Coherence exceeds 0.6. Magnitude-Squared Coherence is indicated by the color scale on the right-hand side.

CHAPTER 7

DISCUSSION

The first objective of this study is to identify and quantify the temporal relationship between various groundwater drivers and the water level of a surficial aquifer on a barrier island. The various groundwater drivers in question are precipitation, evapotranspiration, tides, and storm surge. The second objective of the study is to assess the spatial variability of various pond levels across the island with respect to the geographical location and the previously mentioned variables. It is hypothesized that precipitation and pond level will have a linear relationship, ET will have an effect on the pond, but minimal, tidal effects will be seen and more strongly during perigean tides, and that spatially the ponds closer to the center of the island will experience more of a rise in water level than those closer to the water.

There are a few key findings noted in this research. Hydrometeorological data from the first time series (2016 – 2017) regarding storm events suggests there is a positive linear relationship between the precipitation and water level of the pond. A positive relationship best modeled by a power regression is observed between the maximum tide and water level of the pond as well. An anomaly in the data is seen during a period of excessive precipitation combined with a prolonged high oceanic water level, where water level of the pond increases exponentially compared to the amount of precipitation.

The CWT analysis identifies all areas of abrupt change in each respective time series and shows where the data is statistically significant. The wavelet coherence between time series shows where the variables have a significant effect on the water level. Tides are seen as having a consistent effect on the water level at the 12 hr 25 min tidal period, and storm surge and precipitation have significant effects at a longer period where they respectively occur in time. Spatially the wavelet coherences are similar, but there are noticeable differences among the precipitation and tide wavelet coherences that will be discussed below.

7.1 Relationship between Precipitation from Storm events and Water Level of Gravel Pond

7.1.1 Precipitation and Water Level of Gravel Pond

The main source for recharge of the surficial aquifer on Sapelo Island is precipitation, so it is no surprise that there is a clear relationship between precipitation and water level of the Gravel Pond. A clear linear relationship can be seen in Figure 18 in both of the datasets with moderate R^2 values of .58 and .39, for the first and second data period respectively. Of note, both of the hurricane data points were removed to see the linearity of the first dataset.

The CWT of precipitation revealed a number of areas with high power during precipitation events with statistical significance starting at less than an hour and peaking at a period of 16 – 256 hours. These areas of higher power line up with the two peaks of significance seen on the CWT of water level of Gravel Pond. The wavelet coherence of these two CWTs reveals these common areas in high coherence specifically in the range from 16 – 256 hours at a phase angle pointing down. This suggests that the water level is lagging precipitation, meaning the peak in water level due to precipitation is expected anywhere from 4 – 64 hours after the precipitation event. While precipitation would have an immediate effect on a pond level, it is probably not shown on the wavelet coherence scalogram due to the fact that it is so small the area of significance does not show up on the graph. The overall lag is likely representative of the variable source hydrology that the Gravel Pond experiences.

The varying sources affecting the pond level resulting from precipitation events would likely occur at varying lags. Direct precipitation on the pond would have an immediate impact. Given the surrounding subsurface areas have exceeded the amount of precipitation that can infiltrate the ground then runoff would occur, seen in a relatively short amount of lag on the terms from a few minutes up to a few hours. Horton overland flow can also be a mechanism of runoff where the precipitation rate exceeds that of infiltration rate creating runoff. After the time it takes for the precipitation to infiltrate through the unsaturated zone, groundwater effects would then be seen affecting the pond levels. Groundwater flow would have a positive effect on the pond level a few hours after a precipitation event up until the last effects from lags are seen, sometimes 64 hours afterwards. This succession of variable sources in the hydrology of the ponds would explain the range of lag seen between precipitation events and the water level of the ponds.

7.1.2 Hurricane Events and Water Level of Gravel Pond

Observed data of the water level of Gravel Pond analyzed from the two hurricane events seen in October of 2016 and September of 2017 displays some interesting behavior. While there was a significant amount of precipitation for each event, 65 and 123 mm respectively, the amount the pond rose was substantially higher. During hurricane Matthew the pond level rose 750 mm and during hurricane Irene the level rose 641 mm, for a ratio of precipitation amount to pond level of 11.6 and 5.2 respectively. The other storms had varying amounts of precipitation, some more than 100 mm, but only saw a maximum rise of 90 mm and no ratios exceeding 2.5.

The notable difference between the rise in pond level during hurricane events and all of the other storm events is the incredibly high tides and storm surge associated with storm events. The phase where the water level of the pond is rising fastest is during a prolonged period of higher than normal high and low tide. This suggests that the pond level rate is a function of both precipitation amount, duration, and height of tide. In theory this extended high tide allows for more continual forcing on the surficial aquifer via saltwater intrusion. Presumably, the denser saltwater moves inland making the freshwater-seawater transition zone retreat further inland from all sides of the island (Figures 2 & 7). This movement inland of the transition zone decreases the total surface area of the freshwater lens from an aerial 2-D view but raises the water level a significant amount as the volume does not change. This results in the large spikes in water level seen in Figures 21 & 22 that are much greater than the total amount of precipitation.

The pond level rate of change during the two hurricane events exhibits a similar pattern. The pond level rate starts off very gradually increasing and then increases at an exponential rate until it reaches the peak. Then, the water level falls at a very fast rate and slowly the rate slows down until finally the water level reaches equilibrium again. During hurricane Matthew the Gravel Pond gained over 521 mm in the pond level and from hurricane Irene the Gravel Pond gained 117 mm in the pond level. This follows the same pattern that the submarine groundwater discharge did in Adyasari et al. (2021) where there is an initial rate that starts off slowly and multiplies to a peak discharge only to reverse and have the rate of SGD slow down rapidly and then come back to normal.

7.2 Relationship between Evapotranspiration and Water Level of Gravel Pond

The cross-correlation coefficient between the temperature on Sapelo Island and the water level of Gravel Pond was calculated to be 0.14 with no lag using MATLAB. This suggests a poor relationship between the two time series, indicating that there is minimal correlation between the two variables. While effects from evapotranspiration are expected to affect the water level of the Gravel Pond the weak relationship between the two could be due to the small effect from evapotranspiration being overshadowed by larger changes from other variables or a instrument error in measuring the water level as the HOBOware pressure sensors have a standard deviation of 5 mm, which is around the expected evapotranspiration.

As seen in table 3, the average water level change per day is very low, with less than 5 mm every day observed in the water level and in the calculated evapotranspiration on the table. This amount is substantially less than other changes seen in the pond level that often exceed centimeters per hour and even sometimes half a meter in less than a day. While the loss due to evapotranspiration is steady, it is not significant enough to factor in when looking at much larger changes due to precipitation, storm surges, and tides.

7.3 Relationship between Tides, Storm Surges, and Water Level of Gravel Pond

When analyzing the hydrometeorological parameters of the storm events, there is a noticeable trend when comparing maximum tides to the change in water level of the pond. Best described by an exponential equation, the larger tides experiencing a significant storm surge create an exponential effect on the amount of water level gained, causing the pond to rise 5 and 11 times higher than the amount rained on two occasions. This power regression model of water level change and maximum tide has a very strong fit with an R^2 of 0.82. The high ratios of pond level rise to precipitation amount could be due to higher than normal tides remaining high and inundating for days areas that are usually underwater for about an hour. This would result in a steady tidal forcing inland causing the water level of the surficial aquifer to rise at an exponential rate.

In the wavelet coherence between the storm surge and water level there are two large significant events during the hurricanes, the first at a period from 16 – 200 hours and the second from 16 – 500 hours. The phase angle shows a quarter phase lag suggesting that the water level is lagging these events. This means that for the two studied storm surge events the water level of the pond was lagging the storm surges by a quarter of the identified frequencies. The effects from the storm surges were seen from 4-50 and 4-125 hours (1-2 days and 1-5 days) respectively. In the wavelet coherence between the tide and water level there can be seen 2 main bands of power, one at 12 hrs 25 mins and one at 25 hours. These intervals are the exact timing apart for high tides in a semidiurnal setting, showing that tides are in fact connected to this pond's water level. The calculated phase angle shows that they are nearly in phase occurring at the same time. This shows that the tides have an effect on the surficial aquifer, with the high tides causing forcing affecting the water table in the ponds. Perigean tides are also seen to have more of an effect on the water level, supporting the idea that the water level is affected most by level of inundation from sea water and duration.

7.4 Spatial variances in storm responses between ponds on Sapelo Island

Four ponds across Sapelo Island were used as proxy for the water level of the island's surficial aquifer across a period of time, creating four time series that were analyzed individually against the hydrometeorological variables. The results from each pond's analyses were then compared to highlight similarities and differences among them.

In Figure 30 all of the CWTs of the ponds are shown, and they are all relatively similar with some minor differences that the wavelet coherence will give more insight on to why these occur. In the CWT of both precipitation and storm surge for this time there is a statistically significant event in April that lines up with an event seen in all of the ponds CWTs. For the CWT of tide there is a band of power across the 12 hour period that matches up to the significant level power on all the ponds CWT as well.

All the scalograms of Figure 34 present a peak of coherence between precipitation and water level of the ponds from mid-February to late May. This peak is most pronounced in the Third Pond and smallest in the Fourth Pond. This can be seen in the time series of the water level where the Third Pond rises significantly more than the others during this time period. Due to its location, the Third Pond could be experiencing higher tidal forcing from the salt marsh or potentially washover from the marsh. Washover is unlikely given that there were no excessive storm surges during the second monitoring period and the conductivity of this pond was above the detection limit when first observed in March 2022 (not reported) and during the second observation (September 2022) of conductivity it was fresher, indicating that the pond salinity had decreased. There is also a large area of coherence in the Alligator Pond from April on in the 256 – 1024 hour period that is not seen on the same scale in the other scalograms but is seen much smaller in the

Third Pond. Given the location of the Alligator and Third ponds they could have had a higher coherence of precipitation to pond level due to their proximity to the ocean and experiencing a higher groundwater flow.

The large lag times indicated by wavelet coherences for all the ponds between precipitation and pond level can be attributed to the variable source hydrology as discussed in 7.1.1. Direct precipitation on the island would have an immediate effect on the pond levels. This would be closely followed by effects from runoff within the following minutes or hours after an event. Then the water that had made it through the unsaturated zone to the saturated zone would attribute to groundwater flow that would affect the pond level for the larger lag times, with the groundwater flow headed from the center of the island to the coasts.

The differences between pond's responses to precipitation may also be due to the differing catchment areas of each respective pond. If one pond has a significant amount more area of surface runoff than another location then it would be reacting much higher. This is true as well if the sediments of the catchment area differ as this would cause less precipitation to infiltrate into the subsurface instead to create runoff that would increase the pond level. In the case of the Gravel Pond experiencing a greater loss of groundwater over the 2nd data acquisition period this could be due to anthropogenic effects. The pond is used in part to collect sand and this act would open space up that previously wasn't available, lowering the pond level at a rate faster than the other ponds. In general, there can commonly be anthropogenic effects that can affect water table changes such as upconing from over pumping of groundwater or mining of the sediments.

There were not any considerably large storm surges during this time period, but it was still considered. The wavelet coherences of the storm surges are mostly similar to the

Gravel Pond having a larger peak than the others in March, but no significant effects were observed on the water level. No discernible effects were observed for storm surge during this time.

The wavelet coherence between tides and water levels of the ponds is seen in Figure 35. They are very similar, having a strong band of coherence at a period of 12 hrs 25 mins, and another clear but sparser band at 25 hours. The main difference between these scalograms is in the phase angle. Calculated using the XWT the phase angle of the 5% significant regions for the Alligator, Gravel, Third, and Lilly Pond are -164±21°, -1±40°, -15±48°, and -132±46°, respectively. The Alligator and Lilly Pond appear to be in anti-phase, whereas the Gravel and Third Ponds appear to be in phase with the tides. The ponds in anti-phase would be experiencing effects from the tides ~6 hours after a high tide occurred and the ponds in phase would be experiencing tidal effects on the water level as high tide is occurring. This is counterintuitive given that the ponds would be experiencing the tidal effects coming from propagations at the coast, but the Gravel Pond is the furthest from the coast and experiencing no lag whereas ponds closer to the coast are in quarter phase lag. We hypothesize that the Gravel Pond is actually a full phase lag behind the tides, leading to the coherence analysis suggesting that it is in phase. This would mean that the time lags seen for tides effect on water table would be 0 hours for the Third Pond, 6 hours for the Lily and Alligator Pond, and 12 hours for the Gravel Pond. The strong correlation seen at both the 12 hr 25 min and 25 hr period indicating tidal effects on the pond levels is good evidence for the assumption made in this study that the ponds on the island are connected to the surficial aquifer.

This study has quite a few limitations that do need to be considered. The first of which is the assumption that the height of the pond level is an accurate estimate for the water level of the surficial aquifer. If this were not the case, then the results would be misleading. There is also a very highly localized climate on islands. Given that one area experiences precipitation does not mean that another area, even close by, has the same amount at all.

This research provides a basis for looking at the properties of a barrier island's surficial aquifer from the top, using water level. This can be coupled with measuring submarine groundwater flow to see both the storage capacity of the aquifer and the transmissivity of the subsurface. If the exact heights of all the ponds water levels are acquired at the same time, then forcing on the aquifer should be able to be seen from all sides of the island as well as insights can be drawn on the height and shape of freshwater lens/surficial aquifer. Over a long-term project, the changes in water level can be used to see the extent of the aquifer via aerial view of vegetation.

CHAPTER 8

CONCLUSION

Barrier islands are a landmark along the East Coast of the US known for tourism and the diverse nature it holds, as well as a crucial landform in protecting mainland coastlines. The source for freshwater upon which the diverse and dynamic nature of these islands depend is found in the form of a freshwater lens, or surficial aquifer if there is an underlying confining unit, lying on top of the denser salinized groundwater. The dynamics of these aquifers is controlled by a combination of factors that fluctuate temporally and spatially: precipitation recharging the aquifer, evapotranspiration removing water, tides and storm surges creating a pressure gradient affecting flow, and submarine groundwater discharge to the ocean. All of these affect the size, shape, and overall groundwater flow of the surficial aquifer of a barrier island.

The change in water level of Sapelo Island's surficial aquifer was observed temporally and spatially to better understand the response of the surficial aquifer of a barrier island to the dynamic conditions it experiences. The water level was inferred using the level of ponds assumed to be a proxy for the water level of the surficial aquifer. Variables affecting the surficial aquifer were gathered through online resources from the Georgia LTER and NOAA. Precipitation, evapotranspiration, tidal heights, and storm surge were variables used to analyze the aquifers response. The analyses were done via cross correlation between the water level and evapotranspiration, and through a series of wavelet analyses for precipitation, tides, and storm surges.

Precipitation, evapotranspiration, tides, and storm surges were found to all have a very clear effect on the water level of a surficial aquifer. Precipitation affects the water level immediately and its effects can continue for hours and days after. Evapotranspiration has a consistent daily effect reducing water levels that peak during the summer months, but overall has a small effect on daily water level compared to the other variables. Tides have a consistent effect seen on the water level of all the ponds at the tidal period of 12 hrs 25 mins with a more pronounced connection during perigean tides. When present, storm surge is seen as having a strong positive effect on the water level increasing. During large storms that couple a storm surge with high tides the water level response is similar to other precipitation events in that it increases, but different for the extent that it increases an exponential amount more than the total amount of precipitation. The overall trends identified during the first monitoring period on the Gravel Pond were also witnessed on the other ponds on the island, however, the extent of the water level changes caused by the studied factors varied for the different ponds.

Spatially, there is a difference seen among the pond levels reactions to precipitation events. The ponds closest to the ocean, the Alligator and the Third Pond, have the highest positive responses to precipitation events. This can be attributed to increased groundwater flow due to proximity to the ocean, or larger amounts of runoff due to sediment permeabilities or catchment size. The tidal effect was easily seen on all the ponds in the scalograms of wavelet coherence, but was seen as being in different time lags for each pond. The further a pond was located from the ocean the larger a lag in time was identified.

The validity of using ponds water levels as a proxy for groundwater level could be verified by measuring the submarine groundwater discharge simultaneously and seeing whether the processes reflect each other and how much time lag is between the two. Additional work is also needed to see the full extent of the relationship between the water level rise of the aquifer from the coupled effects of precipitation and lengthened inundation from high tides and storm surge and to quantify the associated flux of nutrients that such events bring out to the marshes and the ocean.

REFERENCES

Adesida, A. O., (2000) The Stratigraphic Framework of Eocene through Miocene Sequences beneath Sapelo Island, Georgia. A Shallow Seismic Reflection Study: University of Georgia, 5-8; 25-28 p.

Adyasari, D., Montiel, D., Mortazavi, B., Dimova, N., (2021). Storm-Friven Fresh Submarine Groundwater Discharge and Nutrient Fluxes From a Barrier Island, *Frontiers in Marine Science*, 8, https://doi.org/10.3389/fmars.2021.679010

Allen, M. R., & Smith, L. A. (1996). Monte Carlo SSA: Detecting irregular oscillations in the Presence of Colored Noise, Journal of Climate, 9(12), 3373-3404.

Anderson, W. P., (2002), Aquifer salinization from storm overwash, *Journal of Coastal research*, v. 18, p.413-420, http://www.jstor.org/stable/4299090

Anderson, W., Evan, D., Snyder, S., (2000). The effects of Holocene barrier-island evolution on water-table elevations, Hatteras Island, North Carolina, USA. *Hydrogeology Journal, 8*, p. 390-404.

Barlow, P.M., Reichard, E.G., (2009). Saltwater intrusion in coastal regions of North America. *Hydrogeology Journal* 18, p. 247–260 (2010). https://doi.org/10.1007/s10040-009-0514-3

Bedekar, V. S., Memari S. S., Clement, T. P., (2019). Investigation of transient freshwater storage in island aquifers. *Journal of Contaminant Hydrology*, 221, 98-107. https://doi.org/10.1016/j.jconhyd.2019.02.004

Breslin, S. (2018, January 17). Hurricane Irma Created a New Island Along the Georgia Coast. *The Weather Channel*. https://weather.com/news/news/2018-01-16-new-island-created-georgia-coast-hurricane-irma

Chalmers, A.G., (1997). The Ecology of the Sapelo Island National Estuarine Research Reserve.

Chang, S., Nemec, K., Kalin, L., Clement, T., (2016). Impacts of Climate Change and Urbanization on Groundwater Resources in a Barrier Island. *Journal of Environmental Engineering, 142(12),* https://doi.org/10.1061/(ASCE)EE.1943-7870.0001123.

Chui, T. F. M., Terry, J. P., (2013). Influence of sea-level rise on freshwater lenses of different atoll island sizes and lens resilience to storm-induced salinization. *Journal of Hydrology*, 502, 18-26. http://dx.doi.org/10.1016/j.jhydrol.2013.08.013

Corbett, D. R., Dillon, K., Burnett, W., (2000). Tracing Groundwater Flow on a Barrier Island in the North-east Gulf of Mexico, *Estuarine, Coastal, and Shelf Science*, 51, 227-242. https://doi.org/10.1006/ecss.2000.0606

Deegan, L., Johnson, D., Warren, R. Peterson, B., Fleeger, J., Fagherazzi, S., & Wollheim, W., (2012). Coastal eutrophication as a driver of salt marsh loss. *Nature* **490**, 388–392 (2012). https://doi.org/10.1038/nature11533

Deegan, L., Johnson, D., Warren, R. *et al.* (2012). Coastal eutrophication as a driver of salt marsh loss. *Nature* **490**, 388–392 (2012). https://doi.org/10.1038/nature11533

Dodd, M. G., and A. H. Mackinnon. 2003. Loggerhead turtle (Caretta caretta) nesting in Georgia, 2003. Annual report submitted to US Fish and Wildlife Service for grant E-5-3 Coastal Endangered Species Management, 46 pp

Donnelly, J. P., & Bertness, M. D. (2001). Rapid shoreward encroachment of salt marsh cordgrass in response to accelerated sea-level rise. *Proceedings of the National Academy of Sciences*, *98*(25), 14218-14223.

Essink, G.H.P.O., (2001). Improving fresh groundwater supply – problems and solutions. *Ocean & Coastal Management, 44*, 429-449. https://doi.org/ 0964-5691/01

Falkland, A. C., (1991), Hydrology and water resources of small islands: A practical guide. A contribution to the International Hydrological Programme. UNESCO Press, Paris, France

Ferguson, G., Gleeson, T. (2012). Vulnerability of coastal aquifers to groundwater use and climate change. *Nature Climate Change*. v. 2, p. 342-345. https://doi.org/10.1038

Georgia Coastal Ecosystems LTER. (2022). GCE Data Portal. Georgia Coastal Ecosystems LTER. https://gce-lter.marsci.uga.edu/portal/

Grinsted, A., J. C. Moore, S. Jevrejeva (2004), Application of the cross wavelet transform and wavelet coherence to geophysical time series, Nonlin. Process. Geophys., 11, 561566

Hayes M.O. (1994) The Georgia Bight Barrier System. In: Davis R.A. (eds) Geology of Holocene Barrier Island Systems. Springer, Berlin, Heidelberg. https://doi.org/10.1007/978-3-642-78360-9_7

Hayes, M.O., (1979). Barrier island morphology as a function of tidal and wave regime. In: S.P. Leatherman (Editor), Barrier Islands. Academic Press, New York, pp. 1-29.

Herrick, S. M., (1961). Well Logs of the Coastal Plain of Georgia. The Geological Survey, Bulletin Number 70, 282-283.

Howard, J., Scott, R., (1983). Comparison of Pleistocene and Holocene barrier island beach-to-offshore sequences, *Georgia Sedimentary Geology*, 34(2-3), p. 167-183. https://doi.org/10.1016/0037-0738(83)90085-4.

Hoyt, J. H. 1968a. Barrier Island formation: reply. *Bull. Geol. Soc. Am.* 79:947.

Hoyt, J., (1967). Barrier Island Formation. *Geological Society of America Bulletin*, 78, p. 1125-1136

Hoyt, J., Henry, V., (1967), Influence of island migration on barrier island sedimentation. *Geol. Soc. Am*, v. 78, p. 78-86

Hoyt, J., Henry, V., (1967), Influence of island migration on barrier island sedimentation. *Geol. Soc. Am*, v. 78, p. 78-86

Koetse, M. J., Reitveld, P., (2009), The impact of climate change and weather on transport: An overview of empirical findings, *Transportation Research part D: Transport and Environment*, v. 14(3), p. 205-221, https://doi.org/10.1016/j.trd.2008.12.004

Krause, R. E., Mathews, S. E., Gill, H. E., (1984), Evaluation of the groundwater resources of coastal Georgia, *Georgia Geological Survey*, Information circular 62, 12

Krest, J. M., Moore, W. S., Gardner, L. R., and Morris, J. T., (2000), Marsh nutrient export supplied by groundwater discharge: Evidence from radium measurements, *Global Biogeochemical Cycles*, v. 14, p. 167-176. https://doi.org/10.1029/1999GB001197

Kumar, P., and Foufoula-Georgiou, E. (1997), Wavelet analysis for geophysical applications, *Rev. Geophys.*, 35(4), 385– 412, doi:10.1029/97RG00427.

Ledoux, J. G., (2015) Drivers of groundwater flow at a back barrier island-marsh transect in coastal Georgia: University of Georgia, 104 p.

Lemke, P., Ren, J., Alley, R.B., Allison, I., Carrasco, J., Flato, G., Fujii, Y., Kaser, G., Mote, P., Thomas, H.R., Zhang, T., (2007). Observation Changes in Snow, Ice and Frozen Ground. In: *Climate Change 2007: The Physical Science Basis. Contribution of Working Group 1 to the Fourth Assessment Report of the Intergovernmental Panel on Climate Change*. Cambridge university Press, Cambridge, United Kingdom and New York, NY, USA

Li, H., Jiao, J. J., (2002). Analytical solutions of tidal groundwater flow in coastal two-aquifer system: *Advances in Water Resources*, v. 25, issue 24, https://doi.org/10.1016/S0309-1708(02)00004-0

NOAA. (2004, February 25). Datums for 8675622, OLD TOWER, SAPELO ISLAND, DOBOY SOUND GA. *NOAA Tides & Currents.* https://tidesandcurrents.noaa.gov/datums.html?id=8675622

Peterson, R. N., Meile, C., Peterson, L. E., Carter, M., and Miklesh, D., (2019), Groundwater discharge dynamics into a salt marsh tidal river: *Estuarine, Coastal and Shelf Science*, v. 218, p.324-333, https://doi.org/10.1016/j.ecss.2019.01.007

Pilkey, O., Cooper, J.A.G., Lewis, A. (2009). Global Distribution and Geomorphology of Fetch-Limited Barrier Islands. *Journal of Coastal Research*, 25(4), p. 819-837. https://doi.org/10.2112/08-1023.1

Porubsky, W.P., Weston, N. B., Moore, W. S., Ruppel, C., Joye, S. B., (2014). Dynamics of submarine groundwater discharge and associated fluxes of dissolved nutrients, carbon, and trace gases to the coastal zone (Okatee River estuary, South Carolina). *Geochimica et Cosmochimica Acta*, 131, 81-97. https://doi.org/10.1016/j.gca.2013.12.030

Post, V. E. A., (2005). Fresh and saline groundwater interaction in coastal aquifers: Is our technology ready for the problems ahead?, *Hydrogeology Journal*, v. 13, p. 120-123, https://doi.org/10.1007/s10040-004-0417-2

Post, V., Abarca, E., (2010). Preface: Saltwater and freshwater interactions in coastal aquifers, *Hydrogeology Journal*, 18, p. 1–4, https://doi.org/10.1007/s10040-009-0561-9

Ruppel, C., Schultz, G. and Kruse, S. (2000), Anomalous Fresh Water Lens Morphology on a Strip Barrier Island. *Groundwater, 38*: 872-881. https://doi.org/10.1111/j.1745-6584.2000.tb00686.x

Sanger, D., Parker, C., (2016), Guide to the Salt Marshes and Tidal Creeks of the Southeastern United States: Columbia, South Carolina, South Carolina Department of Resources

Schneider, J., Kruse, S. (2003). A comparison of controls on freshwater lens morphology of small carbonate and siliciclastic islands: examples from barrier islands in Florida, USA. *Journal of Hydrology, 284(1-4)*, p. 253-269. https://doi.org/10.1016/j.jhydrol.2003.08.002.

Schultz, G., Rupel, C., (2002). Constraints on hydraulic parameters and implication for groundwater flux across the upland-estuary interface. *Journal of Hydrology, 260 (1-4),* p. 255-269. https://doi.org/10.1016/S0022-1694(01)00616-3

Schutte, C.A., Hunter, K., Mckay, P., Diiorio, D., Joye, S.B., & Meile, C. (2013). Patterns and Controls of Nutrient Concentrations in a Southeastern United States Tidal Creek. *Oceanography*, *26*(3), p. 132–139. http://www.jstor.org/stable/24862074

Terry, J., Falkland, A. (2009). Responses of atoll freshwater lenses to storm-surge overwash in the Northern Cook Islands. *Hydrogeology Journal*, *18,* p. 749-759. https://doi.org/10.10007/s10040-009-0544-x

Timmerman, C. M., & Chapman, L. J. (2004). Patterns of hypoxia in a costal salt marsh: implications fofr ecophysiology of resident fishes. *Florida Scientist*, v. 67, p. 80–91. http://www.jstor.org/stable/24321201

Torrence, C., & Compo, G. P. (1998). A Practical Guide to Wavelet Analysis, Bulletin of the American Meteorological Society, 79(1), 61-78. Retrieved Nov 5, 2022, from https://journals.ametsoc.org/view/journals/bams/79/1/1520-0477_1998_079_0061_apgtwa_2_0_co_2.xml

U.S. Geological Survey, 2012, USGS NED ned19_n31x50_w081x25_ga_17counties_lot3_2011 1/9 arc-second 2012 15 x 15 minute IMG: U.S. Geological Survey.

Vacher, H.L., (1988).Dupuit-Ghyben-Herzberg analysis of strip-island lenses. *GSA Bulletin*, 100 (4): p. 580–591, https://doi.org/10.1130/0016-7606(1988)100<0580:DGHAOS>2.3.CO;2

Werner, A. D., Sharp, A. K., Galvis, S. C., Post, V. E. A., and Sinclair, P., (2017). Hydrogeology and management of freshwater lenses on atoll islands: Review of current knowledge and research needs, *Journal of Hydrology*, v. 551, p. 819-844. https://doi.org/10.1016/j.jhydrol.2017.02.047

Wilson, A. M., W. S. Moore, S. B. Joye, J. L. Anderson, and C. A. Schutte (2011), Storm-driven groundwater flow in a saltmarsh: Water Resources. Res., 47, W02535, https://doi.org/10.1029/2010WR009496

Wilson, A., Morris, J., (2012). The influence of tidal forcing on groundwater flow and nutrient exchange in a salt marsh-dominated estuary: *Biogeochemistry* 108:27-38, https://doi.org/10.1007/s10533-010-9570-y

Zotarelli, L., Dukes, M. D., Romero, C. C., Migliaccio, K. W., Morgan, K. T., (2020). Step by Step Calculation of the Penman-Monteith Evapotranspiration (FAO-56 Method), *IFAS Extension,* AE459, 1-10.